5859

Microwave Spectroscopic Studies of Simple Free Radicals

1981

Yasuki Endo

Division of Molecular Structure

Institute for Molecular Science

Okazaki, Japan

Acknowledgement

The author wishes to express his gratitude to Professors Eizi Hirota and Shuji Saito for their invaluable advices and encouragements throughout the works covered by the present thesis.

He also wishes to thank Dr. Tetsuo Suzuki and Mr. Kazuhiko Yoshida for their cooperative works in constructing the microwave spectrometers at Institute for Molecular Science.

Thanks are due to all the colleagues in our laboratory, Drs. Chikashi Yamada, Kentarow Kawaguchi, and Masao Kakimoto for their helpful discussions.

Contents

Part I. Introduction

Theory

Experimental

Chapter I. Introduction

Free radicals have attracted much attention in various fields of molecular spectroscopy, because they are important not only in spectroscopy but also in many other related fields. The term "Free radical" has usually been used for a group of atoms split off from a parent molecule with one or more unpaired electrons. The existence of unpaired electrons makes them reactive and short-lived. Free radicals are detected only as transient intermediates in reaction systems, and their investigations are quite difficult compared with stable molecules which have closed shell electron configurations. Sometimes molecules without unpaired electrons are included in free radicals if they are generated as short-lived chemical fragments. Spectroscopic knowledge on such free radicals is still rather restricted because of the difficulties in their detections, and it is still quite challenging for molecular spectroscopists to detect unknown short-lived species and firmly establish their existence. Identification of a free radical in a particular reaction system has a key importance to understand the reaction system. If high enough resolution is attained, spectroscopy is also capable of providing their structural informations. It is interesting, for example, to compare the structures of a precursor molecule and a free radical split off from the molecule, since they are helpful to understand a nature of chmical bonds.

spectroscopy of free radicals has also been motivated by

the existence of unpaired electrons. They cause complexities on their spectra which are not seen in molecules without them. Analyses of the spectra of free radicals are thus often more difficult than those of stable molecules. These complexities, on the other hand, afford many useful informations concerned with their electronic structures even in spectroscopy within the ground electronic state.

So far, many spectroscopic techniques have been applied to investigate simple free radicals in gas phase. The most fruitful among them is conventional optical spectroscopy observing electronic transitions either by emission or absorption. Optical spectroscopy has succeeded in detecting various free radicals thoughout its long history (1). Microwave spectroscopy of free radicals also has been tried since an earlier stage of the method. In fact, first successful detections were those of CS (2) and OH (3) both in 1953. Since then, owing to gradual improvements of the detection systems, many free radicals have now been studied by microwave spectroscopy (4-14). Gas phase electron paramagnetic resonance (EPR) spectroscopy, which is closely related to microwave spectroscopy, has also been used to investigate various free radicals since early 1960's (15). Various laser techniques, such as laser magnetic resonance (LMR) spectroscopy in far-infrared (16) and mid-infrared (17) regions, laser-microwave or laser-radiowave

double resonance spectroscopy (18-20), and diode laser spectroscopy (21), have recently been vitally applied to investigate many free radicals.

Compared with these other spectroscopic techniques, microwave spectroscopy has a few shortcomings which have made its application to free radical spectroscopy difficult. One problem is its lower sensitivity than that of most of other spectroscopic methods. Roughly speaking, sensitivity of a spectroscopic technique becomes higher if spectra are observed in higher frequency region. In fact, sensitivity of optical spectroscopy is so high that many short-lived free radicals and molecular ions which have not yet been observed by other spectroscopic methods have been observed by optical spectroscopy. Once a laser technique is introduced, even individual atoms or molecules are detectable in the optical region. Other laser techniques operating in far-infrared or mid-infrared regions also have higher sensitivity than microwave spectroscopy (16). Even the EPR method which operates in a cm wave region has comparble or higher sensitivity, because EPR uses a high Q resonance cavity as an absorption cell (15).

Another problem is that it is difficult to scan wide frequency regions by microwave spectrometers. This problem is amplified by the fact that the rotational transitions spread into wide frequency regions. Especially for simple light molecules, numbers of observable transitions become so small that this

problem becomes quite serious. It has been almost impossible to search an unknown species by microwave spectroscopy alone unless spectra are strong and rich in microwave region. So far, most free radicals observed by microwave spectroscopy have been limited to those already detected by other techniques, and fairly precise molecular constants for them had been obtained. These results have been utilized to restrict the search region. The low sensitivity also has been overcome by using a slow scanning rate with a long time constant in the narrow frequency region. Sometimes the reaction schemes adopted by other methods to generate free radicals have been used, because it is almost impossible to repeat the search by changing the observation conditions in microwave spectroscopy.

In spite of such difficulties, one of the advantages of microwave spectroscopy is its high resolution and precision. Althouth the new laser techniques often state their higher resolution and accuracy over conventional optical spectroscopy, accuracy obtained by microwave spectroscopy is still higher than that of such new methods in most cases. Resolution of microwave spectroscopy is usually high enough to resolve the magnetic hyperfine splittings of free radicals; the hyperfine instractions are a source of valuable information on electronic structures of free radicals. Furthurmore, these high resolution and accuracy are essential in many cases to firmly and unambiguously establish the molecular species observed.

Once a free radical is detected by microwave spectroscopy, the precise molecular constants obtained enable us to accurately evaluate the molecular structures. Dipole moments which also can be determined by microwave spectroscopy gives means to qualitatively estimate the absolute concentrations of the radicals in various reaction systems.

Microwave spectroscopy of free radicals has found its important application in radioastronomy. About fifty molecules including many free radicals have been identified in interstellar space through their microwave spectral lines observed by radiotelescopes (22). The free radicals which are short-lived in the terrestrial medium could have longer lifetime in interstellar space because of their low concentrations. In fact, owing to recent advances in radioastronomy, some species were detected and identified prior to laboratory observations. And there exist several species which have not been observed in laboratory yet. The free radicals observed in interstellar space are considered to be taking important roles in the molecular evolution. Therefore, laboratory observations of free radicals have given important means for their identifications and helped the understanding of the reaction mechanisms. At the same time, microwave spectroscopy have gained many stimulations as to the existence of usually unstable species from radioastronomy.

Free radicals so far observed by microwave spectroscopy are simple diatomic and triatomic species. Theories to analyze the rotational spectra of these free radicals are now well established. The unpaired electron(s) on the free radicals cause complex couplings of the various angular momenta. The unpaired electron spin $\underset{\sim}{S}$ couples with the orbital angular momentum $\underset{\sim}{L}$ for diatomic and linear triatomic species with non-zero orbital angular momentum. This coupling, the spin-orbit coupling, gives rise to the fine structure for such species. The spin angular momentum also couples with overall molecular rotaion; the coupling is called the spin-rotation coupling. The spin-rotation coupling gives rise to the fine structure for molecules without orbital angular momentum, e. g. bent triatomic radicals. If there exist one or more atoms with nonzero nuclear spin $\underset{\sim}{I}$, the electron spin $\underset{\sim}{S}$ couples with the nuclear spin(s). This coupling gives rise to the magnetic hyperfine structure.

Rotational energy levels of such species were first discussed by Hill and Van Vleck (23) for diatomic radicals and Van Vleck (24) for asymmetric rotor species. The theory for diatomic radicals, especially in $^2\Pi$ electronic states, has been later extended by many authors (15,25-31). Among these studies the analysis of OH (3) was the first application of the theory to the microwave spectrum. Extensive studies on ClO_2 (32-38) and NO_2 (39) by Curl et al. in the microwave region greatly promoted the refinement of the theory for asymmetric

rotors with an unpaired electron.

Microwave spectrometers for stable molecules have well established configurations, where the Stark modulation is usually used with an absorption cell made of a waveguide. For free radical spectroscopy the spectrometers should be changed considerably to fit the observation of short-lived species. Sensitivity of the spectrometer becomes an important factor to detect free radicals because it is difficult in most cases to obtain sufficient concentrations for the species to be studied. Specially designed absorption cells are required to generate the desired species efficiently. Thus, various types of spectrometers have so far been tried including the adoption of Zeeman modulation or video detection with a free space cell or modified waveguide mode cells (3,41-43). However, the most successful and easy to handle among them was the one which used Stark modulation with a parallel-plate absorption cell (4); a fairly large vacuum pump was connected directly to the cell to pump continuously the gases in the cell. Most of the components and techniques used for spectroscopy of stable molecules also can be used for this type of spectrometers, except the absorption cell and the vacuum system, so that it has been easier to obtain high enough sensitivity required for free radical spectroscopy than other methods adopted. The characteristic Stark patterns

for observed transitions are also quite useful to assign the unknown species. One problem of this type of cells is that long path length is not obtained compared with that of the absorption cells for stable molecules, because the concentrations of the unstable species are limited by the lifetime of the species and by the pumping speed. Cell length of several ten cm is optimum for this type of cells, which as a result has limited the minimum detectable concentrations for the free radicals to be studied. The cell length is also limited by the microwave propagation. In fact, even by a cell of 40 cm long, it becomes quite difficult to get sufficient transmitted microwave power above 100 GHz. Absorption cells with lower transmission loss are required to operate the spectrometer above 100 GHz, where absorption becomes much stronger and it becomes easier to obtain high enough sensitivity for free radical spectroscopy. In higher frequency regions up to sub-mm, free space cells have been used for spectroscopy of both stable and unstable molecules (41) because it has very low transmission loss at high frequency region.

Woods (44) has shown recently that microwave can be fairly well transmitted even through a discharged plasma if the plasma density is sufficiently low. He and his coworkers used a free space cell 3 m in length, and successfully detected molecular ions and free radicals (45-50) in the discharged plasma at frequency regions from 80 to 120 GHz. This type of cells seems to have greater possibilities for future studies

as the lifetime of the species to be observed is not limited primarily by the pumping speed in the cell because the species are generated where they are observed. Fairly good microwave transmission enabled them to use very long cell, and thus minimum detectable concentrations become quite low in their apparatus. In fact, according to their estimation of the absorption coefficient, the concentration of CO^+ is an order of 10^{-6} times that of parent CO (45).

In this thesis, microwave spectroscopic studies of three free radicals are presented. The SF radical is a diatomic free radical with the $^2\Pi$ ground electronic state, and spectra in the $^2\Pi_{1/2}$ state have been observed for the first time. From a combined analysis of the result with that of the $^2\Pi_{3/2}$ state (13), detailed and precise molecular constants which fully characterize a molecule in the $^2\Pi$ electronic state have been determined. Among them is included the determination of all four hyperfine coupling constants of the fluorine nucleus, which are useful to discuss the electronic structure of the radical.

Studies of two bent triatomic radicals are also given. The HSO radical and its fluorinated derivative FSO are both new species which had not been known until a few years ago. Especially, no spectroscopic results on the FSO radical had been published before. The present study of FSO is an exceptional example that the microwave spectrum was observed without utilizing results of other spectroscopic studies.

On the other hand, for the study of the HSO radical, results of recent investigations by dye laser excitation spectroscopy were fully utilized (51, 52), since the spectrum was much weaker and sparce in the microwave region. These results were quite useful to restrict the search region, and consequently we were able to detect very weak spectrum for this radical. Greatly improved and detailed informations have been obtained for the radical.

In the next chapter, theories of the molecular Hamiltonians appropriate to analyze the spectra of the free radicals observed are summarized. As the theories for diatomic species and polyatomic species have been developed separately and consequently quite different nomenclature is used, the chapter was divided into two to explain each of them. Numerical analyses of the spectra were performed with computer programs in all the cases. The programs, which were developed in the cource of present works, are also explained there.

The third chapter is devoted to the explanations of our experimental set up. Two types of absorption cells were constructed; one is a parallel plate Stark cell with a conventional Stark modulation scheme, and others are free space cells where internal glow discharges were used with a source modulation scheme. A minicomputer was used to obtain high sensitivity. Source modulation has rarely been used so far because of its difficulty in scanning wide

frequency range and the severe baseline distortions due to reflections of the microwave power. Use of the minicomputer has greatly remedied these difficulties and widened the applicabilities of the source modulation method.

Results of the individual radicals are presented in Part II. The last chapter of Part II is devoted to general discussions of the results. Special emphasis is put on the interaction constants which exist only for free radicals, such as the spin-rotation interaction constants and the magnetic hyperfine interaction constants. Especially the hyperfine interaction constants of fluorine nuclei are compared for SF and FSO along with CF (53) and NF_2 (54).

Chapter II. Theory

1. Rotational Hamiltonian for diatomic molecules in $^2\Pi$ electronic state

Rotational energy levels of molecules in $^2\Pi$ electronic state were first discussed by Hill and Van Vleck (23). They considered a rotational Hamiltonian with couplings between rotational angular momentum $\underset{\sim}{R}$, unpaired electron spin angular momentum $\underset{\sim}{S}$, and electron orbital angular momentum $\underset{\sim}{L}$, and derived an energy level equation for general intermediate coupling cases between Hund's (a) and (b). Van Vleck (25), and Mulliken and Christy (26) discussed the Λ-type doubling of molecules in $^2\Pi$ electronic state. Almy and Horsfall (27) introduced the centrifugal distortion effect in rotation to explain the spectra of BH^+. First application of the theory to microwave spectroscopy was done by Dousmanis et al. (3) in their analyses of the Λ-doubling transitions of the OH and OD radicals. They refined the theory applicable to microwave spectroscopy. James (29) introduced the centrifugal distortion effect of the spin-orbit coupling, viz. A_J. He also explicitly introduced the spin-rotation interaction term γ_v. However, more recently, Brown and Watson (55) discussed that A_J and γ_v cannot be determined simultaneously unless data on different isotopic species were used.

The rotational Hamiltonian for a $^2\Pi$ molecule can be written as follows;

$$\underset{\sim}{H} = \underset{\sim}{H}_{rot} + \underset{\sim}{H}_{fs} + \underset{\sim}{H}_{sr}, \tag{1-2-1}$$

where

$$\underset{\sim}{H}_{rot} = B_v(\underset{\sim}{J}-\underset{\sim}{L}-\underset{\sim}{S})^2 - D_v(\underset{\sim}{J}-\underset{\sim}{L}-\underset{\sim}{S})^4, \tag{1-2-2}$$

$$\underset{\sim}{H}_{fs} = A_v\underset{\sim}{L}\cdot\underset{\sim}{S} + A_J[(\underset{\sim}{L}\cdot\underset{\sim}{S})\underset{\sim}{N}^2 + \underset{\sim}{N}^2(\underset{\sim}{L}\cdot\underset{\sim}{S})], \tag{1-2-3}$$

$$\underset{\sim}{H}_{sr} = \gamma_v\underset{\sim}{N}\cdot\underset{\sim}{S}. \tag{1-2-4}$$

Here, B_v and D_v are the rotational constant and its centrifugal distortion constant; A_v and A_J the spin-orbit interaction constant and its centrifugal distortion constant; γ_v the spin-rotation interaction constant. $\underset{\sim}{J}$ is the total angular momentum, $\underset{\sim}{S}$ the spin angular momentum, $\underset{\sim}{L}$ the orbital angular momentum and $\underset{\sim}{R}$ the molecular rotation angular momentum. The appropriate coupling scheme for them is $\underset{\sim}{N} = \underset{\sim}{R} + \underset{\sim}{L}$, and $\underset{\sim}{J} = \underset{\sim}{N} + \underset{\sim}{S}$.

Matrix elements of the above Hamiltonian terms are evaluated with the case (a) basis set wave functions,

$$|J\Omega S\Sigma\Lambda\rangle = |J\Omega\rangle|S\Sigma\rangle|\Lambda\rangle. \tag{1-2-5}$$

They transform as follows under reflection σ_v in the xy-plane of the molecule fixed axis system (30,56),

$$\sigma_v|J\Omega\rangle = (-1)^{J-\Omega}|J,-\Omega\rangle, \tag{1-2-6}$$

$$\sigma_v|S\Sigma\rangle = (-1)^{S-\Sigma}|S,-\Sigma\rangle, \tag{1-2-7}$$

$$\sigma_v|\Lambda\rangle = (-1)^{\Lambda+s}|-\Lambda\rangle, \tag{1-2-8}$$

where

$$s = 0 \quad \text{for} \quad \Sigma^+, \ \Pi, \ \Delta, \ \ldots \text{ states}, \tag{1-2-9}$$

$$s = 1 \quad \text{for} \quad \Sigma^- \text{ state}.$$

Therefore, for doublet electronic states,

$$\sigma_v|J\Omega S\Sigma\Lambda\rangle = (-1)^{J-S-s}|J,-\Omega,S,-\Sigma,-\Lambda\rangle. \tag{1-2-10}$$

By using the above basis set functions, following matrix elements are obtained for the S = 1/2 and $\Delta\Lambda$ = 0 block (31):

$$\langle J\Omega=\tfrac{1}{2},S\Sigma=-\tfrac{1}{2},\Lambda=1|\underset{\sim}{H}|J\Omega=\tfrac{1}{2},S\Sigma=-\tfrac{1}{2},\Lambda=1\rangle$$

$$= -\frac{A_v}{2} + (B_v - A_J - D_v)(J + \tfrac{1}{2})^2$$

$$-D_v(J + \tfrac{1}{2})^4, \tag{1-2-11}$$

$$\langle J\Omega=\tfrac{3}{2},S\Sigma=\tfrac{1}{2},\Lambda=1|\underset{\sim}{H}|J\Omega=\tfrac{3}{2},S\Sigma=\tfrac{1}{2},\Lambda=1\rangle$$

$$= \frac{A_v}{2} + (B_v + A_J + 3D_v)[(J + \tfrac{1}{2})^2 - 2]$$

$$-D_v(J + \tfrac{1}{2})^4, \tag{1-2-12}$$

$$\langle J\Omega=\tfrac{3}{2},S\Sigma=\tfrac{1}{2},\Lambda=1|\underset{\sim}{H}|J\Omega=\tfrac{1}{2},S\Sigma=-\tfrac{1}{2},\Lambda=1\rangle$$

$$= -\{B_v - \frac{\gamma_v}{2} - 2D_v[(J + \tfrac{1}{2})^2 - 1]\}$$

$$\times[(J + \tfrac{1}{2})^2 - 1]^{1/2}. \tag{1-2-13}$$

H_{rot} and H_{fs} contain terms with $\Delta\Lambda = \pm 1$ matrix elements. The terms are rewritten as follows:

$$\hat{H}_{\Lambda} = -B_v(J_+L_- + J_-L_+) + (B_v + \frac{A_v}{2})(L_+S_- + L_-S_+). \qquad (1\text{-}2\text{-}14)$$

They connect different electronic states differing by one in Λ, and cause the Λ-doubling in $^2\Pi$ state (25,26). To account for the Λ-doubling, wavefunctions with definite parity are required; following linear combinations are adopted here:

$$|^2|\Lambda|^S_{\Omega},J,\pm> = \frac{1}{\sqrt{2}}[|J\Omega S\Sigma\Lambda> \pm (-1)^{J-S-s}|J,-\Omega,S,-\Sigma\Lambda>], \qquad (1\text{-}2\text{-}15)$$

where the $\pm$ signs and the e and f notations by Kopp and Hougen (30) are related as follows for $^2\Pi$ electronic states:

$$\text{when} \quad (-1)^{J-\frac{1}{2}} = 1 \qquad |\Pi+> : e, \qquad (1\text{-}2\text{-}16)$$
$$|\Pi-> : f,$$
$$\text{or} \quad (-1)^{J-\frac{1}{2}} = -1 \qquad |\Pi+> : f,$$
$$|\Pi-> : e \text{ levels, respectively.}$$

The contributions from excited $^2\Sigma^s$ states (those from Δ states are negligible) are treated by the second-order perturbation method and the wavefunctions in eq. (1-2-15) are used as basis set wavefunctions; following matrix elements within the $^2\Pi$ electronic state are obtained:

$$<^2\Pi_{1/2},J,\pm|H_{\mathcal{C}\Lambda}|^2\Pi_{1/2},J,\pm>$$

$$= \frac{q_v^*}{2}[(J+\tfrac{1}{2})^2+1] + \frac{p_v^*}{2} + o_v^* \mp(-1)^{J-S}(J+\tfrac{1}{2})$$

$$\times(q_v + \frac{p_v}{2}), \qquad (1\text{-}2\text{-}17)$$

$$<^2\Pi_{3/2},J,\pm|H_{\mathcal{C}\Lambda}|^2\Pi_{3/2},J,\pm>$$

$$= \frac{q_v^*}{2}[(J+\tfrac{1}{2})^2-1], \qquad (1\text{-}2\text{-}18)$$

$$<^2\Pi_{3/2},J,\pm|H_{\mathcal{C}\Lambda}|^2\Pi_{1/2},J,\pm>$$

$$= -(\frac{p_v^*}{4}+\frac{q_v^*}{2})[(J+\tfrac{1}{2})-1]^{1/2}$$

$$\pm(-1)^{J-S}(J+\tfrac{1}{2})[(J+\tfrac{1}{2})^2-1]^{1/2}\frac{q_v}{2}, \qquad (1\text{-}2\text{-}19)$$

where

$$p_v = 4\Sigma(-1)^s\frac{<\Pi|\frac{A_v}{2}L_+|\Sigma^s><\Sigma^s|B_vL_+|\Pi>}{E_\Pi - E_\Sigma}, \qquad (1\text{-}2\text{-}20)$$

$$q_v = 2\Sigma(-1)^s\frac{|<\Pi|B_vL_+|\Sigma^s>|^2}{E_\Pi - E_\Sigma}, \qquad (1\text{-}2\text{-}21)$$

and

$$o_v^* = \Sigma\frac{|<\Pi|\frac{A_v}{2}L_+|\Sigma^s>|^2}{E_\Pi - E_\Sigma}, \qquad (1\text{-}2\text{-}22)$$

$$p_v^* = 4\Sigma\frac{<\Pi|\frac{A_v}{2}L_+|\Sigma^s><\Sigma^s|B_vL_+|\Pi>}{E_\Pi - E_\Sigma}, \qquad (1\text{-}2\text{-}23)$$

$$q_v^* = 2\Sigma \frac{|\langle \Pi | B_v L_+ | \Sigma^s \rangle|^2}{E_\Pi - E_\Sigma} . \qquad (1\text{-}2\text{-}24)$$

Here, p_v and p_v^*, and q_v and q_v^* are not identical in general because of the factor $(-1)^s$, which causes opposite contributions when $^2\Sigma^-$ states are concerned (26,29). As is easily seen, eqs. (1-2-11) through (1-2-13) are not affected when the wavefunctions with parity are adopted (see also eq. (1-2-10)). When eqs. (1-2-17) through (1-2-19) are compared with eqs. (1-2-11) through (1-2-13), it is seen that the contributions of o_v^*, p_v^*, and q_v^* are not distinguishable with those of A_v, B_v, and γ_v.

So far, so called single perturber model(23)has been used for the analyses of the Λ-doubling in most cases (3,7,57,58), where only one Σ^+ (or Σ^-) perturber state was assumed. And p_v^* and q_v^* were considered to be equal to p_v and q_v (or $-p_v$ and $-q_v$). However, this assumption does not hold in general, and it is not a good approximation for precise analysis of the observed data (59), although the assumption is useful in many cases to understand the Λ-doublings qualitatively. When the single perturber model is not adopted, determined constants A_v, B_v, and γ_v should be considered to be effective constants including the contributions from excited $^2\Sigma$ states,

$$A_v^{(eff.)} = A_v - \frac{1}{2}(p_v^* + 2o_v^*), \qquad (1\text{-}2\text{-}25)$$

$$B_v^{(eff.)} = B_v + \frac{1}{2}q_v^*, \qquad (1\text{-}2\text{-}26)$$

$$\gamma_v^{(eff.)} = \gamma_v - \frac{1}{2}p_v^*. \qquad (1\text{-}2\text{-}27)$$

Finally, combining the eqs. (1-2-11) through (1-2-13) with the eqs. (1-2-17) through (1-2-19) by using redefined A_v, B_v, and γ_v, we obtain the following matrix elements to analyze rotational energy levels of $^2\Pi$ molecules,

$$\langle {}^2\Pi_{1/2}J\pm|\underset{\sim}{H}|{}^2\Pi_{1/2}J\pm\rangle = -\frac{A_v}{2} + (B_v - A_J - D_v)(J+\tfrac{1}{2})^2 - D_v(J+\tfrac{1}{2})^4 \mp(-1)^{J-S}(J+\tfrac{1}{2})(q_v + \frac{p_v}{2}), \qquad (1\text{-}2\text{-}28)$$

$$\langle {}^2\Pi_{3/2}J\pm|\underset{\sim}{H}|{}^2\Pi_{3/2}J\pm\rangle = \frac{A_v}{2} + (B_v + A_J + 3D_v)[(J+\tfrac{1}{2})^2 - 2] - D_v(J+\tfrac{1}{2})^4, \qquad (1\text{-}2\text{-}29)$$

$$\langle {}^2\Pi_{3/2}J\pm|\underset{\sim}{H}|{}^2\Pi_{1/2}J\pm\rangle = -\{B_v - \frac{\gamma_v}{2} - 2D_v[(J+\tfrac{1}{2})^2 - 1] \mp(-1)^{J-S}(J+\tfrac{1}{2})\frac{q_v}{2}\}[(J+\tfrac{1}{2})^2 - 1]^{1/2}, \qquad (1\text{-}2\text{-}30)$$

where A_v etc. are in fact $A_v^{(eff.)}$ etc.

To access constants without the contributions from excited Σ states, we have to know precisely the electronic energy levels of the molecule and also have to know the matrix elements between

the $^2\Pi$ state and those states. The largest contribution from the states comes through the constant p_v^*, which makes the meaning of γ_v unambiguous. Moreover, the indeterminacy between γ_v and A_J (55) makes the problem quite difficult for quantitative discussions.

2. Hyperfine interactions for diatomic molecules in $^2\Pi$ electronic state

When one or two nuclei of a diatomic molecule have nonzero nuclear spin(s), the nuclear spin angular momentum interacts with the unpaired electron spin and electron orbital angular momentum. The interactions give rise to hyperfine structures. Frosch and Foley (28), and Mizushima (60) discussed the hyperfine interactions for molecules in $^2\Pi$ electronic state. Dousmanis (61) later reexamined the treatment of Frosch and Foley, and redefined the hyperfine interaction constants they introduced in ref. 28.

The explicit expressions for the hyperfine Hamiltonian are written as follows (61),

$$\begin{aligned} \underset{\sim}{H}_{hf} = {} & a\underset{\sim}{I}\cdot\underset{\sim}{L} + (b + c)I_zS_z + \tfrac{1}{2}b(I_+S_+ + I_-S_-) \\ & + d(e^{2i\phi}I_-S_- + e^{-2i\phi}I_+S_+) \\ & + e[e^{i\phi}(S_-I_z + I_-S_z) + e^{-i\phi}(S_+I_z + I_+S_z)], \end{aligned} \tag{1-2-31}$$

where

$$I_\pm = I_x \pm iI_y,$$

and

$$a = 2g_I\beta\beta_I\left\langle\frac{1}{r^3}\right\rangle_{av.},$$

$$b = -\tfrac{1}{2}g_Sg_I\beta\beta_I\left\langle\frac{3\cos^2\chi-1}{r^3}\right\rangle_{av.} + \frac{8\pi}{3}g_Sg_I\beta\beta_I|\Psi(0)|^2,$$

$$c = \frac{3}{2} g_S g_I \beta\beta_I \left\langle \frac{3\cos^2\chi - 1}{r^3} \right\rangle_{av.},$$

$$d = \frac{3}{2} g_S g_I \beta\beta_I \left\langle \frac{\sin^2\chi}{r^3} \right\rangle_{av.},$$

$$e = \frac{3}{2} g_S g_I \beta\beta_I \left\langle \frac{\sin\chi\cos\chi}{r^3} \right\rangle_{av.}. \qquad (1\text{-}2\text{-}32)$$

β and β_I are the values of the Bohr and nuclear magnetons, and g_S and g_I are the electron spin and nuclear spin g-factors. The term containing d in eq. (1-2-32) has $\Delta\Lambda = \pm 2$ matrix elements and contributes to each of the Λ-doublet. The term containing e has $\Delta\Lambda = \pm 1$ matrix elements; they can be ignored in most cases because there is no first order contributions within $^2\Pi$ electronic state. Other terms are diagonal in Λ.

Matrix elements within the $^2\Pi$ electronic state have been given by Frosch and Foley (28), and Lin and Mizushima (62). However, we used the following matrix elements in our analysis which are expressed using Racah coefficients (15, 63, 64),

$$\langle {}^2\Pi_{1/2} J\pm | H_{hf} | {}^2\Pi_{1/2} J'\pm \rangle = G(JJ'IF)\{(-1)^{J'-1/2} \begin{pmatrix} J & 1 & J' \\ -1/2 & 0 & 1/2 \end{pmatrix} \times (a - \frac{b+c}{2}) \mp \begin{pmatrix} J & 1 & J' \\ -1/2 & 1 & -1/2 \end{pmatrix} \frac{d}{\sqrt{2}} \}, \qquad (1\text{-}2\text{-}33)$$

$$\langle {}^2\Pi_{3/2} J\pm | H_{hf} | {}^2\Pi_{3/2} J'\pm \rangle = G(JJ'IF)(-1)^{J'-3/2} \begin{pmatrix} J & 1 & J' \\ -3/2 & 0 & 3/2 \end{pmatrix} \times (a + \frac{b+c}{2}), \qquad (1\text{-}2\text{-}34)$$

$$<^2\Pi_{3/2}J\pm|H_{hf}|^2\Pi_{1/2}J'\pm> = G(JJ'IF)(-1)^{J'-3/2}\begin{pmatrix} J & 1 & J' \\ -3/2 & 1 & 1/2 \end{pmatrix}\frac{b}{\sqrt{2}} , \tag{1-2-35}$$

where

$$G(JJ'IF) = (-1)^{J+I+F}[I(I+1)(2I+1)(2J+1)(2J'+1)]^{1/2}\begin{Bmatrix} I & J & F \\ J' & I & 1 \end{Bmatrix} . \tag{1-2-36}$$

3. Asymmetric rotor molecules in doublet electronic state

Because the electron orbital angular momentum is quenched owing to the asymmetry, there is no first order spin-orbit interaction as is observed for diatomic molecules in $^2\Pi$ electronic state. The spin-rotation interaction gives rise to the fine structure for rotational energy levels of such asymmetric rotor molecules. However, the treatment of the spectrum becomes slightly complicated because the rotational energy levels of asymmetric rotors are not simple. Van Vleck (24) gave a general theory for the couplings of the angular momentum vectors in molecules, where he presented relevant matrix elements for asymmetric rotors in doublet electronic states including the spin-rotation interaction. Lin (65) discussed the rotational energy levels of NO_2, where he included a treatment of the hyperfine interaction. Curl and Kinsey (32) discussed the coupling in general by using Racah coefficients (spherical tensor method). Curl et al. also applied their theory to analyze the rotational spectra of ClO_2 (33-38), and NO_2 (39,40). Bowater et al. (66) derived general matrix elements for such molecules including the hyperfine interaction, the Stark effect, and the Zeeman effect by using the spherical tensor method. Centrifugal distortion corrections to the spin-rotation interaction were discussed by Dixon and Duxbury (67), Cook et al. (68), and Brown and Sears (69). Brown and Sears (70) discussed that there are indeterminacies among the spin-rotation

interaction constants and its centrifugal distortion constants by a way Watson (71) first discussed for ordinary centrifugal distortion constants in rotation. They gave matrix elements for the centrifugal corrections in spin-rotation both in so called S-reduction and A-reduction (72).

The Hamiltonian for asymmetric rotors in doublet electronic state is given by,

$$\underset{\sim}{H} = \underset{\sim}{H}_{rot} + \underset{\sim}{H}_{cd} + \underset{\sim}{H}_{sr} + \underset{\sim}{H}_{srcd} + \underset{\sim}{H}_{hfs} , \qquad (1\text{-}2\text{-}37)$$

where $\underset{\sim}{H}_{rot}$ and $\underset{\sim}{H}_{cd}$ denote the ordinary asymmetric rotor Hamiltonian and its centrifugal distortion correction (72). The third term, $\underset{\sim}{H}_{sr}$, is the spin-rotation interaction operator, and $\underset{\sim}{H}_{srcd}$ its centrifugal correction. The last term, $\underset{\sim}{H}_{hfs}$, denotes the magnetic hyperfine interaction. Explicit expressions for the last three terms are,

$$\begin{aligned}\underset{\sim}{H}_{sr} &= \varepsilon_{aa}N_aS_a + \varepsilon_{bb}N_bS_b + \varepsilon_{cc}N_cS_c \\ &\quad + 1/2(\varepsilon_{ab}+\varepsilon_{ba})(N_aS_b+N_bS_a),\end{aligned} \qquad (1\text{-}2\text{-}38)$$

$$\begin{aligned}\underset{\sim}{H}_{srcd} &= \Delta_N{}^S\underset{\sim}{N}^2(\underset{\sim}{N}\cdot\underset{\sim}{S}) + 1/2\Delta_{NK}{}^S\{\underset{\sim}{N}^2N_aS_a+N_aS_a\underset{\sim}{N}^2\} + \Delta_{KN}{}^SN_a{}^2(\underset{\sim}{N}\cdot\underset{\sim}{S}) \\ &\quad + \Delta_K{}^SN_a{}^3S_a + \delta_N{}^S(N_+{}^2+N_-{}^2)(\underset{\sim}{N}\cdot\underset{\sim}{S}) \\ &\quad + 1/2\delta_K{}^S\{(N_+{}^2+N_-{}^2)N_aS_a + N_aS_a(N_+{}^2+N_-{}^2)\} ,\end{aligned} \qquad (1\text{-}2\text{-}39)$$

$$\underset{\sim}{H}_{hfs} = a_F\underset{\sim}{S}\cdot\underset{\sim}{I} + \underset{\sim}{S}\cdot\underset{\sim}{T}\cdot\underset{\sim}{I} , \qquad (1\text{-}2\text{-}40)$$

where ε_{ij} denotes a component of the spin-rotation interaction tensor $\underset{\sim}{\varepsilon}$, Δ^S's and δ^S's the centrifugal distortion constants in the spin-rotation interaction, a_F the Fermi coupling constant, and T_{ij} a component of the magnetic dipole-dipole interaction tensor $\underset{\sim}{T}$. There are nine components for the spin-rotation interaction tensor in general. And it is easily be shown that five out of them are non-zero for molecules with C_s symmetry from symmetry considerations. As discussed by Brown et al. (70), however, only four out of five constants are determinable for C_s molecules; we retained three diagonal components ε_{aa}, ε_{bb}, and ε_{cc} and a linear combination for the off-diagonal component, $1/2(\varepsilon_{ab}+\varepsilon_{ba})$, for four determinable constants. The parameters given above for the centrifugal distortion constants in the spin-rotation interaction are those for molecules belonging to the orthorhombic symmetry (70). There are five components for T_{ij} in general; three of them are non-zero for molecules with C_s symmetry.

Matrix elements of the Hamiltonian terms given above are evaluated using the basis set functions $|NKSJIFM_F\rangle$ with Hund's case (b) coupling scheme, viz. $\underset{\sim}{J} = \underset{\sim}{N} + \underset{\sim}{S}$ and $\underset{\sim}{F} = \underset{\sim}{J} + \underset{\sim}{I}$. The matrix elements are listed in Table I, where the spin-rotation constants and the hyperfine interaction constants expressed in irreducible tensor notations are related to those expressed in the molecule fixed Cartesien coordinate system as follows (66),

$$T_0^0(\varepsilon) = -3^{-1/2}[\varepsilon_{aa}+\varepsilon_{bb}+\varepsilon_{cc}] ,$$

$$T_1^1(\varepsilon) = T_0^1(\varepsilon) = T_{-1}^1(\varepsilon) = 0 ,$$

$$T_0^2(\varepsilon) = 6^{-1/2}[2\varepsilon_{aa}-\varepsilon_{bb}-\varepsilon_{cc}] ,$$

$$T_1^2(\varepsilon) = T_{-1}^2(\varepsilon) = -1/2(\varepsilon_{ab}+\varepsilon_{ba}) ,$$

$$T_2^2(\varepsilon) = T_{-2}^2(\varepsilon) = 1/2(\varepsilon_{bb}-\varepsilon_{cc}) , \qquad (1\text{-}2\text{-}41)$$

and

$$g_S g_I \beta\beta_I T_0^2(C) = -1/2 T_{aa} ,$$

$$g_S g_I \beta\beta_I T_1^2(C) = -g_S g_I \beta\beta_I T_{-1}^2(C) = -6^{-1/2} T_{ab}$$

$$g_S g_I \beta\beta_I T_2^2(C) = g_S g_I \beta\beta_I T_{-2}^2(C) = 24^{-1/2}(T_{aa}+2T_{bb}) .$$

(1-2-42)

The Hamiltonian for the Stark effect is given by,

$$\underset{\sim}{H}_S = -\underset{\sim}{\mu}\cdot\underset{\sim}{E} = \sum_g \mu_g \phi_{zg} E_z . \qquad (1\text{-}2\text{-}43)$$

The matrix elements for this Hamiltonian with the spherical tensor notations (66) are expressed as follows:

$$\langle N'K'SJ'IF'M_F' | H_S | NKSJIFM_F \rangle$$

$$= -\sum_p (-1)^p T_p^1(\underset{\sim}{E})(-1)^{F'-M_F'} \begin{pmatrix} F' & 1 & F \\ -M_F' & -p & M_F \end{pmatrix}$$

$$\times(-1)^{J'+I+F+1}[(2F'+1)(2F+1)]^{1/2}\begin{Bmatrix} J' & F' & I \\ F & J & 1 \end{Bmatrix}$$

$$\times(-1)^{N'+S+J+1}[(2J'+1)(2J+1)]^{1/2}\begin{Bmatrix} N' & J' & S \\ J & N & 1 \end{Bmatrix}$$

$$\times\sum_q T^1_q(\underset{\sim}{\mu})(-1)^{N'-K'}[(2N'+1)(2N+1)]^{1/2}\begin{pmatrix} N' & 1 & N \\ -K' & q & K \end{pmatrix} , \qquad (1\text{-}2\text{-}43)$$

where, $T^1_0(\underset{\sim}{E}) = E_z$ and $T^1_{\pm 1}(\underset{\sim}{E}) = 0$, if the applied static electric field is parallel to the microwave electric field, and

$$T^1_0(\mu) = \mu_a ,$$

$$T^1_1(\mu) = -2^{-1/2}(\mu_c + i\mu_b) ,$$

$$T^1_{-1}(\mu) = 2^{-1/2}(\mu_c - i\mu_b) , \qquad (1\text{-}2\text{-}44)$$

where μ_a, μ_b, and μ_c are components of the dipole moment along the three inertial axes, a, b, and c respectively.

Table I. Matrix elements of the asymmetric top Hamiltonian in doublet electronic state

1. Spin-rotation terms

$$\langle N'K'SJ'IF'M_F'|H_{sr}|NKSJIFM_F\rangle = \delta_{M_FM_F'}\delta_{FF'}\delta_{JJ'}\sum_{k=0}^{2}(2k+1)^{1/2}$$

$$\times[S(S+1)(2S+1)]^{1/2}[(2N+1)(2N'+1)]^{1/2}(-1)^{J+S+N'}\begin{Bmatrix} N & S & J \\ S & N' & 1 \end{Bmatrix}$$

$$\times\frac{1}{2}[(-1)^k\{N(N+1)(2N+1)\}^{1/2}\begin{Bmatrix} 1 & 1 & k \\ N' & N & N \end{Bmatrix}+\{N'(N'+1)(2N'+1)\}^{1/2}$$

$$\times\begin{Bmatrix} 1 & 1 & k \\ N & N' & N' \end{Bmatrix}]\sum_q(-1)^{N'-K'}\begin{pmatrix} N' & k & N \\ -K & q & K \end{pmatrix}T_q^k(\varepsilon).$$

2. Centrifugal corrections for the spin-rotation interaction

$$\langle NKSJ|H_{srcd}|NKSJ\rangle = \{\Gamma(NSJ)/2N(N+1)\}$$

$$\times\{\Delta_K{}^sK^4+(\Delta_{NK}{}^s+\Delta_{KN}{}^s)K^2N(N+1)+\Delta_N{}^sN^2(N+1)^2\},$$

$$\langle N-1KSJ|H_{srcd}|NKSJ\rangle = -\{\Phi(NSJ)/(2N-1)(2N+1)\}^{1/2}(K/2N)$$

$$\times(N^2-K^2)^{1/2}\{\Delta_K{}^sK^2+\Delta_{NK}{}^sN^2\},$$

$$\langle NK\pm2SJ|H_{srcd}|NKSJ\rangle = \{\Gamma(NSJ)/2N(N+1)\}$$

$$\times[\{N(N+1)-K(K\pm1)\}\{N(N+1)-(K\pm1)(K\pm2)\}]^{1/2}\{\delta_N{}^sN(N+1)$$

$$+\frac{1}{2}\delta_K{}^s[K^2+(K\pm2)^2]\},$$

$$\langle N-1K\pm2SJ|H_{srcd}|NKSJ\rangle = -\{\Phi(NSJ)/(2N-1)(2N+1)\}^{1/2}$$

$$\times[(N\mp K-1)(N\pm K+1)(N\mp K-2)(N+K)]^{1/2}$$

$$\times\{K(N\pm K)+(K\pm2)(N\pm K+2)\}\delta_K{}^s/4N,$$

where

$$\Gamma(NSJ) = J(J+1)-N(N+1)-S(S+1),$$

and

$$\Phi(NSJ) = (N-J+S)(N+J+S+1)(S+J-N+1)(N+J-S).$$

3. Hyperfine interaction terms

$$\langle N'K'SJ'IF'M_F'|H_{hfs}|NKSJIFM_F\rangle = \delta_{M_FM_F'}\delta_{FF'}\delta_{NN'}\delta_{KK'}(-1)^{N+S+J'}$$

$$\times(-1)^{J+I+F+1}[(2J'+1)(2J+1)S(S+1)(2S+1)I(I+1)(2I+1)]^{1/2}$$

$$\times\begin{Bmatrix} I & J' & F \\ J & I & 1 \end{Bmatrix}\begin{Bmatrix} S & J' & N \\ J & S & 1 \end{Bmatrix} a_F$$

$$-\delta_{M_FM_F'}\delta_{FF'}(30)^{1/2}g_Sg_I\beta\beta_I(-1)^{J+I+F}[I(I+1)(2I+1)S(S+1)(2S+1)]^{1/}$$

$$\times[(2J+1)(2J'+1)(2N+1)(2N'+1)]^{1/2}\begin{Bmatrix} I & J' & F \\ J & I & 1 \end{Bmatrix}\begin{Bmatrix} N' & N & 2 \\ S & S & 1 \\ J' & J & 1 \end{Bmatrix}$$

$$\times\sum_q(-1)^{N'-K'}\begin{pmatrix} N' & 2 & N \\ -K & q & K \end{pmatrix} T_q^2(C).$$

4. Numerical Calculations

Using the matrix elements given in sections 1 through 3, we wrote computer programs for numerical evaluations of the rotational energy levels and for least squares fittings. We usually set up Hamiltonian energy matrices on appropriate basis set functions, which have been given in each section, and numerically diagonalize the matrices to obtain the energy levels. The calculated energy levels are then fitted to the observed transition frequencies by the least-squares method.

Instead of expanding the Racah coefficients in eqs. (1-2-33) through (1-2-36), eqs. in Table I, and eq. (1-2-43), we wrote function subroutines which numerically calculate the 3J, 6J, and 9J symbols using equations (106.14), (108.10), and (108.12) in ref. (73). Numerical calculations of the Racah coefficients greatly simplified the programs, because, if they are expanded, many types of functions are required for each element of the matrix. For the hyperfine interactions, for example, the matrix is diagonal only in F, and $\Delta J = 0, \pm 1$ and $\Delta N = 0, \pm 1, \pm 2$ matrix elements are required for asymmetric top molecules.

For diatomic molecules, a Hamiltonian energy matrix as shown in Fig. 1 is constructed, where the matrix is divided into two blocks, one for $\Omega = 1/2$ and the other for $\Omega = 3/2$. Each block consists of 2I+1 elements since the matrix is diagonal

in F, and $\Delta J = \pm 1$ matrix elements are required for the hyperfine interactions. Some of the 2I+1 elements are missing for matrices with small F number because J should be greater than or eaqual to Ω. Two types of matrices are constructed for a given F value for positive and negative parities of the basis functions. The energy matrices are then diagonalized numerically, and fitted to the observed values by a least-squares fitting. These procedures are well known and firmly established, and are not explained here.

Hamiltonian energy matrices for asymmetric top molecules become much larger in dimension and more complicated. Fig. 2 illustrates a matrix for I = 1/2. Here, also the matrices are diagonal in F, and since the case (b) coupling scheme is used, not only $\Delta J = 0, \pm 1$ but also $\Delta N = 0, \pm 1, \pm 2$ matrix elements should be considered. Each subblock should contain hyperfine matrix elements as shown in the figure. Matrix elements for rotation and the spin-rotation interaction have non-zero elements where designated in the figure. Each diagonal subblock is diagonal in N and consists of different K ($K \leq N$) elements, which corresponds to the Hamiltonian matrix for usual singlet molecules. For usual singlet molecules, however, each matrix consists only of odd K or even K, because rotational Hamiltonian has matrix elements only $\Delta K = 0, \pm 2$ (, ± 4 ... in some cases). This is also the case for e.g. molecules with C_{2v} symmetry, where no $\Delta K = \pm 1$ matrix elements

Ω =	1/2	1/2	3/2	3/2
J =	F+1/2	F-1/2	F+1/2	F-1/2
	ROT SO HF	HF	SO HF	HF
		ROT SO HF	HF	SO HF
			ROT SO HF	HF
				ROT SO HF

Fig. 1. Hamiltonian energy matrix for $^2\Pi$ molecules with I = 1/2.

N =	F-1	F	F	F+1
J =	F-1/2	F-1/2	F+1/2	F+1/2
	ROT SR HF	SR	HF	HF
		ROT SR HF	HF	HF
			ROT SR HF	SR HF
				ROT SR HF

Fig. 2. Hamiltonian energy matrix for asymmetric top molecules with S = 1/2 and I = 1/2.

exists. For molecules with C_s symmetry, e.g. bent XYZ type molecules, there are $\Delta K = \pm 1$ matrix elements arising from the spin-rotation interaction and the hyperfine interaction. Consequently, each subblock is twice as large as that of ordinary molecules. So called Wang transformation (74), viz.

$$S_{NKM\gamma} = 2^{-1/2}[\ \psi_{NKM} + (-1)^{\gamma}\psi_{N-KM}\ ], \quad \text{for } K \neq 0$$

and

$$S_{N0M0} = \psi_{N0M}\ , \quad \text{for } K = 0 \qquad (1\text{-}2\text{-}45)$$

are performed on the original basis functions, so that each energy matrix is divided into two different matrices for a given F value. Thus, the dimension of the energy matrix for a given F value becomes 4F+2 for I = 1/2 molecules with doublet electronic state and C_s symmetry, which is the case for FSO and HSO.

For molecules with I = 1 or larger, larger matrices are required, e.g. 6F+6 for I = 1. We wrote two different programs for I = 1/2 species and I = 1 species. The former one has been used for FSO and HSO, and the latter for DSO. For the analysis of e.g. ClSO (I = 3/2), the program should be extended to handle larger energy matrices, which is now in progress.

Once the Hamiltonian energy matrix is constructed, other processes are the same as that of diatomic molecules mentioned before or ordinary asymmetric rotor molecules.

As will be explained later, for the analysis of the Stark effect of the FSO radical, another program was required where the Stark effect was evaluated numerically by matrix diagonlization. Since the Stark Hamiltonian has matrix elements, $\Delta F = 0, \pm 1$, we combined matrices in Fig. 2 together to construct larger matrices as shown in Fig. 3, and diagonalized them to calculate Stark shifted transition frequencies. Because of the memory size and the computation time, the matrix was truncated at $F = 3$.

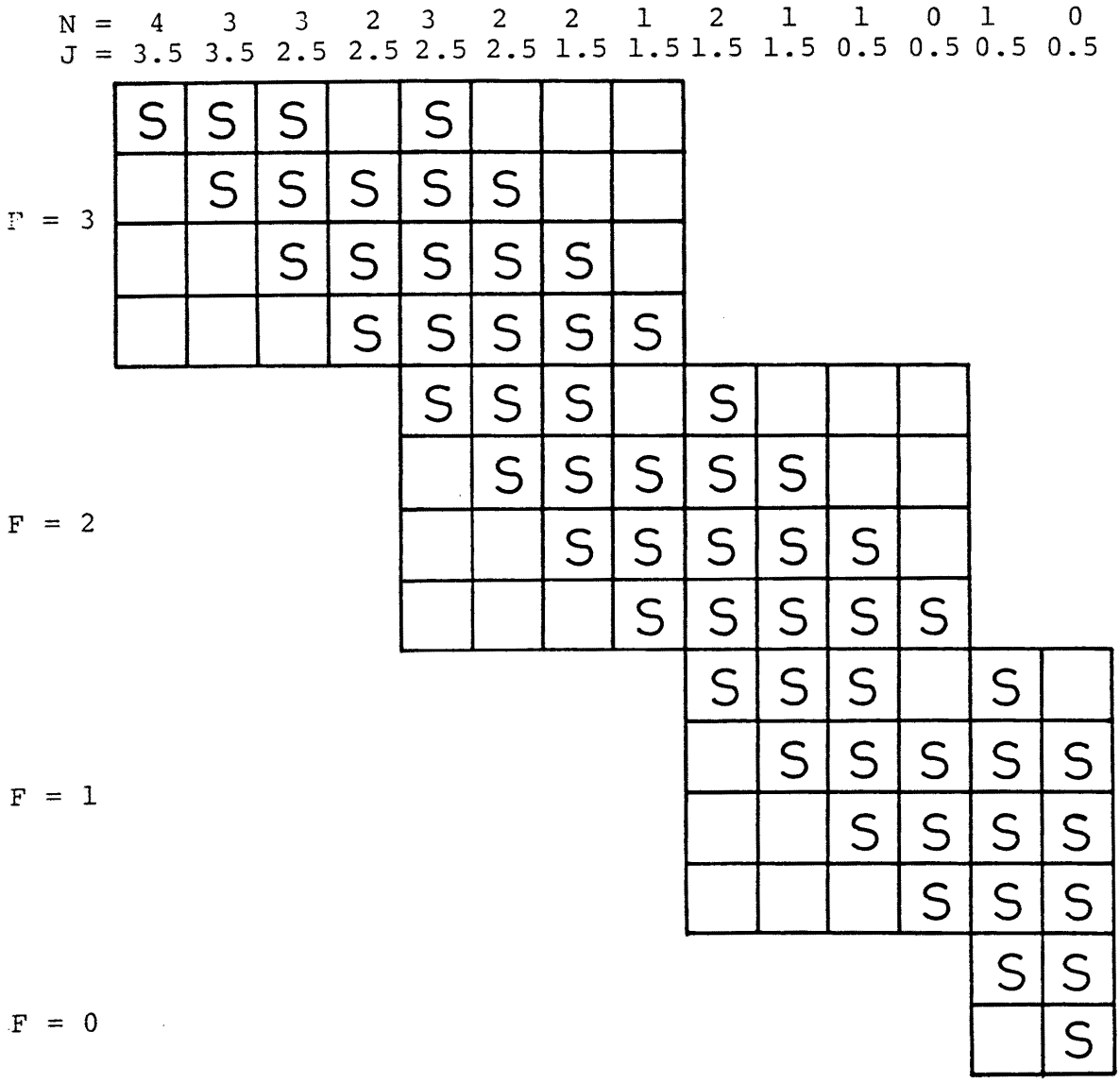

Fig. 3. Hamiltonian energy matrix for calculating the Stark effect with S = 1/2, I = 1/2, M_F = 0. The energy matrix is truncated at F = 3, so that calculated energy levels with F < 3 are accurate enough. Each submatrix is twice as large as in Fig. 2, and the K selection rule and the parity selection rule obey a and b type selection rules.

Chapter III. Experimetal

1. Stark spectrometer

Experimental set up of the Stark spectrometer is essentially the same as used widely in spectroscopy of stable molecules except the design of the absorption cell (75). A block diagram of the spectrometer used in the present study is shown in Fig. 1. 100 kHz square wave modulation field up to 1000 V_{pp} is applied for most cases. Sine wave modulation with D. C. electric field superimposed is used when dipole moments are measured. A series of OKI klystrons are used as microwave sources. They are phase-locked to a harmonic of a Varian X-13 klystron by a Microwave Systems PLS-60 with 1N26 crystal as a mixer. The frequency of the X-13 is measured by a YHP 5340A microwave counter. Although no wavemeter have been used for the measurement of the frequencies of the mm-wave klystrons, it is not difficult to determine the order of a harmonic of X-13. The X-13 klystron, when immensed in an oil bath, is stable to about 10 kHz without any stabilization, as is readily used for spectral searches over a wide frequency region. When accurate measurements of the frequencies of transitions are required, the X-13 klystron is further phase-locked to a temperature stabilized crystal oscillator by using a Microwave Systems MOS-5. The frequency of the crystal can be varied up to 0.1 % by feeding a D. C. voltage of 0 - 10 V to a variable capacitor in MOS-5. However, because the frequency of the

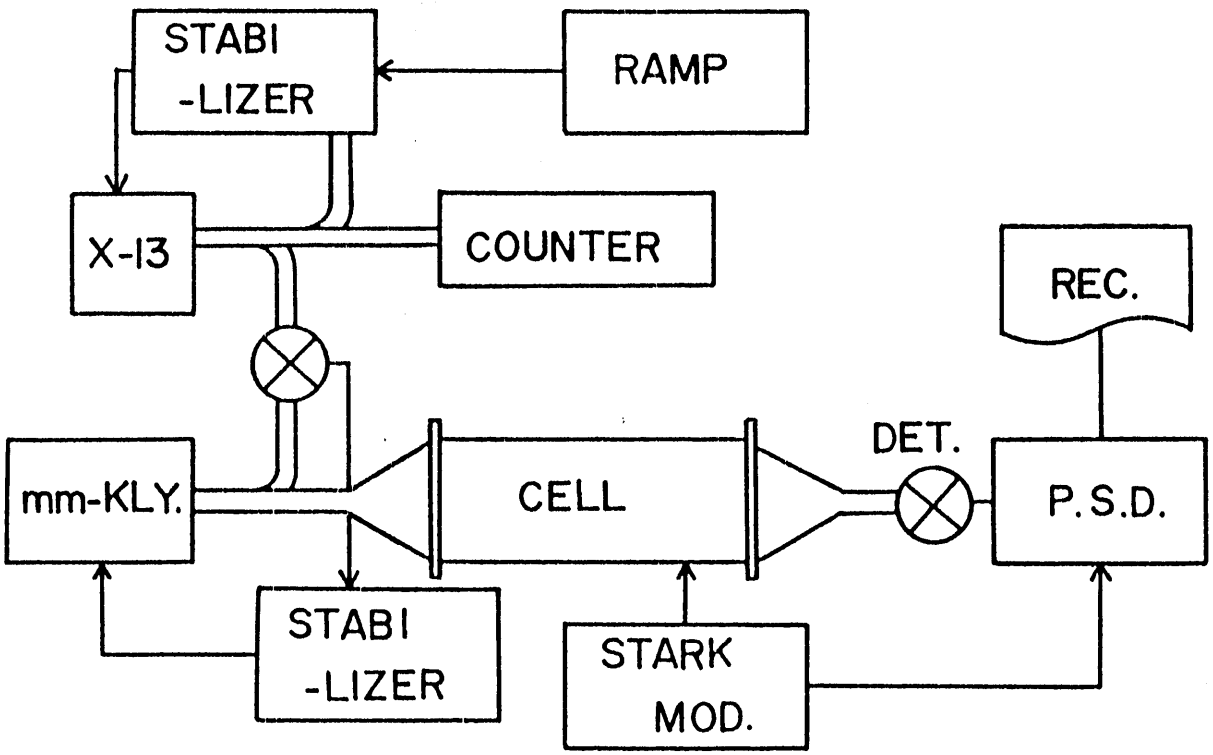

Fig. 1. Block diagram of the Stark spectrometer

crystal oscillator was found to change nonlinearly with the tuning voltage, a circuit as shown in Fig. 2 is added to compensate for the nonlinearity. Usually an output of a ramp generator, the circuit of which is also shown in the figure, is connected to the compensation circuit. The ramp generator enabled us to use a slow scan required for the accurate measurements of line frequencies. If higher sensitivity is required, an output of a digital to analog convertor in the minicomputer system, which is explained in detail later in a separate section, is connected to the input of the compensation circuit. In this case the frequency of the source klystron is controlled by the computer, and signal averaging is performed by the computer.

In the frequency regions below 70 GHz, a 1N53C diode is used as a detector. In the region from 70 to 100 GHz, a Hitachi GaAs shottky barrier diode W3420A is used, and above 100 GHz, GaAs diode T3420A is used.

The design of the absorption cell is shown in Fig. 3, where the Stark electrodes are made of gold-plated brass parallel plates with a spacing of 10 mm. The plates are 40 mm wide and 3 mm in thickness, and are installed in a Pyrex glass tube 55 mm in inner diameter and 400 mm in length. These plates are supported by teflon blocks. At each end of the cell, a mica plate is attached to keep vacuum sealing

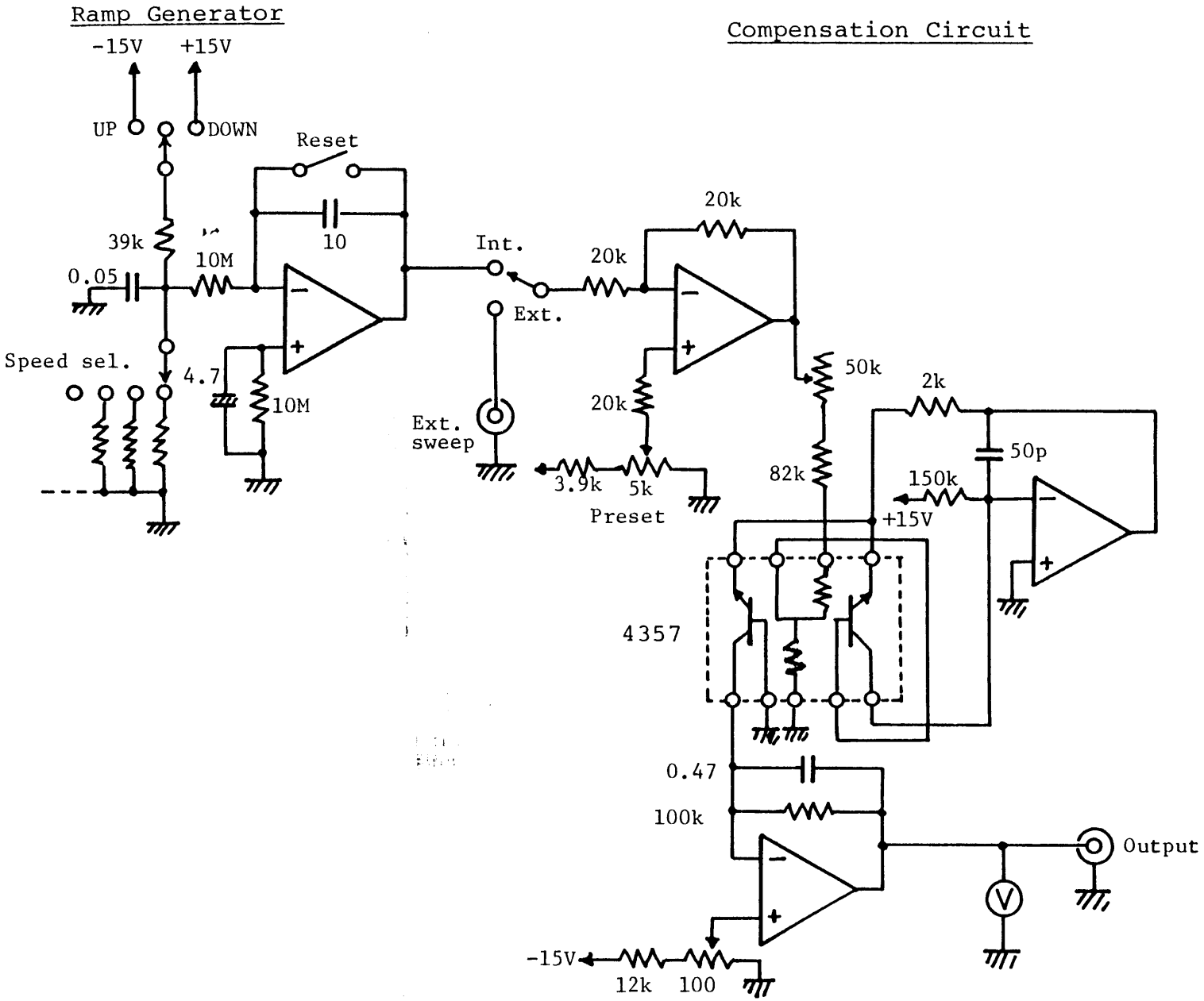

Fig. 2. Sweep and compensation circuit for MOS-5 crystal oscillator. The compensation circuit consists of an anti-Log circuit.

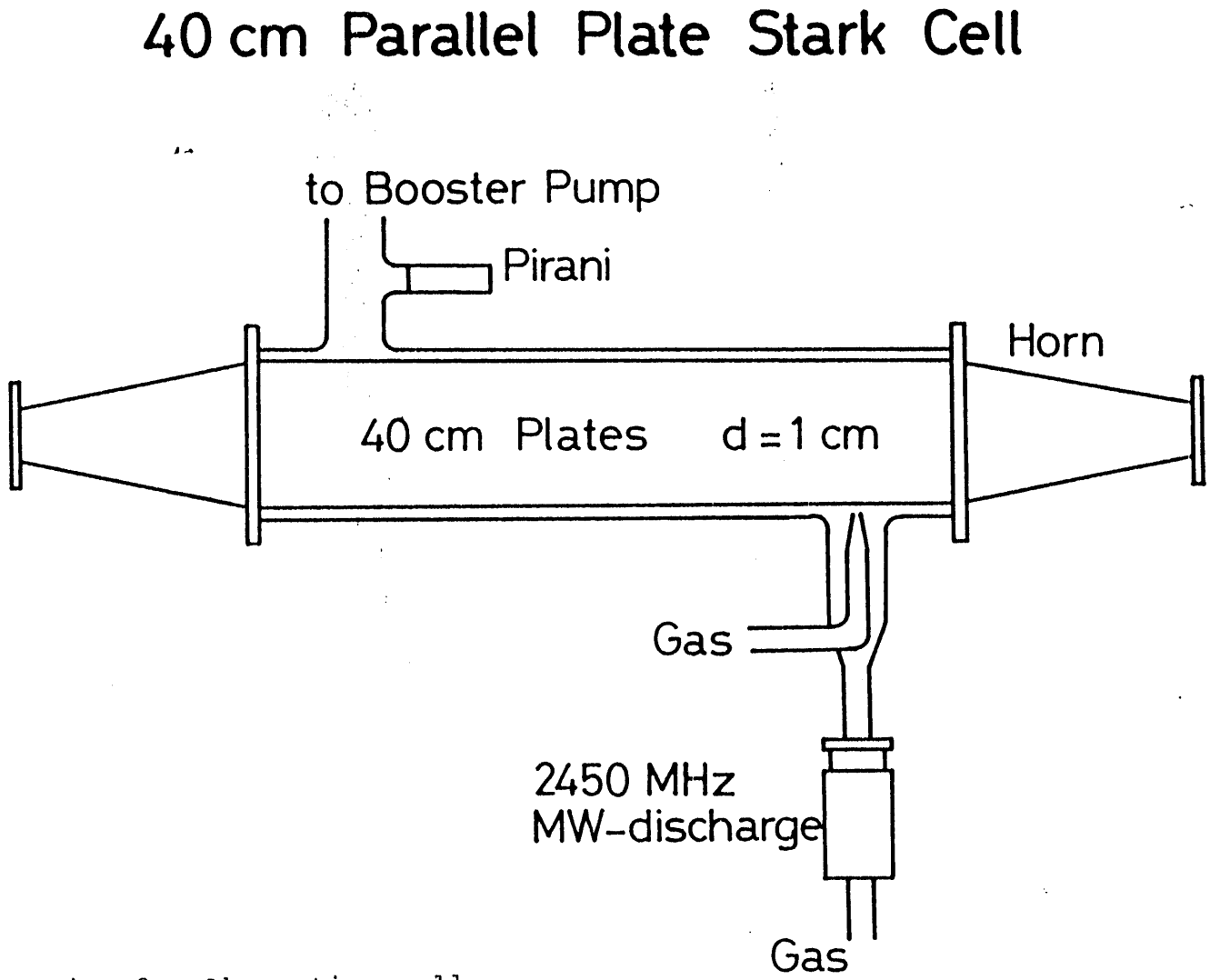

Fig. 3. Absorption cell.

and a horn which interfaces the K-band waveguide to the parallel plates is also installed.

The cell is evacuated by a mechanical booster pump (1800 liters/min.) followed by two liqid nitrogen traps and a rotary pump. Details of the gas inlet is shown in Fig. 4, where 2450 MHz microwave discharge products are reacted with another gas at the mixing point near the inlet. Because the linear velocity in the cell is estimated to be several meters/sec., species of e.g. 10 msec lifetime can live for several cm in the cell. The 2450 MHz microwave is obtained from a magnetron which was taken off from a commercial microwave oven with its power supply circuits and other components.

Because lines of paramagnetic species are affected by the earth's magnetic field ($\sim$0.5 Gauss.), two coils are wound on the cell, one along the cell which is placed north to south and compensates the horizontal field, and the other perpendicular to the ground to compensate the vertical field. The currents fed to the coils are adjusted to make linewidth narrower and line intensity stronger. The coil along the cell is also used in picking out paramagnetic lines from among diamagnetic lines; a current up to 10 A supplied to the coil produces a few ten of Gauss in the cell.

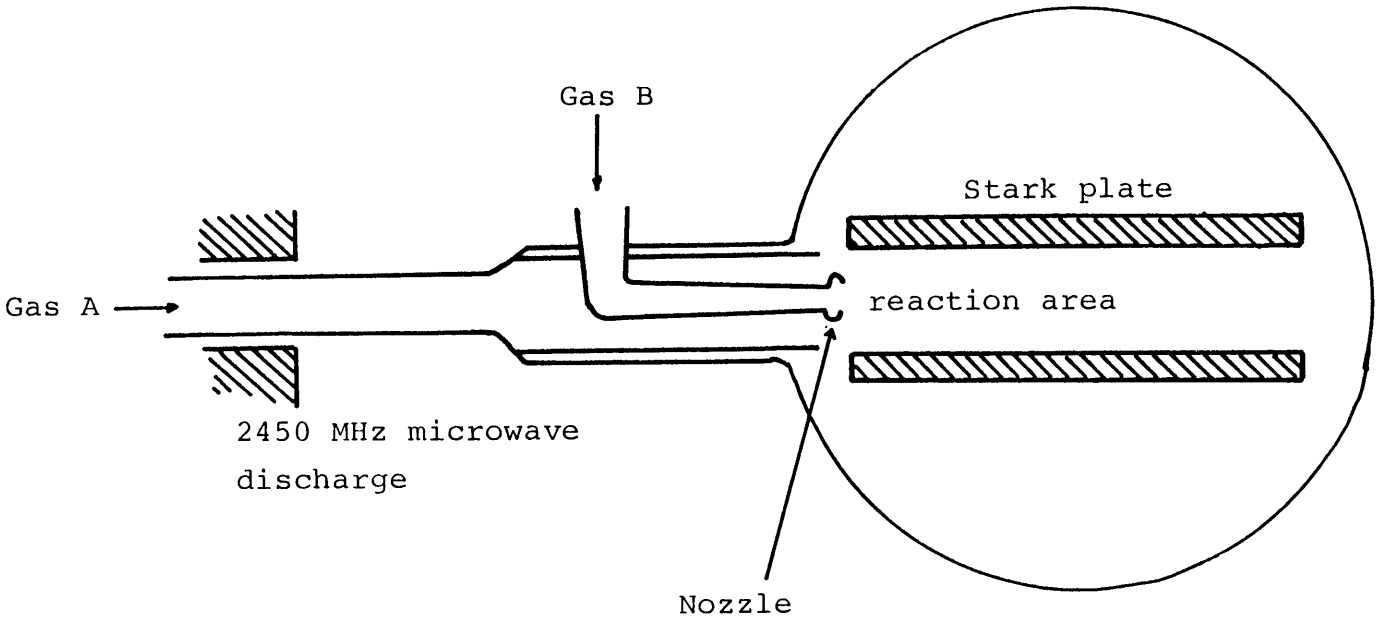

Fig. 4. Cross section of the Stark cell. Microwave discharge products of gas A are reacted with gas B between the Stark electrodes.

2. Source modulation spectrometer

A block diagram of the source modulation spectrometer is shown in Fig. 5. The same OKI klystrons are used as microwave sources. However, they are operated at free running conditions, since it was not easy to phase-lock frequency modulated microwaves. The Varian X-13 klystron, which is phase-lock stabilized by MOS-5, is also used as a frequency standard. The frequency of the X-13 klystron is monitored by the YHP 5340A microwave counter. Beat notes between the source klystron and a harmonic of the X-13 klystron generated by a 1N26 or 1N78 mixer diode are detected by an all-wave receiver JRC NRD-10.

The modulation waveform consists of two identical square waves of 50 kHz with a phase-difference of $\pi/2$ (see Fig. 6) (76), which is applied to the reflector circuit of the klystron power supply. Fig. 7 shows the modulator circuit which generates the required waveform. In Fig. 8 is shown the circuit around the klystron, in which the point where the modulation signal is applied is designated. Rectified microwave signals are demodulated by a phse-sensitive detector (PAR 124A) operated at 100 kHz. A demodulated signal such as shown in Fig. 6 is obtained. This modulation waveform gives second derivative waveforms for broad variations of the microwave power, whereas narrow absorption signals are affected only slightly. Thus, undesirable baseline variations, which limit

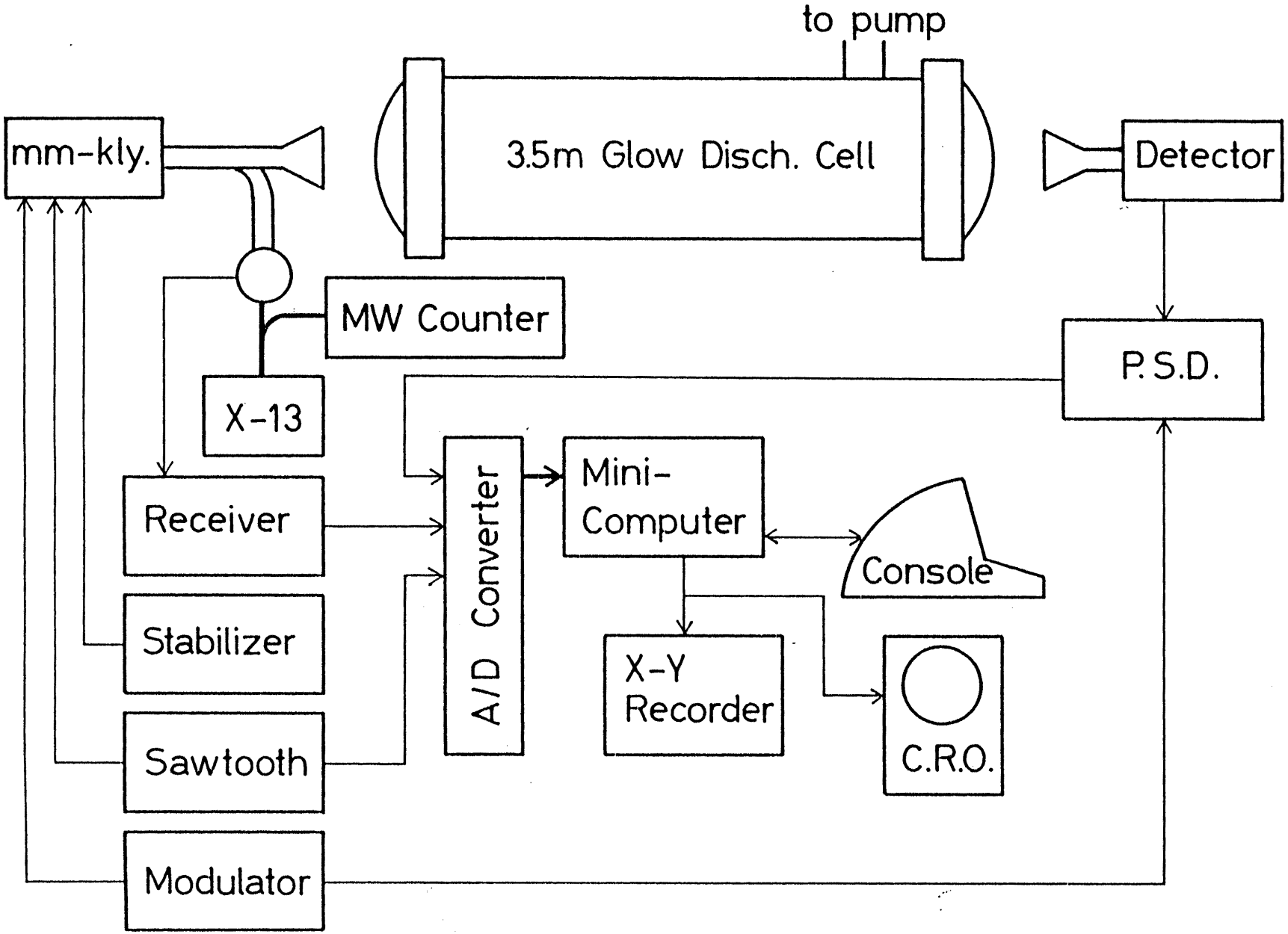

Fig. 5. Block diagram of the source modulation spectrometer

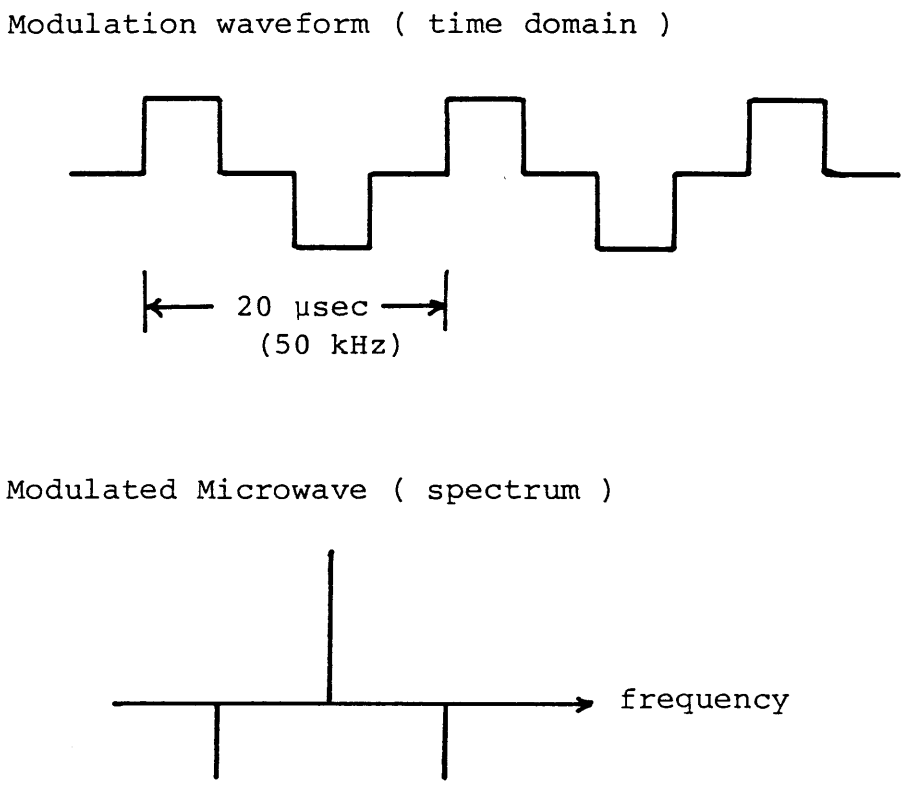

Fig. 6. Modulation waveform and demodulated signal.

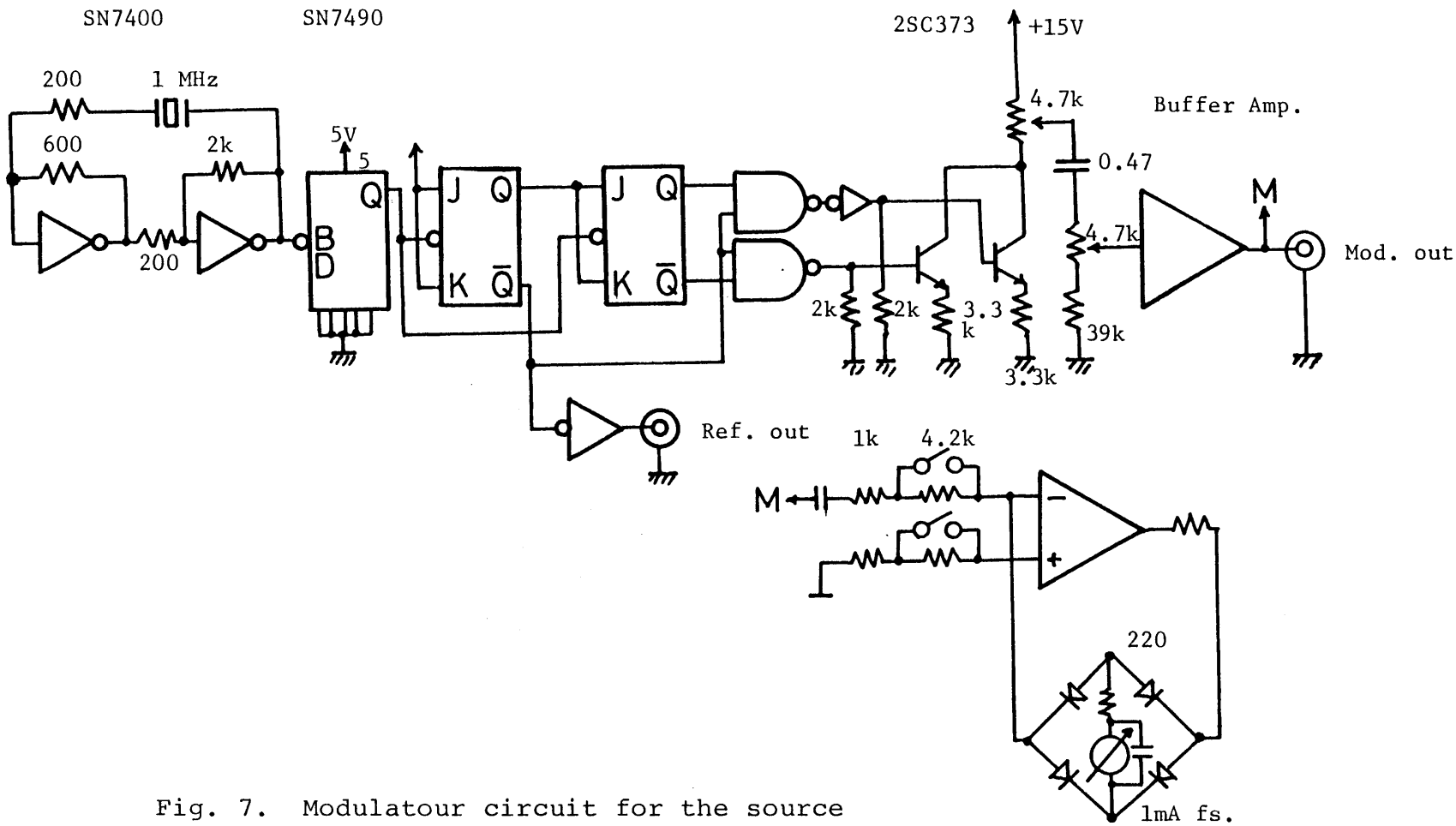

Fig. 7. Modulatour circuit for the source modulation spectrometer.

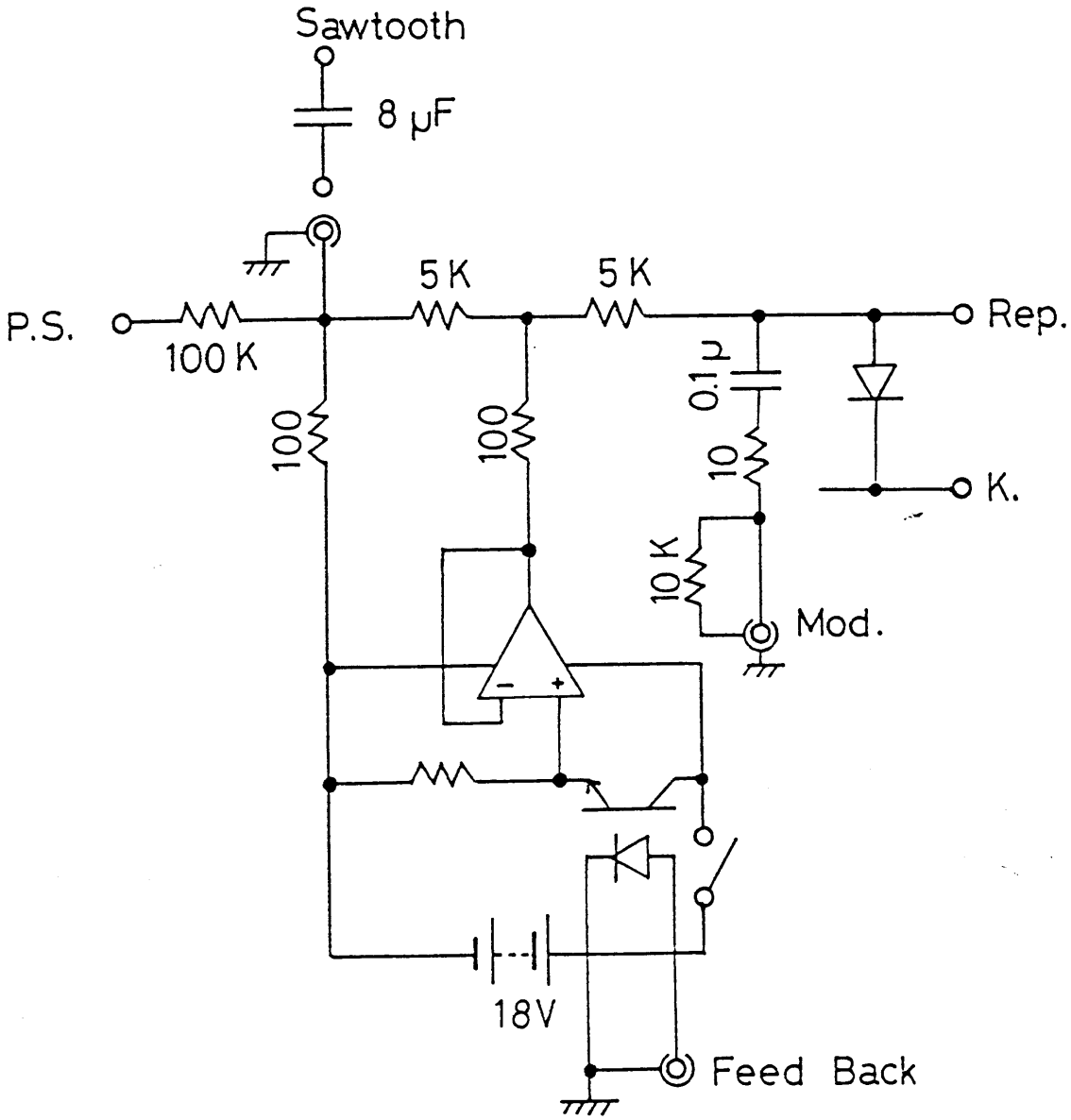

Fig. 8. Circuit in the klystron mount

the sensitivity of the source modulation spectrometer, are suppressed to a tolerable amount. However, for the source modulation method to be used widely, some furthur consideration is required (77, 78).

The absorption cell is made of a Pyrex glass tube 350 cm in total length and 15 cm in inner diameter, which is designed after Woods (44). The cell is sealed with a teflon lens at each end, which is used to collimate and focus the microwave power through the cell to the detector. Waveguide horns are used to feed the microwaves into the cell and collect them at the detector.

Stainless steel electrodes are installed coaxially inside the cell near both ends. They are supported by teflon pieces of 1 cm thick to keep them off from the inside wall of the cell. These supports are necessary to prevent arc discharges to take place through the cell walls, which cause serious noises to the electronics circuits. The separation between the two electrodes is 250 cm. Copper sheets with copper tubes are wrapped around the cell in the region between the electrodes, in order to cool the cell by liquid nitrogen flows through the tubes. The liquid nitrogen is fed from two liquid nitrogen vessels 100 liters in volume. The cell can be kept at nearly any temperature by adjusting the amount of the nitrogen flow, from minus several ten centigrade to almost the liquid nitrogen

temperature. In the same region, two coils are also wound as in the case for the parallel plate cell explained earlier to compensate the earth's magnetic field and to pick out paramagnetic lines.

The cell is pumped by a mechanical booster pump (3300 liters/min.) followed by two liquid nitrogen traps and a rotary pump. Although a larger booster pump is used for this cell than for the parallel plate cell, the pumping speed inside the cell is much slower because of the larger cell volume (about 62 liters).

A smaller cell with teflon lenses and discharge electrodes inside the cell was also constructed. The cell length is 1 m and the diameter of the glass tube used is 10 cm. This cell has higher pumping speed than the 3.5 m cell, and larger D. C. magnetic field, up to 50 Gauss, can be applied. The larger magnetic field was useful to assign the spectrum of SF radical in the $^2\Pi_{1/2}$ state; details will be given later.

The source modulation spectrometer works together with a YHP 2170A mini-computer system. The computer averages the PSD output to get as high sensitivity as possible, processes furthur the averaged signals, and stores the spectra on its disc storage. Details of the operation is given in the next section, separately.

3. Data processing for the source modulation spectrometer

In the mini-computer are installed 64 k words of memory, an 8 channel analog to digital convertor (A/D convertor), a 2 channel 8 bit digital to analog (D/A) convertor, a 2 channel 12 bit D/A convertor, and an IEEE-488 bus interface. A character display terminal which works as a console of the mini-computer, a 4.9 M byte disc storage, and a line printer are also attached (see Fig. 9).

The 8 bit D/A convertor is connected to a CRO to monitor the averaged spectra, where each channel drives X or Y axis of the CRO. The 12 bit D/A convertor, which has higher accuracy, drives an X-Y recorder to obtain hard-copies of the spectra. Input channels of the 8 channel A/D convertor are connected to the output of the PSD, shaped signals of the beat notes from the interpolation receiver, and a gate signal generated from the saw-tooth signal.

The operation of the signal averaging is shown in Fig. 10. The saw-tooth signal, the frequency of which is usually set to 2 to 5 Hz, is applied to the reflector circuit of the source klystron (see Fig. 8). The saw-tooth signal sweeps the klystron in a small frequency region, e.g. 2 to 10 MHz. As explained in Fig. 10, a gate opens with a fixed time delay from the start of a saw-tooth, and the mini-computer is initiated to digitize both the PSD output and the shaped output

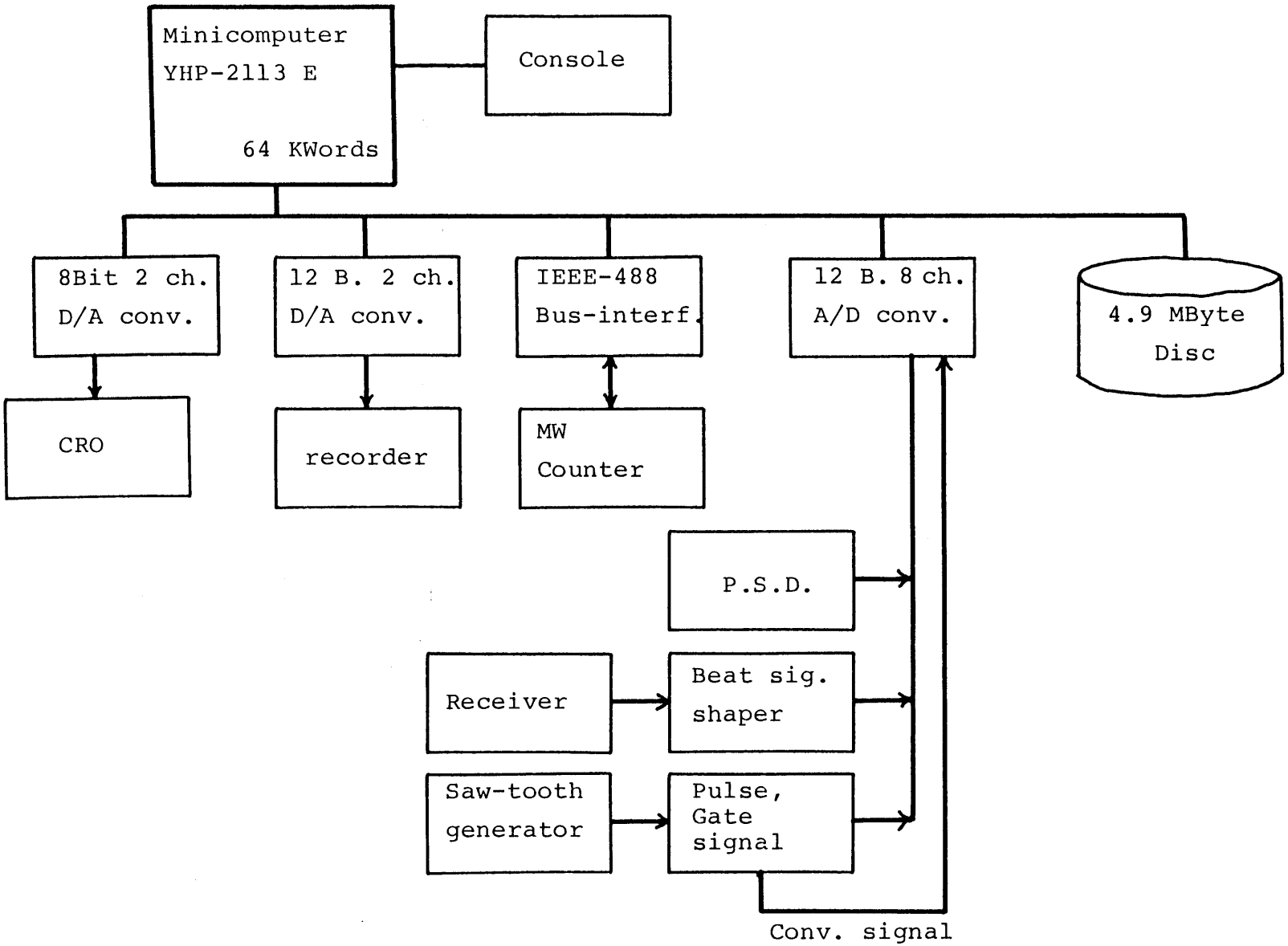

Fig. 9. Block diagram of the mini-computer system.

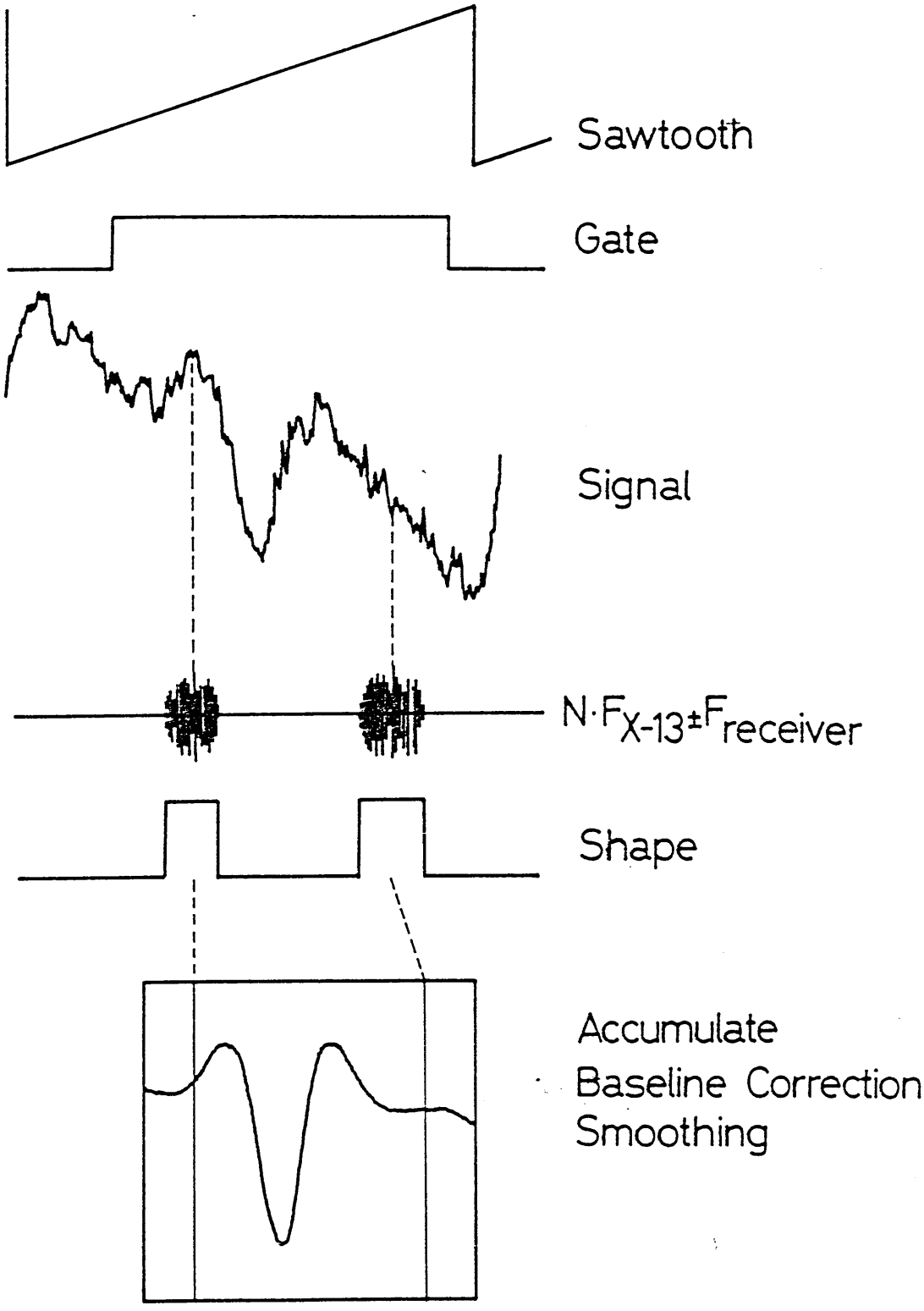

Fig. 10. Timing diagram of the data accumulation. Signal is accumulated with respect to the frequencies of the beat notes.

of the beat notes, simultaneously, through the A/D convertor. 1000 data points are digitized at uniform time intervals in one scan for both the signals. The gate signal and the beat notes are monitored on a CRO. The receiver dial is usually set to 0.5 - 3 MHz depending on the conditions or the purposes. The amplitude of the saw-tooth is adjusted so that both plus and minus beat notes are digitized in one scan. The computer finds the centers of the beat notes which are broadened by the frequency modulation, interpolates or extrapolates the frequency of each data point digitized, and accumulates the data to appropriate words in the memory. An array of 500 words is allocated for the accumulation, where the 50th and 450th words are assigned to the positions of the centers of the beat notes. This process is repeated for every scan. If one of the beat notes goes out of the range covered by the sweep, no data accumulation is performed and the computer waits until the beat notes come in the appropriate positions. A stabilizer circuit is attached to maintain the positions of the beat notes within the range. The stabilizer senses the position of the first beat note with respect to the rising edge of the gate signal, and feeds back an error signal to the reflector circuit. Fig. 11 shows a block diagram of the stabilizer and the timing generator, and a timing chart for the stabilization.

Thus, the signal averaging does not affected by slow

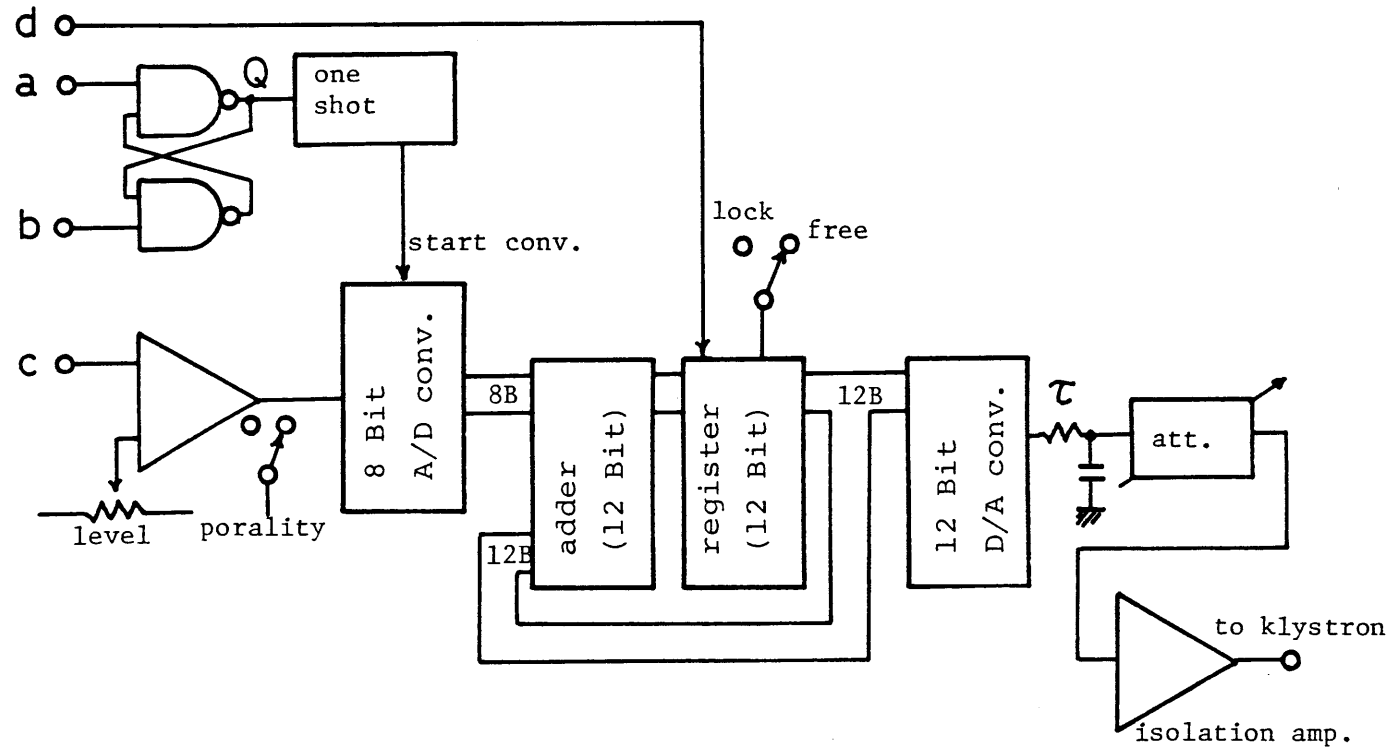

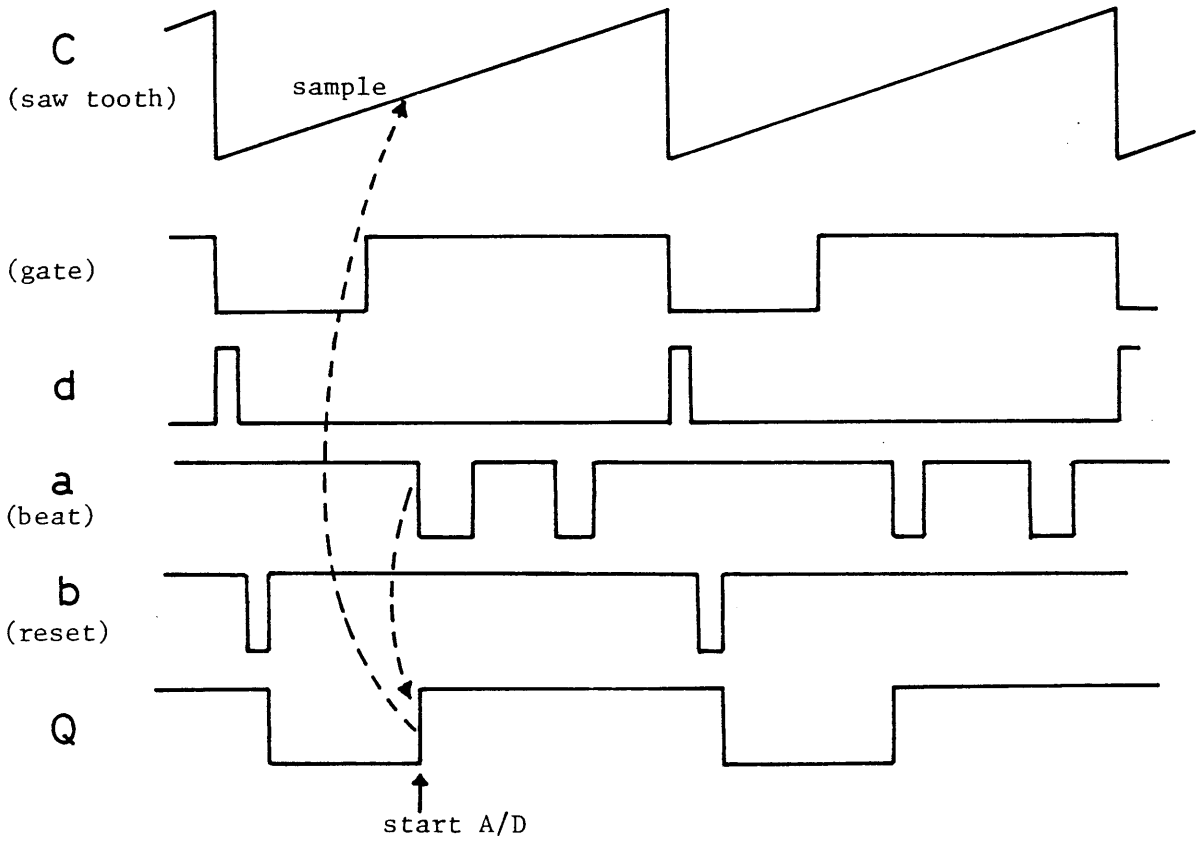

Fig. 11. Block diagram of the frequency stabilizer, and timing charts for the stabilization.

drift of the free running source klystron. In fact, this system enables us to accumulate signals even for longer than 30 minutes without broadening of absorption lines. Fast frequency fluctuations, however, are not reduced by this process, e.g. those due to hams from the power supply circuit or mechanical vibrations. To reduce such flactuations stable and low noise power supply circuit is required, and mechanical vibrations should be reduced by using a heavy and stable klystron mounting.

When the signal averaging process described above is completed, the averaged data are processed and displayed on the monitor CRO. The data processing consists of correction of the baseline distortions, smoothing of the data, and gain setting.

As mentioned earlier, because the baseline distortions of the spectra obtained by the source modulation method have limited the sensitivity of the spectrometer although the modulation waveform introduced here reduces them to some extent (79), following method is introduced to eliminate numerically the baseline distortions. At the first step, the averaged signal is fitted by a least-squares method to a polynomial function, where the fitting is performed to all data points irrespective of the existence of absorption lines. Then, the fitted polynomial function is evaluated and subtracted

from the original signal. Functions from linear to tenth order polynomial are selectable in the present system. The selection can be performed by monitoring the corrected spectrum.

The numerical smoothing is a well known procedure in the data processing to reduce noise levels, which is equivalent to a numerical convolution of the observed spectrum with a given filter function. Coefficients which correspond a least-squares fitting of the quadratic function to the observed data are used as a filter function (80). They are:

$$\bar{x}_k = \frac{1}{R_L} \sum_{k=-L}^{L} p_k x_k,$$

$$p_k = (3L^2+3L-1) - 5k^2,$$

$$R_L = (2L+1)(4L^2+4L-3)/3,$$

where x_k's are the original data, $\bar{x}_k$'s are the smoothed values, and 2L+1 is the total number of points used to smooth each data point of the data. Here, the number of points, 2L+1, can also be selected to obtain optimum noise suppression.

After these processes have completed, an arbitary gain factor is multiplied, and the result is displayed on the CRO. When one of the parameters for above processes is not adequate, the parameter can be easily changed, and a new result is seen on the CRO. Thus, the system allows us considerable freedom after the data averaging process has completed. This freedom reduces many tedious parameter settings before starting the data accumulation, such as proper gain setting, time constant setting, or critical adjustments of the microwave components

to reduce baseline distortions. The original data are stored with several experimental parameters on the disc storage. Hard-copies of the spectra are obtained on the X-Y recorder if desired.

The stored spectra are monitored on the CRO or plotted on the X-Y recorder at any time with another program, which runs independently of the data accumulation program. The program also reads the line frequencies of the observed lines. Line frequencies of the spectra on the disc storage are usually read after a series of experiments are finished. The frequency readout method adopted here is as follows. At first, we designate an approximate position of a line to be read. Then, the program finds the maximum and minimum points around the designated point. The line is sliced at six different levels as shown in Fig. 12, centers of the intersects are computed, the center positions are fitted to a linear function, and the intersect of the fitted line with the minimum level (peak of the line) is printed out as the line frequency. The slope and the difference of the determined frequency from the peak frequency are also printed out as a check of the quality of the frequency determination.

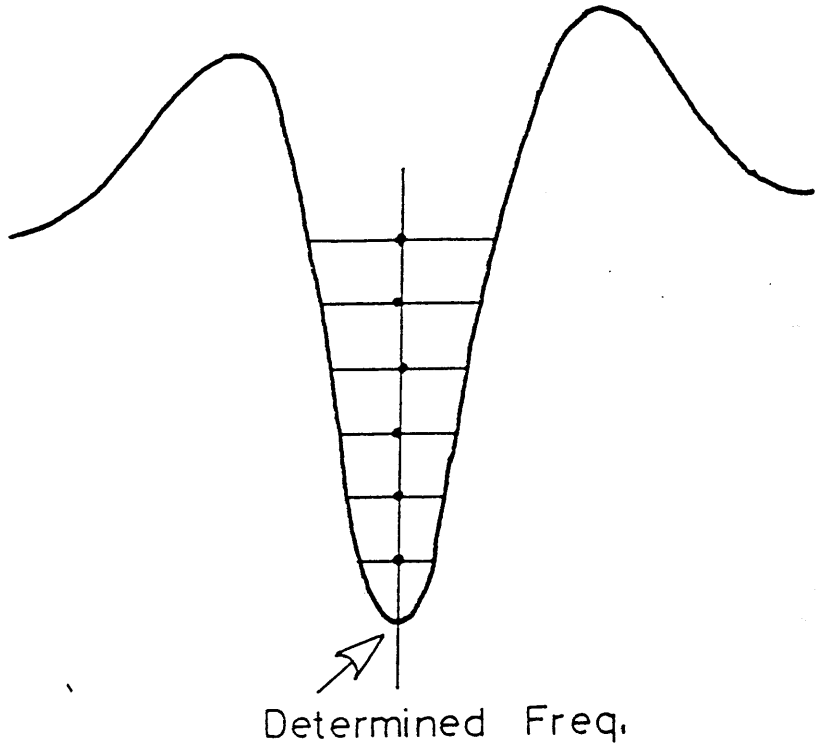

Fig. 12. Computer frequency read out is performed as shown in this figure.

4. Signal averaging for the Stark spectrometer

In most cases, the Stark spectrometer is used without the mini-computer system. However, when higer sensitivity is required, which is not attainable with the usual slow scan method, the computer can be used for long time signal averaging. We wrote a computer program which controls the data accumulation of the Stark modulated spectra, where we do not used the same high repetition rate scan with the free runing klystron. The source klystron is phase-lock stabilized as explained in section 2. The frequency of the klystron is controlled by the computer through MOS-5 and PLS-60. To determine the order of the harmonics of 15 MHz crystal oscillator in MOS-5, frequency of the X-13 klystron is monitored by the YHP 5340A microwave counter, and the output of the counter is connected to the computer via the IEEE-488 interface bus.

The output of the 12B D/A convertor is repetitively swept by the computer, and thus the frequency of the mm-klystron is swept. At the same time, the PSD output is digitized and accumulated. The repetition rate is about 0.25 Hz, so that only accumulation of e.g. 10 minutes or longer is effective for Stark spectra. The same smoothing routine is used in this program also to reduce noise levels, and the result is displayed on the CRO. An example of the averaged spectra is shown in the next section.

5. Performances of the spectrometers

To check the sensitivity of a constructed spectrometer has great importance to see possibility that a free radical to be studied is detectable or not. As for the Stark spectrometer, there are little to be mentioned because it was made mostly on well established techniques (12,75). In Fig. 13 are shown examples of the spectra of an isotope of OCS in natural abundance, where results obtained by usual slow scan method and by using computer averaging are compared. Here, the S/N improvement by computer averaging is mainly of longer observation time. In both cases, the S/N ratio is mainly determined by the detector noise. Sometimes, excess noises are observed, for example, those due to pick ups from high amplitude Stark modulation electric field, from 2450 MHz microwave discharges, or from improper setting of the time constant of the phase-lock loop. However they could be reduced by careful settings of the spectrometer.

As for the source modulation spectrometer, we had to be more careful because many new factors are introduced into this system; some results of the sensitivity tests are explained in detail here. Fig. 14 shows a result of the baseline distortion correction described in section 3, where the baseline distortions are completely removed by the process explained there. As seen in the figure a larger gain factor

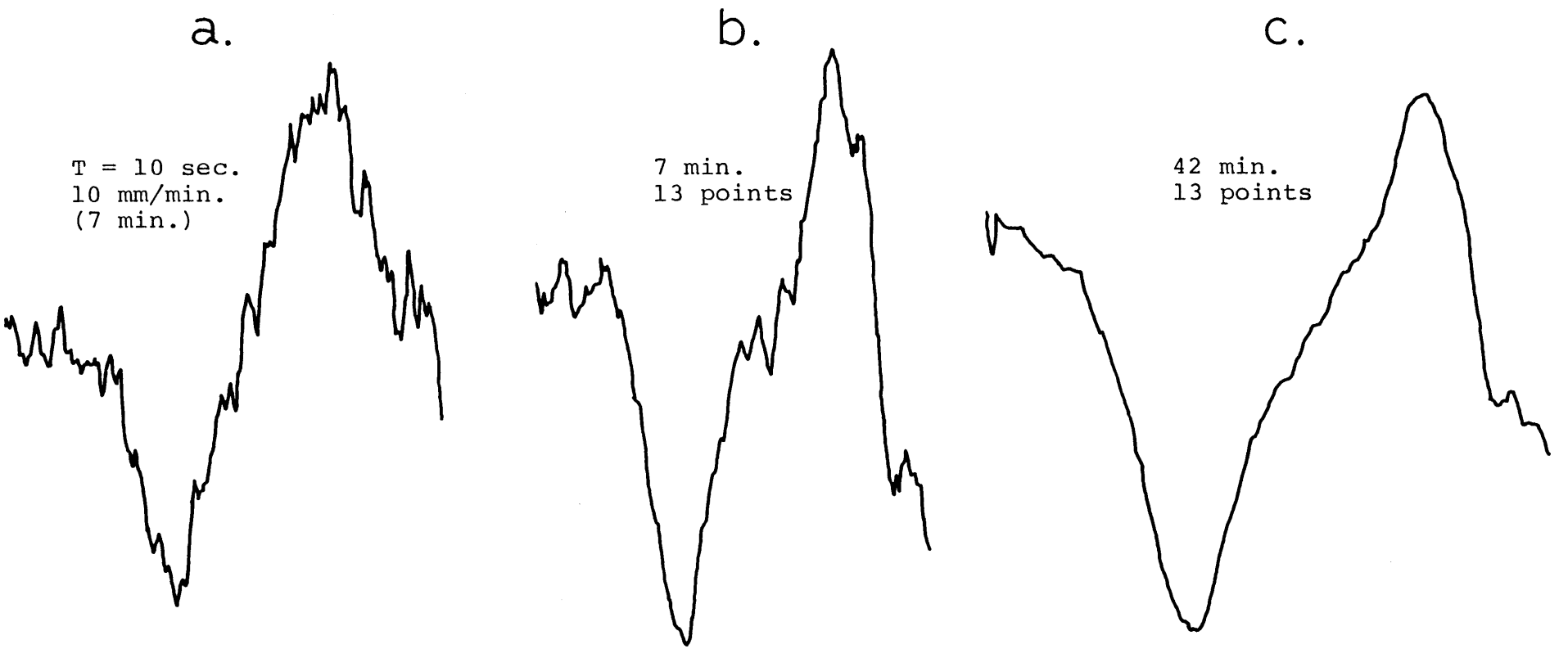

Fig. 13. The J = 1 - 0 transition of $^{18}OC^{34}S$ observed by the Stark spectrometer. a) was obtained by an ordinary slow scan method. b) and c) were obtained by the minicomputer averaging. Total observation times for the traces a) and b) were nearly the same (c.a. 7 min.), while c) is a result of about 42 min. integration. All the spectra were observed at room temperature.

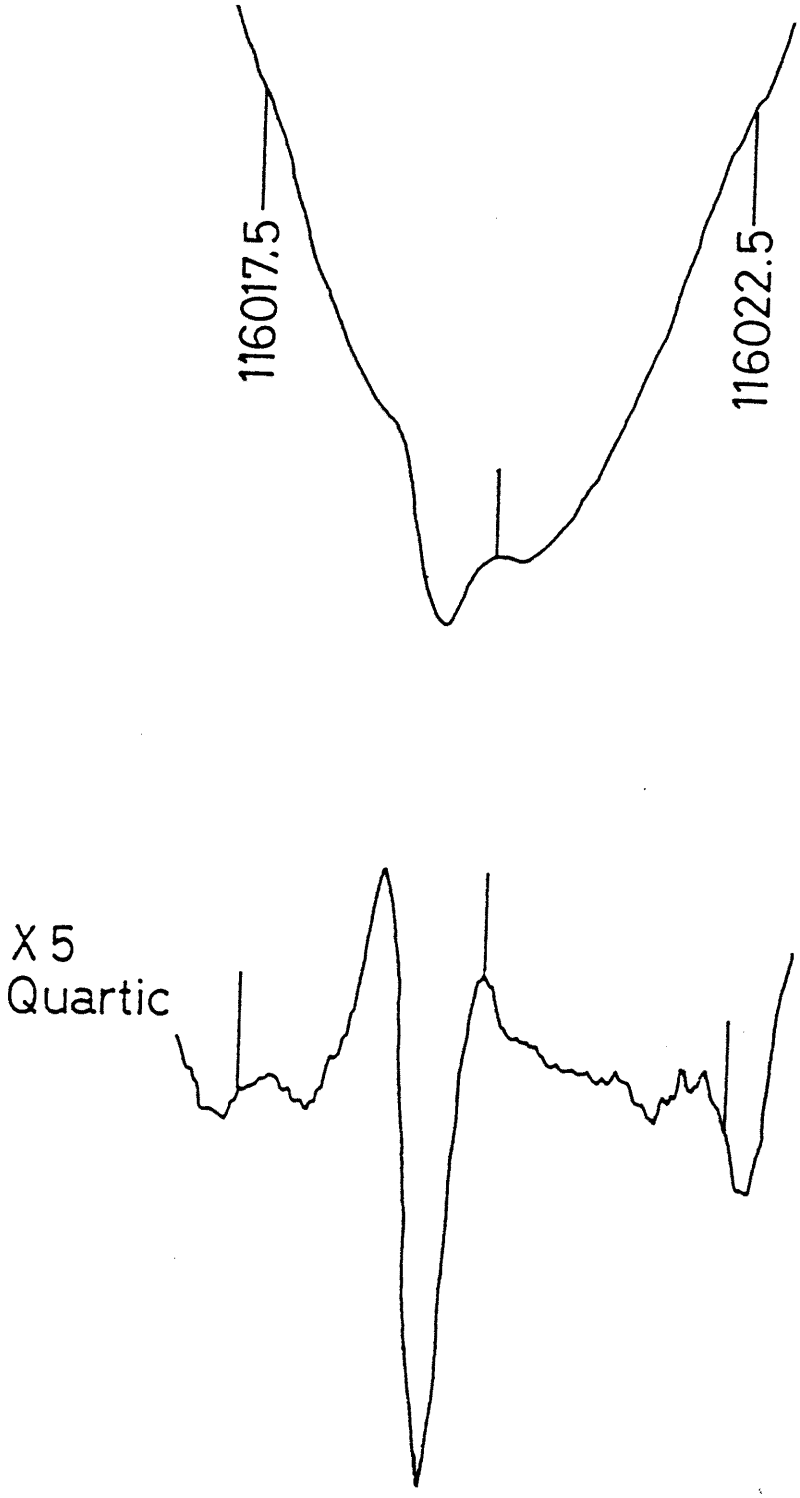

Fig. 14. These spectra illustrate the effect of the baseline correction. Upper trace is uncorrected and lower corrected by a quartic polynomial function.

is used for the corrected spectrum. Sometimes it introduces undesirable distortions to the corrected spectrum especially near the both ends of the observation region. However, it is not difficult to distinguish them with true lines by changing the order of a polynomial to be fitted. It is better to make another run for data accumulation by slightly changing the alignment of the microwave components to make completely sure.

For accurate measurement of the line frequencies, the receiver dial is usually set as low as possible, 1 MHz is a typical setting, so that baseline distortions affect little to the measurement. Linear or quadratic functions are enough for such cases when careful alignment of the microwave components are done. We confirmed that the correction introduces almost nothing bad to the quality of the frequency measurement. Higher order polynomial functions are useful for spectral searches, where a wider frequency region, e.g. 5 - 10 MHz, is observed in one scan.

Effects of smoothing are shown in Fig. 15. PSD time constant is set to be 1 msec or 3 msec depending on the width of a region covered by the sweep. Those time constants are small enough not to distort the observed lines. As seen in the figure, the smoothing affects little on the observed line-shape although the noise is reduced considerably. It should be noted that because the numerical smoothing is a symmetrical process without time lags, which are always observed for RC

time constant, no change of the center frequency due to this process is observed. This assures us of accurate measurements of frequencies of very weak lines.

Fig. 15 also illustrates a result of long time data integration. No linewidth broadening is observed, and the peak intensity is affected only slightly owing to the integration method described in section 3. The S/N ratio is improved by the factor expected, i. e. square root of the total integration time ratio. The concentration of the isotope $^{18}O^{13}C^{34}S$ in natural abundance is 10^{-6} of that of most abundant $^{16}O^{12}C^{32}S$. That means, in favourable cases, the spectrometer can detect less than ppm order of concentrations of species in a reaction system with respect to those of parent molecules. In other words, minimum detectable concentration is 10^{8} molecules/cm^{3} or less.

As to the transmission of the microwave through the cell, the 3.5 m free space cell is much better than the 40 cm Stark cell, because there is no metal conductors in the cell which cause losses and undesirable reflections. In fact, measurements become quite difficult above 130 GHz with the Stark cell, while the free space cell works very well above 180 GHz which is the highest frequency region attained by the OKI klystrons. Although there exist some frequency dependent variations of microwave powers due mainly to the reflections,

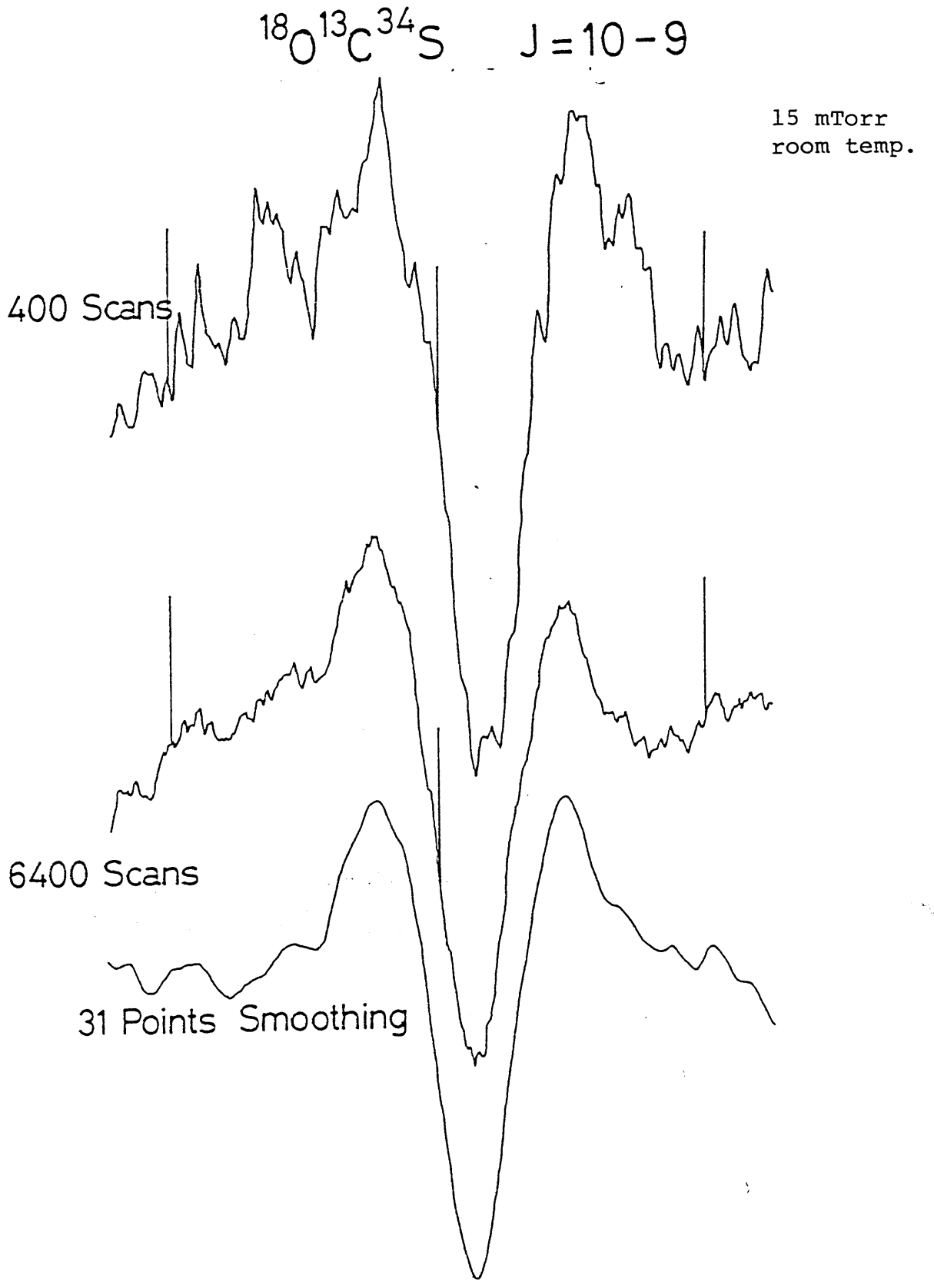

Fig. 15. Spectrum of OCS rare isotope. Lower two traces are results of c. a. 28 minutes accumulation. Lowest trace is smoothed with 31 points smoothing.

loose couplings between the microwave components and the cell assures us freedom for critical adjustments of the components, so that we can make the region to be observed not to be suffered from such reflections.

Part II. Results of individual species
General discussions

Chapter I. Microwave spectroscopy of the SF radical

1. Introduction

As has been reviewed in Part I, Chapter II, observations of both $^2\Pi_{1/2}$ and $^2\Pi_{3/2}$ states are indespensable to completely characterize a molecule in a $^2\Pi$ electronic state. The SF radical was first identified in gas phase by Carrington et al. (81) with the EPR method. Usually the EPR method can detect species only in a $^2\Pi_{3/2}$ state, since the method uses external magnetic field to bring transitions into resonances with a fixed frequency microwave field. They concluded that the ground electronic state of this radical was an inverted $^2\Pi$, and determined values for the spin-orbit interaction constant, an effective rotational constant for the $^2\Pi_{3/2}$ state, and an axial component of the fluorine hyperfine interaction constant. Lonardo et al. (82) observed its electronic transitions ($^2\Pi \leftarrow {}^2\Pi$) in the region 4000 - 3300 Å. They confirmed the spin-orbit interaction constant and the rotational constant Carrington et al. had obtained. However, because the spectrum was not strong enough nor had sufficient resolution, no furthur information on the ground electronic state for this radical had been obtained. Amano and Hirota (13) observed its zero-field rotational transitions in the $^2\Pi_{3/2}$ state by microwave spectroscopy around 83 GHz. They obtained improved values for the effective rotational

constant and the hyperfine interaction constant. They also tried to observe the spectrum in the $^2\Pi_{1/2}$ state. However, they were not able to assign the spectrum among many interfering lines, mainly of SF_2 (13). So far, therefore, nothing had been known for the spectrum in the $^2\Pi_{1/2}$ state. Only a few effective constants in the $^2\Pi_{3/2}$ state had been known for the ground state of this radical.

There had been some difficulties for the observation of the spectrum in the $^2\Pi_{1/2}$ state when compared with the observation in the $^2\Pi_{3/2}$ state. Intensity of the spectrum in the $^2\Pi_{1/2}$ state is about 1/16 of that of the $^2\Pi_{3/2}$ state, because the $^2\Pi_{1/2}$ state lies about 400 cm^{-1} above the ground $^2\Pi_{3/2}$ state and the spectrum is expected to split into two by the Λ-doubling. Another difficulty is that the Stark effect for the $^2\Pi_{1/2}$ state is second order, while that of the $^2\Pi_{3/2}$ state is first order; large Stark field required for the observation of the spectrum in the $^2\Pi_{1/2}$ state also considerably modulates absorption lines of other undesirable species. For example, absorption lines of SF_2, which is also efficiently generated by the same reaction system (83), interfere with the observation of the spectrum in the $^2\Pi_{1/2}$ state, whereas they interfere little when observing the spectrum in the $^2\Pi_{3/2}$ state because of low Stark fields required. Furthermore, it had not been easy to distinguish the $^2\Pi_{1/2}$ lines of SF by the Zeeman effect, because its magnetic moment is nearly

cancelled in the $^2\Pi_{1/2}$ state.

In our present study, however, we utilized a small Zeeman effect in the $^2\Pi_{1/2}$ state which is induced by the spin-uncoupling with the $^2\Pi_{3/2}$ state in order to pick up $^2\Pi_{1/2}$ lines. The use of small Zeeman effect was suggested by the observation of CF spectrum in the $^2\Pi_{1/2}$ state by diode laser spectroscopy which utilized Zeeman modulation (107). Although the spin-uncoupling effect is quite small for this radical, which is close to pure Hund's case (a) coupling ($\lambda = A_0/B_0 \sim -700$) as will given in the next section, we were able to assign the spectrum by using the source modulation spectrometer. At the same time, measurements in the $^2\Pi_{3/2}$ state, which had already reported (13), were extended to higher J transitions. Simultaneous analysis for both the states enabled us to determine detailed ground state molecular constants of the SF radical.

2. Zeeman effect in the $^2\Pi_{1/2}$ state

The magnetic moment for $^2\Pi$ molecules in the intermidiate case (ab) is expressed as (3)*,

$$g_J = -\frac{1}{J(J+1)}\{ g_L + \frac{g_S}{4} \pm \frac{(g_L+g_S)(\lambda-2) + g_S(J-1/2)(J+3/2)}{2[4(J+1/2)^2 + \lambda(\lambda-4)]^{1/2}} \}, \qquad (2\text{-}1\text{-}1)$$

where $\lambda = A_0/B_0$. The positive sign in the above equation applies to the $^2\Pi_{3/2}$ state of the inverted doublets and the negative sign to the $^2\Pi_{1/2}$ state, as is the case for the SF radical. If we neglect smaller terms, the above equation is simplified to be, for the $^2\Pi_{1/2}$ state,

$$g_J = -\frac{1}{J(J+1)} \frac{(J-1/2)(J+3/2)}{\lambda - 2} \quad . \qquad (2\text{-}1\text{-}2)$$

Here, λ is about -700 for the SF radical. Therefore, for example, $g_J = 0.0026$ ($J = 5/2$), which corresponds to a splitting of c.a. 0.45 MHz at 60 Gauss. This splitting is large enough to discriminate lines of SF in the $^2\Pi_{1/2}$ state among many diamagnetic lines, if we use the source modulation spectrometer explained in Part I, Chapter III.

* In fact, we must discuss by g_F instead of g_J for SF. However, the difference is not essential for the above discussion.

3. Experimental

The microwave spectrometer used in this study was the source modulation spectrometer described in Part I, Chapter III. The glow discharge cell 1 m in length was used, since larger magnetic field was obtained with this cell than the 3.5 m cell. The cell was made of a pyrex glass tube 100 mm in diameter and 1 m in length, onto which 1 mm resine-coated cupper wire was wound to apply a magnetic field. We were able to apply D. C. current up to 5.5 A with a 35 V stabilized power supply. The current produced a magnetic field c.a. 60 Gauss (calculated field strength is about 70 Gauss). As explained in the previous section, the magnetic field is large enough to pick up lines of SF in the $^2\Pi_{1/2}$ state. The cell was pumped by a mechanical booster pump 67 liter/sec, followed by two liquid nitrogen traps and a rotary pump.

The spectrum of SF was observed in a glow discharge in mixtures of OCS and CF_4 with pressures of 10 mTorr and 35 mTorr, respectively, measured by a thermocouple gauge near the outlet. Optimum D. C. current was about 10 mA. The conditions were optimized by monitoring the spectrum in the $^2\Pi_{3/2}$ state (13).

We scanned about 500 MHz with and/or without the magnetic field, since the Λ-doubling constant had not been known at all. Finally we picked up lines as shown in Fig. 1, where the upper trace was obtained without the external magnetic field and the lower with the magnetic field of 60 Gauss along

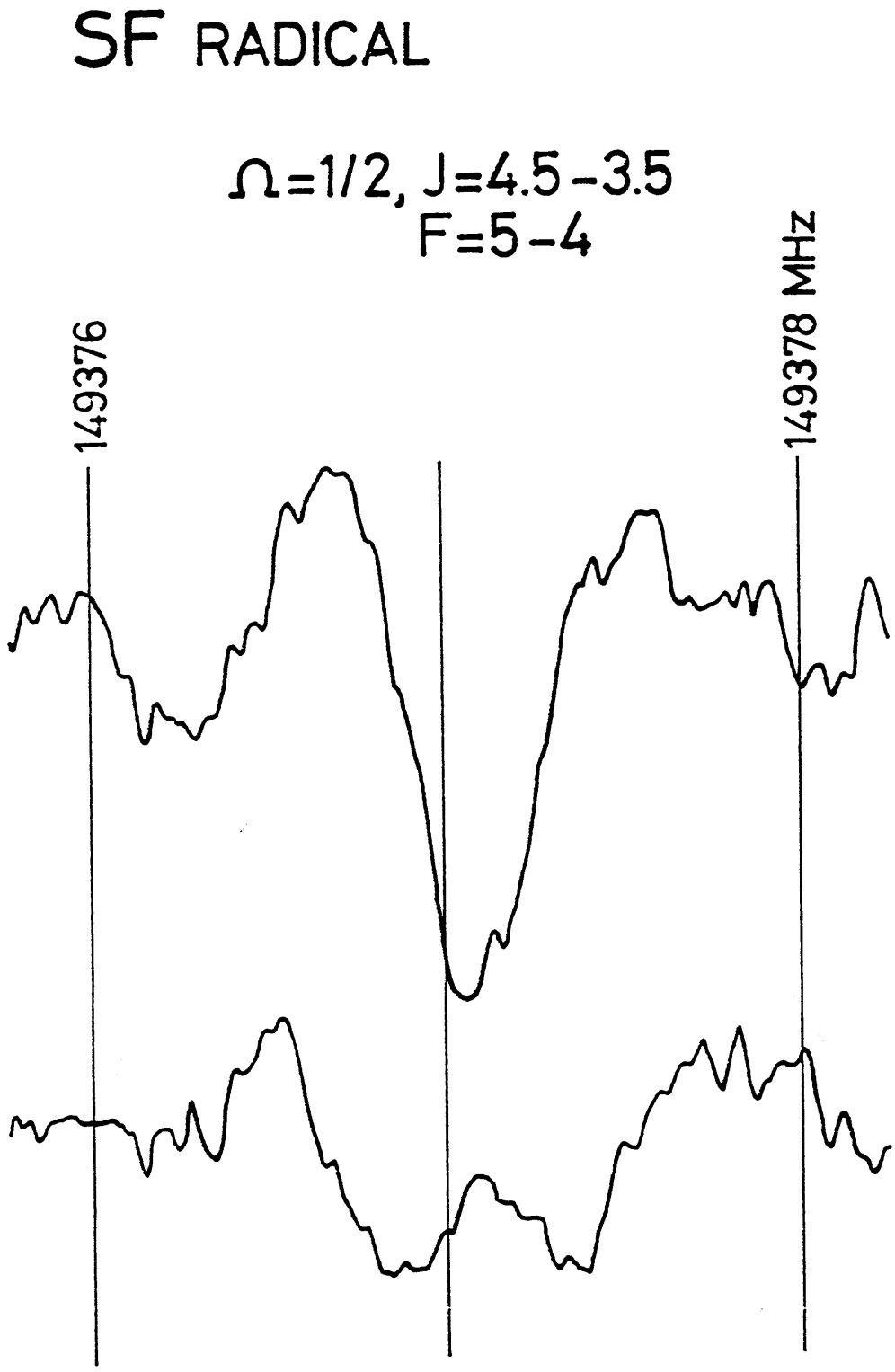

Fig. 1. Observed spectrum of SF in the $^2\Pi_{1/2}$ state, J = 4.5 - 3.5, F = 5 - 4, e level. Upper trace was obtained without external magnetic field, and lower with 60 Gauss magnetic field. 100 scans were integrated at a rate 2.5 scans/sec., and PSD time constant was 3 msec.

the absorption cell. The splitting thus observed corresponded quite well with that expected for the Zeeman effect of SF in the $^2\Pi_{1/2}$ state. In this manner, we assigned and measured 17 transitions from J = 1.5 ← 0.5 near 50 GHz to J = 5.5 ← 4.5 near 182 GHz. The previous measurement in the $^2\Pi_{3/2}$ state near 83 GHz was also extended up to transitions J = 5.5 ← 4.5. 10 transitions, including the remeasurement of the 3 transitions already reported (13), were measured for this state, where no splittings due to the Λ-doubling were observed. The observed transition frequencies in both states are listed in Table I.

Table I. Observed and Calculated Frequencies of SF (in MHz)

State	J′ - J"	F′- F"		Obs.	O-C
$^2\Pi_{1/2}$	1.5 - 0.5	2 - 1	f	49784.486	0.029
		1 - 0	f	50080.847	0.029
		2 - 1	e	49742.764	0.026
	2.5 - 1.5	3 - 2	f	82991.666	-0.018
		3 - 2	e	82971.962	0.036
		2 - 1	e	83011.439	0.028
	3.5 - 2.5	3 - 2	f	116218.374	0.025
		4 - 3	e	116178.536	-0.032
		3 - 2	e	116198.545	-0.039
	4.5 - 3.5	5 - 4	f	149386.243	-0.028
		4 - 3	f	149401.895	0.025
		5 - 4	e	149377.090	-0.008
		4 - 3	e	149389.390	0.007
	5.5 - 4.5	6 - 5	f	182577.633	-0.046
		5 - 4	f	182587.883	0.035
		6 - 5	e	182570.296	0.013
		5 - 4	e	182578.656	-0.007
$^2\Pi_{3/2}$	2.5 - 1.5	3 - 2		82732.093	-0.025
		2 - 1		82511.597	-0.004
		2 - 2		82545.533	-0.001
	3.5 - 2.5	4 - 3		115853.472	-0.006
		3 - 2		115910.215	0.001
		3 - 3		115689.709	0.012
	4.5 - 3.5	5 - 4		148963.452	-0.020
		4 - 3		148996.466	0.003
	5.5 - 4.5	6 - 5		182066.927	0.019
		5 - 4		182088.511	0.005

Standard deviation of the fit was 0.027 MHz.

4. Analysis and results

The molecular Hamiltonian used in the analysis of this radical has been given in Part I, Chapter II, eqs. (1-2-28) through (1-2-30), and (1-2-33) through (1-2-35). All the transition frequencies listed in Table I were analyzed by a least squares fitting. However, the transition frequencies in the $^2\Pi_{3/2}$ state were fitted to the averages of the Λ-doublets, because no Λ-doubling was observed for the transitions in the state. Furthermore, q_v could not be determined from the present data; we fixed it to be zero in the least squares analysis.

As for the assignments of the e and f levels for the Λ-doublets in the $^2\Pi_{1/2}$ state (see eq. (1-2-16)), two possible choices gave essentially the same quality of fit. They yielded two sets of constants, one with positive p_v and the other negative p_v; at the same time, the hyperfine interaction constant d changes its sign. We chose the assignment which gave positive d and, consequently, in the present case, gave positive p_v. As discussed by Amano et al. (7), the sign for d should be positive if a single electron approximation for the hyperfine interaction is valid, whereas the sign of p_v could be either positive or negative in accordance with the cases whether the $^2\Sigma^+$ contributions or $^2\Sigma^-$ contributions are larger for the Λ-doubling.

The determined molecular constants are listed in Table II,

where the spin-orbit interaction constant A_0 was fixed to the EPR value(81). The values in the parentheses denote 2.5 times the standard errors of the least-squares fitting. Because the constants A_J and b are affected by the change of A_0, we estimated how much the uncertainty of A_0 affects these constants. They are also given in the Table. Other constants are not affected so much, well within the least-squares errors, and were not listed.

Table II. Molecular Constants of SF (in MHz)[a]

A	387. cm^{-1} [b]	$\pm$25 cm^{-1}
A_J	0.7083(18)	$\mp$1.7[c]
B_0	16576.9140(46)	
D_0	0.02924(10)	
p_v	3.409(44)	
a+(b+c)/2	428.51(12)	
a-(b+c)/2	535.67(44)	
b	210.(15)	$\pm$14
d	589.76(92)	
a	482.09(24)[d]	
c	-317.(15)[d]	$\mp$14

a. Values in parentheses denote 2.5 times standard deviations and apply to the last digit.

b. Carrington et al. (81).

c. Changes of the constants due to the uncertainty of A.

d. Derived constants.

5. Discussion

As seen in Table II, most of the constants which characterize a molecule in a $^2\Pi$ electronic state were determined precisely for the SF radical. Especially, the Λ-doubling constant, p_v, and all four hyperfine interaction constants of the fluorine nucleus were obtained for the first time. The rotational constant, B_0, determined here is not affected by the contributions of the spin-uncoupling and the centrifugal distortion effect of the spin-orbit interaction (see eqs. (1-2-28) through (1-2-30) in Part I, Chapter II).

It should be noted that the Λ-doubling constant, p_v, is extremely small for this radical. On the other hand, for example, p_v of ClO, which is an isoelectronic radical with SF, is 670 MHz (57). p_v is expressed as a sum of second order perturbations from excited $^2\Sigma$ states (see eq. (1-2-20)). Usually a unique perturber approximation has been applied to explain the magnitude of p_v, where only one $^2\Sigma$ state is considered to be mainly contributing to the Λ-doubling. If we assume a $^2\Sigma$ state contributing to the Λ-doubling to be 50,000 cm^{-1} above the ground state and use the ground state constants for A_v and B_v in eq. (1-2-20), p_v is calculated to be c. a. 500 MHz for the SF radical. This value is very close to the observed value for ClO but far from that of SF. The observed small value suggests that close lying $^2\Sigma^+$ and $^2\Sigma^-$ states are both contributing to the Λ-doubling simultaneously, and their

contributions are nearly cancelled owing to the factor $(-1)^S$ in the summation in eq. (1-2-20). Although no $^2\Sigma$ state is known so far, our conclusion may be of some use for future investigations of its electronic spectra.

The parity independent constant, p_v^*, can be several hundred MHz, however, because there is no $(-1)^S$ factor in the definition of p_v^* (eq. (1-2-23)). The unknown contribution of p_v^* is contained effectively in the constant, A_J, together with that of γ_v.

The rotational constant, B_0, is used to calculate r_0 to be 1.55946 Å, which agrees well with the EPR value(81), since the contribution of A_J was found to be small for this species. In fact, the bond length should be discussed in its equilibrium value for the discussion to be suitable for the accuracy obtained by the microwave spectroscopy, which is a future plan for the study of this radical.

Since we determined the centrifugal distortion constant, D_0, accurately, we estimated the vibrational frequency from the well known relation,

$$\omega_e^2 = \frac{4B_e^3}{D_e} . \qquad (2\text{-}1\text{-}3)$$

If B_0 and D_0 are used for B_e and D_e in the above equation, ω_e is calculated to be 833 cm^{-1}.

A linear combination of the magnetic hyperfine constants, a+(b+c)/2, has already been determined(13,81). Present value agrees very well with them, while the accuracy is much improved. From the determined hyperfine constants in the Frosch and Foley's notations (see eq. (1-2-32)), the Fermi contact constant, $\frac{8\pi}{3}g_S g_I \beta\beta_I |\psi(0)|^2 \equiv b + c/3$ is calculated to be 105(15) MHz. Also the dipole-dipole interaction constant, $g_S g_I \beta\beta_I \langle 1/r^3 \rangle_{spin} \equiv d + c/3$ is calculated to be 484.1(87) MHz, which agrees quite well with $a \equiv 2g_I \beta\beta_I \langle 1/r^3 \rangle_{orbit} = 482.1$ MHz; the former constant is that averaged on the unpaired electron orbital, while the latter is that of the electron with the orbial angular momentum. Thus, the single electron approximation is found to be a good one for this radical. The spin density on the florine atom is calculated to be 0.13 from $\langle 1/r^3 \rangle_{spin}$ of the atomic fluorine (84).

Chapter II. Microwave spectroscopy of the HSO and DSO radicals

1. Introduction

The first evidence of the existence of HSO in the gas phase was given by Schurath et al. (85) in 1977. They observed low-resolution chemiluminescence spectra of HSO (or DSO) in the visible region by using a reaction of atomic oxygen with H_2S (or D_2S) and then O_3. Kakimoto et al. (51) studied the $\tilde{A}^2A'(003) \leftarrow \tilde{X}^2A''(000)$ band of HSO by means of high-resolution excitation spectroscopy using a single mode dye laser. They observed the spectrum by a reaction of 2450 MHz microwave discharge products of oxygen with H_2S, and determined the rotational, centrifugal distortion, and spin-rotation interaction constants for both the ground and excited electronic states. Resolution of their method is completely limited by the Doppler width, which is higher than that of conventional optical spectroscopy. The constants thus determined have fairly high precision for optical spectroscopy.

Ohashi et al. (52) observed the corresponding laser excitation spectrum of DSO and determined the molecular constants for it. They calculated the structure of this radical by combining the rotational constants of HSO and DSO. They also estimated an approximate force field to understand the vibrational frequencies, inertia defects, and centrifugal distortion constants of both HSO and DSO.

In the present study, we intended to determine their hyperfine interaction constants which have not been determined because the resolution in the visible region was limited by the Doppler width, as well as to refine and confirm the results obatained by dye laser excitation spectroscopy. Two halogenated derivatives of HSO, viz. FSO, results of which are given in the next chapter, and ClSO (86), have been studied also by microwave spectroscopy in our laboratory.

This radical is the first radical which has been observed by the glow discharge cell in our laboratory. The present result have shown us great possibility of the method for studying various free radicals.

2. Experimental

Source modulation spectrometer with the 3.5 m glow discharge cell was used in the present study, which have been explained in Part I, Chapter III. The HSO radical was generated by a D. C. glow discharge in a mixture of hydrogen sulfide and molecular oxygen. Pressures of 15 mTorr for H_2S and 10 mTorr for O_2 measured at the outlet of the cell by an uncalibrated thermocouple gauge, and discharge current of 15 - 20 mA were the optimum conditions. These conditions, however, were not critical. The cell temperature was kept at about 180 K by adjusting the flow rate of the liquid nitrogen. We also tried to use CH_3SH instead of H_2S, at an earlier stage of the experiment, which gave the spectrum nearly the same intensity as the case of H_2S. However, we did not use CH_3SH, since this molecule caused many undesirable spectral lines which seriously disturbed the spectrum of HSO.

The spectrum of DSO was observed by discharging a mixture of D_2S and O_2. The D_2S sample was synthesized from FeS and DCl. The synthesized sample was used without special purifications.

μ_a of HSO was expected to be much larger than μ_b when we assumed the bond moments derived from those of SO_2 and H_2S, and used the structure parameters determined by laser excitation spectroscopy (52). Therefore, a-type R-branch

transitions were searched at first. As the spectrometer has the highest sensitivity around 120 GHz, fine structure components of the $3_{03} - 2_{02}$ transition were searched based on the calculated frequencies using the constants of laser spectroscopy (51). Thus, we successfully observed a few lines near the predicted frequencies. The measurements were, then, extended to other R-branch lines and higher K_a lines. Several strong transitions, especially of $K_a = 0$, were observed even at room temperature. Fig. 1 shows a typical X-Y recorder trace of the observed lines. When K_a of the transitions became larger, the signal intensity became weaker considerably, because of the decrease in population for low temperature (180 K) and fairly large rotational constant A; thus measurements were not easy for higher K_a transitions.

Several low-N b-type transitions with $K_a = 1 - 0$ fall in the available frequency region (below 180 GHz). Two $K_a = 1 - 0$ b-type transitions were observed for HSO, and three for DSO. Other b-type transitions, however, were so weak that we could not observe them. Intensity ratio between the a-type and b-type trasitions roughly corresponded to the expected ratio of about 7 to 1.

Low N transitions, especially N = 1 - 0 transitions, are important to accurately determine the hyperfine interaction constants, because the splittings become larger for lower N transitions. However, we could not observe N = 1 - 0

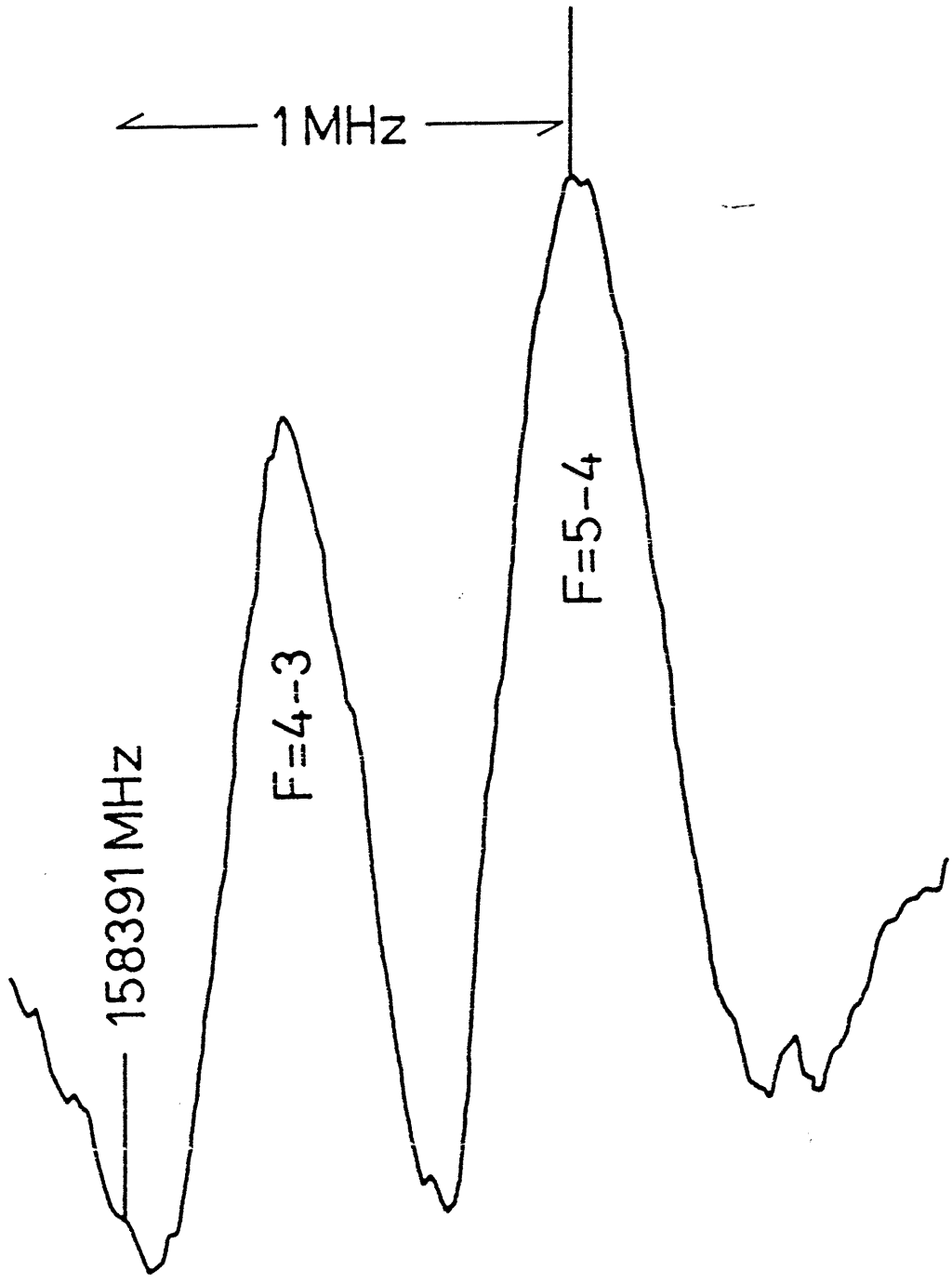

Fig. 1. Observed spectrum of the HSO $4_{04} - 3_{03}$ J = 4.5 - 3.5 transition. 200 scans were integrated at a rate 2.5 scans/sec. The PSD time constant was 3 msec. A linear function of the frequency was used to compensate baseline distortions.

transitions for HSO, nor N = 2 - 1, or 1 - 0 transitions for DSO.

For HSO, however, the magnetic hyperfine splittings due to the hydrogen nuclear spin were easily resolved and assigned. The measured transition frequencies are listed in Table I. On the other hand, we could not resolve those of DSO because the splittings due to the deuterium nuclear spin were much smaller. Partly resolved splittings were observed only for a-type N = 3 - 2 transitions. Therefore, we corrected and removed the contributions of the hyperfine interactions from the observed spectra, and analyzed them with a Hamiltonian which does not include the hyperfine interaction; detailes will be given in the next section. The corrected frequencies for DSO are listed in Table II.

Before the successful detection of the radical by the glow discharge cell, we tried to observe the spectrum of HSO by utilizing the parallel plate Stark cell 40 cm in length with the same reaction system used by the laser excitation spectroscopic study (51), viz. reaction of H_2S with atomic oxygen produced by a 2450 MHz microwave discharge of molecular oxygen. Although we searched the predicted regions carefully for several times, no paramagnetic lines ascribable to the HSO radical have been observed.

Table I. Observed and Calculated Frequencies of HSO (MHz)

Transition	J' ← J"	F' ← F"	obs.	Obs.-Calc.
$^{2}_{02} \leftarrow {}^{1}_{01}$	1.5 ← 0.5	1 ← 0	79373.524	0.028
	1.5 ← 0.5	2 ← 1	79378.688	-0.026
	2.5 ← 1.5	2 ← 1	79162.482	0.022
	2.5 ← 1.5	3 ← 2	79164.923	-0.006
$^{3}_{03} \leftarrow {}^{2}_{02}$	2.5 ← 1.5	3 ← 2	118997.266	0.024
	3.5 ← 2.5	4 ← 3	118786.810	0.009
$^{3}_{13} \leftarrow {}^{2}_{12}$	2.5 ← 1.5	2 ← 1	116019.400	0.019[a]
	2.5 ← 1.5	3 ← 2	116019.400	0.060[a]
	3.5 ← 2.5	3 ← 2	117258.597	0.019
	3.5 ← 2.5	4 ← 3	117260.309	0.010
$^{3}_{12} \leftarrow {}^{2}_{11}$	2.5 ← 1.5	2 ← 1	120227.178	-0.028
	2.5 ← 1.5	3 ← 2	120227.716	0.009
	3.5 ← 2.5	3 ← 2	121254.318	0.037
	3.5 ← 2.5	4 ← 3	121256.207	0.022
$^{3}_{21} \leftarrow {}^{2}_{20}$	2.5 ← 1.5	2 ← 1	116069.147	-0.048
	2.5 ← 1.5	3 ← 2	116065.814	-0.028
	3.5 ← 2.5	3 ← 2	120465.037	-0.001
	3.5 ← 2.5	4 ← 3	120468.134	-0.086
$^{3}_{22} \leftarrow {}^{2}_{21}$	2.5 ← 1.5	2 ← 1	116047.515	0.001
	2.5 ← 1.5	3 ← 2	116044.173	0.001
	3.5 ← 2.5	3 ← 2	120446.404	0.006
	3.5 ← 2.5	4 ← 3	120449.551	-0.024
$^{4}_{04} \leftarrow {}^{3}_{03}$	3.5 ← 2.5	3 ← 2	158597.989	0.025
	3.5 ← 2.5	4 ← 3	158598.747	-0.010
	4.5 ← 3.5	4 ← 3	158391.353	0.001
	4.5 ← 3.5	5 ← 4	158391.984	0.035
$^{4}_{13} \leftarrow {}^{3}_{12}$	3.5 ← 2.5	3 ← 2	160962.286	-0.012
	3.5 ← 2.5	4 ← 3	160962.817	0.019
	4.5 ← 3.5	4 ← 3	161385.603	0.018
	4.5 ← 3.5	5 ← 4	161386.598	0.001
$^{4}_{14} \leftarrow {}^{3}_{13}$	4.5 ← 3.5	4 ← 3	156021.814	-0.017
	4.5 ← 3.5	5 ← 4	156022.759	0.012
$^{4}_{22} \leftarrow {}^{3}_{21}$	3.5 ← 2.5	3 ← 2	157009.280	-0.056
	3.5 ← 2.5	4 ← 3	157008.312	-0.000
	4.5 ← 3.5	4 ← 3	159505.794	-0.045
	4.5 ← 3.5	5 ← 4	159507.528	0.048
$^{4}_{23} \leftarrow {}^{3}_{22}$	3.5 ← 2.5	3 ← 2	156956.395	0.005
	4.5 ← 3.5	4 ← 3	159458.454	-0.033
	4.5 ← 3.5	5 ← 4	159460.017	-0.103
$^{4}_{31} \leftarrow {}^{3}_{30}$	3.5 ← 2.5	3 ← 2	155355.641	0.014
	4.5 ← 3.5	4 ← 3	160536.683	-0.120
	4.5 ← 3.5	5 ← 4	160539.528	0.136
$^{4}_{32} \leftarrow {}^{3}_{31}$	3.5 ← 2.5	3 ← 2	155355.641	0.089

Table I. (Continued)

Transition	J' ← J"	F' ← F"	Obs.	Obs.-Calc.
$4_{32} \leftarrow 3_{31}$	4.5 ← 3.5	4 ← 3	160536.683	-0.058
	4.5 ← 3.5	5 ← 4	160539.528	0.199
$9_{09} \leftarrow 8_{18}$	8.5 ← 7.5	8 ← 7	100131.718	-0.016
	8.5 ← 7.5	9 ← 8	100130.411	-0.011
	9.5 ← 8.5	9 ← 8	100412.611	0.004
	9.5 ← 8.5	10 ← 9	100413.829	0.024
$10_{0,10} \leftarrow 9_{19}$	9.5 ← 8.5	9 ← 8	145329.634	-0.002
	9.5 ← 8.5	10 ← 9	145328.434	0.033
	10.5 ← 9.5	10 ← 9	145397.168	-0.023
	10.5 ← 9.5	11 ← 10	145398.303	-0.009

Standard deviation is 0.048 MHz.

a. Weight is 0.5.

Table II. Observed and Calculated Frequencies of DSO (MHz)

Transition	J' ← J"	Obs.	Obs.-Calc.
$^{3}_{03} \leftarrow {}^{2}_{02}$	2.5 ← 1.5	112197.580	0.022
	3.5 ← 2.5	112012.794	-0.018
$^{3}_{13} \leftarrow {}^{2}_{12}$	3.5 ← 2.5	108990.649	0.047
$^{3}_{12} \leftarrow {}^{2}_{11}$	3.5 ← 2.5	115621.195	0.012
$^{3}_{22} \leftarrow {}^{2}_{11}$	2.5 ← 1.5	110621.065	0.045
	3.5 ← 2.5	113005.422	-0.008
$^{3}_{21} \leftarrow {}^{2}_{20}$	2.5 ← 1.5	110735.485	-0.060
	3.5 ← 2.5	113111.186	-0.040
$^{4}_{04} \leftarrow {}^{3}_{03}$	3.5 ← 2.5	149498.382	0.002
	4.5 ← 3.5	149254.856	-0.039
$^{4}_{13} \leftarrow {}^{3}_{12}$	3.5 ← 2.5	153994.155	0.024
	4.5 ← 3.5	154132.999	0.007
$^{4}_{14} \leftarrow {}^{3}_{13}$	3.5 ← 2.5	144841.900	-0.039
	4.5 ← 3.5	145130.076	-0.006
$^{4}_{22} \leftarrow {}^{3}_{21}$	3.5 ← 2.5	149055.594	0.035
	4.5 ← 3.5	150304.793	0.018
$^{4}_{23} \leftarrow {}^{3}_{22}$	3.5 ← 2.5	148772.953	-0.028
	4.5 ← 3.5	150038.224	0.026
$^{3}_{12} \leftarrow {}^{3}_{03}$	2.5 ← 2.5	148093.186	0.009
	3.5 ← 3.5	145982.736	0.017
$^{4}_{13} \leftarrow {}^{4}_{04}$	3.5 ← 3.5	152588.906	-0.023
	4.5 ← 4.5	150860.831	0.014
$^{5}_{14} \leftarrow {}^{5}_{05}$	4.5 ← 4.5	158629.326	0.002
	5.5 ← 5.5	156979.039	-0.019

Standard deviation is 0.039 MHz.

3. Analysis and results

The molecular Hamiltonian applicable to HSO and DSO has been given in Part I, Chapter II. Two different programs were used for HSO and DSO since I = 1/2 for HSO and I = 1 for DSO. All the transition frequencies in Table I were subjected to a least squares analysis. Δ_K was fixed to the value determined by dye laser spectroscopy (51), because the b-type transitions observed were only those of $K_a = 1 - 0$. Δ_{NK}^S and Δ_K^S were required to fit the observed spectrum. Other centrifugal distortion constants in the spin-rotation interaction could not be determined, and were fixed to be zero. We also fixed the constant T_{ab}, off-diagonal component of the dipolar hyperfine interaction, to -7.8 MHz derived from the constant of DSO, which will be explained later. However the quality of the fit was not affected if T_{ab} = -7.8 MHz or 0.0 MHz was assumed. The determined constants of HSO are listed in Table III along with those obtained by dye laser spectroscopy (51) for comparison.

Analysis of the DSO spectrum was somewhat complicated. Traces denoted as a) in Figs. 2 and 3 are examples of the spectra of the partly resolved transitions and entirely unresolved transitions, respectively. To account for such partly resolved transitions, we assumed the hyperfine interaction constants for DSO to be 1/6.5144 times those for

Table III. Molecular Constants of HSO (MHz)[a]

	this work	dye laser[b]
A	299484.63(49)	299478(20)
B	20504.56(59)	20504.4(17)
C	19133.93(58)	19135.6(17)
Δ_N	0.03070(52)	0.0318(25)
Δ_{NK}	0.8960(26)	0.857(58)
Δ_K	27.2[c]	27.2(20)
δ_N	0.00193(22)	0.00202(56)
δ_K	0.89(29)	0.45(38)
ε_{aa}	-10365.99(55)	-10292(64)
ε_{bb}	-426.656(109)	-433(32)
ε_{cc}	0.226(161)	-5(32)
$\frac{1}{2}\lvert\varepsilon_{ab}+\varepsilon_{ba}\rvert$	378.0(27)	
Δ_{NK}^S	0.038(43)	
Δ_K^S	2.953(115)	
a_F	-36.37(142)	
T_{aa}	-11.96(24)	
T_{bb}	10.44(38)	
$\lvert T_{ab}\rvert$	-7.8[c,d]	

a. Values in parentheses denote 2.5 times standard deviations and apply to the last digits of the constants.

b. Ref. 51.

c. Fixed.

d. The negative sign means the sign of T_{ab} is opposite to that of $(1/2)(\varepsilon_{ab}+\varepsilon_{ba})$.

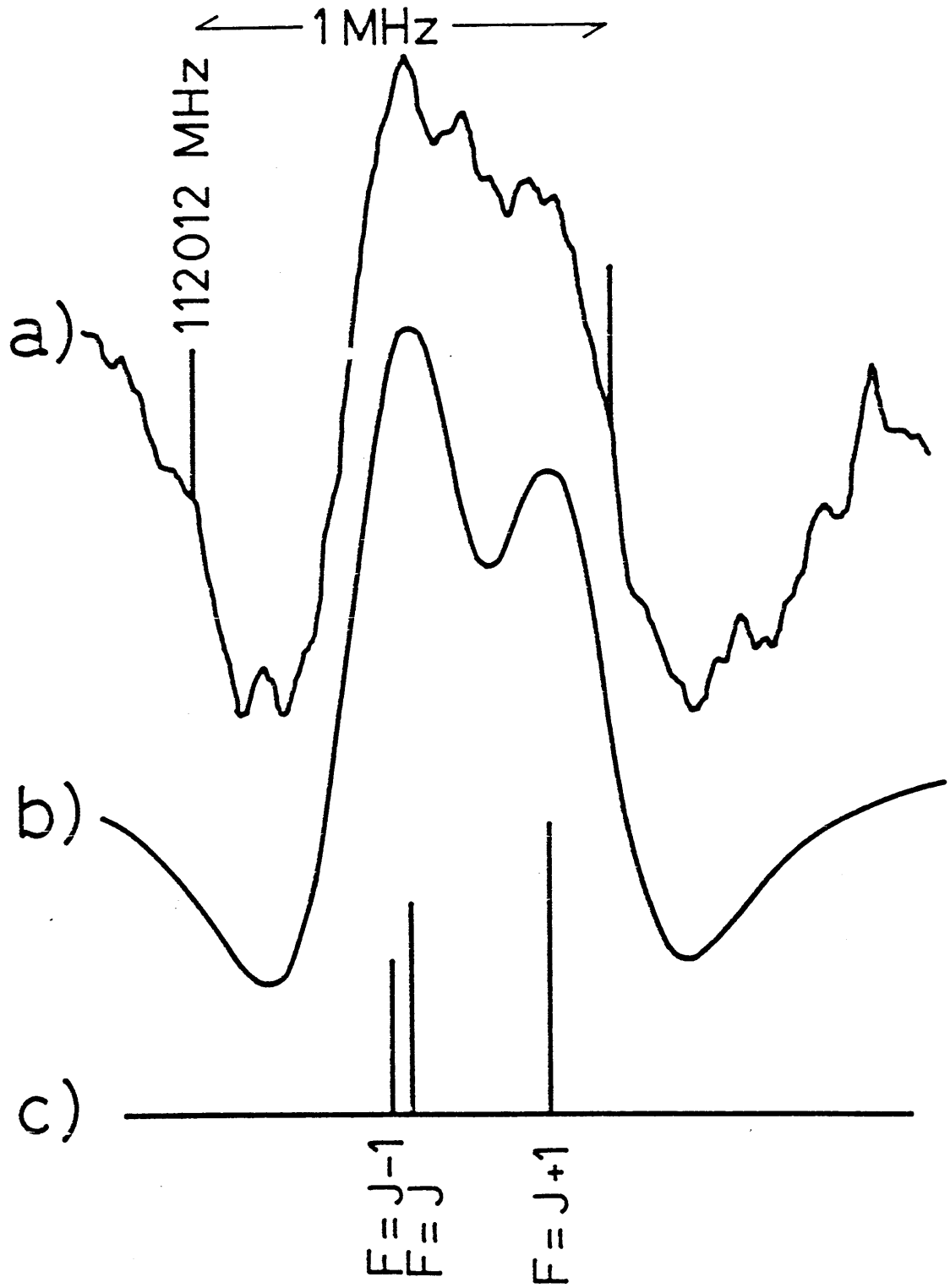

Fig. 2. The $3_{03} - 2_{02}$ J = 3.5 - 2.5 transition of DSO.
a) observed spectrum, b) simulated spectrum, and
c) calculated hyperfine structure.

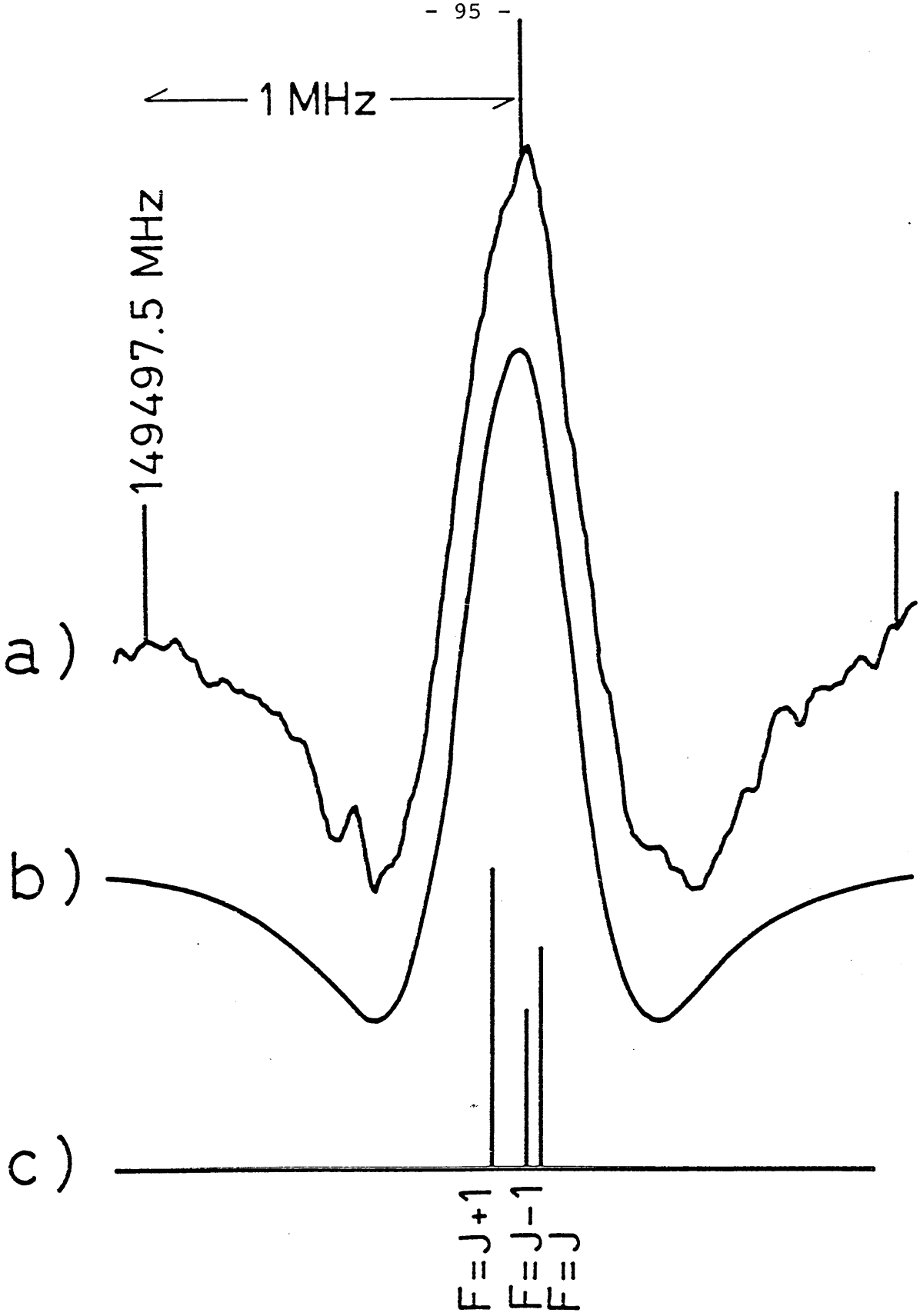

Fig. 3. The $4_{04} - 3_{03}$ J = 3.5 - 2.5 transition of DSO. a), b), and c) are the same as in Fig. 2.

HSO, which were determined by the least-squares analysis. This number is the gyromagnetic ratio of the deuterium nucleus to the hydrogen nucleus. The quadrupole couplings by the deuterium nucleus were ignored. Those denoted as c) in the figures show the thus calculated splittings. Traces denoted as b) are simulated spectra assuming the Lorenzian line shape, where the assumed linewidth was 0.6 MHz FWHM and the modulation depth was ±0.2 MHz for both traces. The simulated spectra fitted very well to the observed spectra for most transitions. However, for the transition $3_{12} \leftarrow 2_{11}$, J = 3.5 ← 2.5, no satisfactory fit was obtained; the observed spectrum is shown in Fig. 4 a).

The discrepancy was later explained as the effect of T_{ab} through a large local perturbation caused by the term containing $\varepsilon_{ab}+\varepsilon_{ba}$; in fact, the 3_{12}, J = 3.5 level lies very close to the 4_{04}, J = 3.5 level, and they are connected by the term containing $\varepsilon_{ab}+\varepsilon_{ba}$. The observed spectrum (Fig. 4 a)) was compared with several simulated traces with different T_{ab} values assumed. As seen in Fig. 4 b), the simulated trace fitted very well to the observed when T_{ab} = -1.2 MHz, where changes of T_{ab} up to ±0.3 MHz were easily discriminated. The negative sign for T_{ab} means that the sign of T_{ab} is opposite to that of $\varepsilon_{ab}+\varepsilon_{ba}$, although the absolute signs are not determinable for T_{ab} nor $\varepsilon_{ab}+\varepsilon_{ba}$. Transitions involving the 4_{04}, J = 3.5 level and the transition $4_{13} \leftarrow 3_{12}$, J = 4.5 ← 3.5 did not split; these facts are consistent with this value for

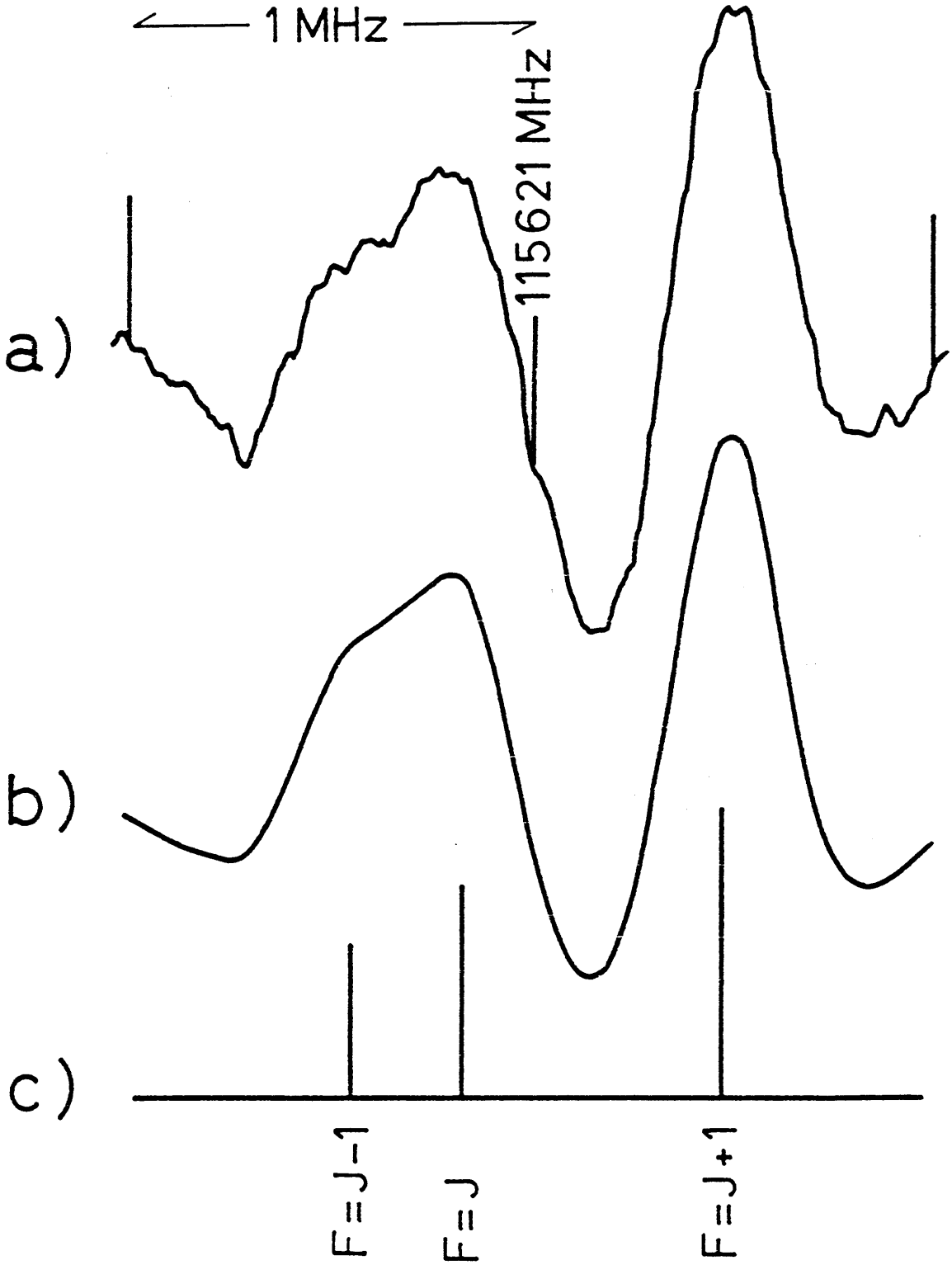

fig. 4. The $3_{12} - 2_{11}$ J = 3.5 - 2.5 transition of DSO. Larege splittings were explained by taking into account the effect of T_{ab}. b) and c) were calculated by assuming T_{ab} to be -1.2 MHz.

T_{ab}. They were also checked by the line shape simulation. Other transitions were not affected by the value of T_{ab}. The T_{ab} value thus obtained for DSO was then transferred to that of HSO to be -7.8(20) MHz. This value for HSO was constrained during the analysis of HSO as mentioned earlier.

From comparisons between the observed and the simulated traces on the recorder charts, we obtained the transition frequencies of DSO which do not include the effects of the hyperfine interactions (see Table II). These frequencies were subjected to a least-squares analysis excluding the hyperfine interactions. Determined molecular constants for DSO are listed in Table IV, where only Δ_K^S was required for the centrifugal distortion constant in the spin-rotation interaction. The constant $1/2|\varepsilon_{ab}+\varepsilon_{ba}|$ was determined much better than the case of HSO, since the energy difference between the 4_{04}, J = 3.5 and 3_{12}, J = 3.5 levels are very small. The constants obtained by dye laser spectroscopy are also listed for comparison (52).

Table IV. Molecular Constants of DSO (MHz)[a]

	this work	dye laser[b]
A	158726.938(71)	158750(18)
B	19836.533(89)	19836.2(28)
C	17570.206(87)	17573.6(26)
Δ_N	0.02646(31)	0.0281(41)
Δ_{NK}	0.66982(134)	0.847(55)
Δ_K	8.9[c]	8.9(10)
δ_N	0.00323(23)	0.00192(84)
δ_K	0.558(42)	-0.15(20)
ε_{aa}	-5646.83(42)	-5668(101)
ε_{bb}	-393.997(37)	-347(38)
ε_{cc}	0.053(56)	51(36)
$\frac{1}{2}\lvert\varepsilon_{ab}+\varepsilon_{ba}\rvert$	322.667(78)	
Δ_K^s	0.677(101)	
a_F	-5.58[d]	
T_{aa}	-1.84[d]	
T_{bb}	1.60[d]	
$\lvert T_{ab}\rvert$	-1.2(3)[e,f,g]	

a. Values in parentheses denote 2.5 times standard deviations and apply to the last digits of the constants.

b. Ref. 52.

c. Fixed.

d. Calculated from the constants of HSO, where axis rotation was ignored.

e. Determined from the $3_{12} - 2_{11}$, J = 3.5 - 2.5 transition.

f. Values in the parenthesis is the error limit estimated from line shape simulation.

g. The negative sign means the sign of T_{ab} is opposite to that of $(1/2)(\varepsilon_{ab}+\varepsilon_{ba})$.

4. Discussion

The small negative value of the Fermi interaction constant in Table III shows that the orbital of the unpaired electron is not extending to the bonding orbital of the hydrogen atom. This is the same tendency with that of its isovalent radical HO_2 (87), but different from that of HCO (11) where the Fermi constant is large and positive. The components of the dipole-dipole interaction tensor in the principal axis system are T_{xx} = -14.4 MHz, T_{yy} = 12.9 MHz, and T_{zz} = 1.6 MHz, where the z-axis coincides with the c-axis and the angle between the x-axis and the a-axis is 17.5(30)°. The direction of the axis rotation is not determined from the constants obtained here; if we rotate it favourably, however, the y-axis nearly coincides with the H-S bond which lies 19.5° from the b-axis for HSO. The T_{yy} component is largest among the three principal axis components of the tensor; this fact means that this dipolar interaction is mainly due to the interaction between the hydrogen nuclear spin and the unpaired electron spin in the p_c orbital on the sulfur atom (84). These arguments on the hyperfine interaction constants support the conclusion (85) that the ground electronic state of this radical is of $^2A''$.

As is seen clearly in Tables III and IV, the rotational, centrifugal distortion, and spin-rotation interaction constants

determined here are in good agreement with the results of dye laser excitation spectroscopy (51,52). Most of the constants agree within the errors given in the laser studies. We can thus assure the accuracy of the dye laser excitation technique, which is rather new and has not been applied to numbers of molecules to obtain accurate molecular constants. The present result also definitely confirmed the sign of ε_{aa} in the ground electronic state. The centrifugal distortion constant, δ_k, of DSO determined by laser spectroscopy had negative value which did not agree with the calculated value from a simple and approximate force field (52). However δ_k determined here is positive and agrees fairly well with the calculated value.

Dixon and Duxbury presented an approximate relation between the centrifugal distortion constants in the spin-rotation interaction and the spin-rotation constants (67). If the relation is adopted, Δ_k^s can be estimated to be c.a. 2 MHz for HSO, which is in order of magnitude agreement with the determined value, 2.953 MHz.

The reaction system, H_2S (or D_2S) + $(O_2)_{MW\ disch.}$, had successfully been used in laser excitation spectroscopy (51,52). However, our attempt to observe the microwave spectrum using a parallel plate Stark cell of 40 cm length with the same reaction system was unsuccessful as mentioned before. This result may partly be ascribed to a very short

lifetime of the HSO radical. Lifetimes of at least 10 msec are required to observe spectra of the species by the Stark cell, because the pumping speed limits the total number of molecules in the cell. In contrast to it, molecules of shorter lifetimes are detectable by dye laser excitation spectroscopy, since the method requires their existence only in small volume. On the other hand, however, reaction takes place all over the cell for the case of the glow discharge cell; the pumping speed is not essential for the detection of short lifetime species.

Another reason why the HSO radical has been observed only in the glow discharge cell is that the minimum detectable concentration is much smaller than that of the 40 cm Stark cell, since the cell length is nearly ten times longer. In fact, the concentration of HSO is estimated to be c. a. 5×10^{-4} of the total number of molecules in the cell, if a dipole moment transferred from those of SO_2 and H_2S, as have been mentioned, and the linewidth parameter of 10 MHz/Torr are assumed.

Chapter III. Microwave spectroscopy of the FSO radical

1. Introduction

Very little has been known so far as for the existence of the FSO radical. Wayne and Radford have observed far-infrared laser magnetic resonance (LMR) spectra for reaction system which involves carbon disulfide and microwave discharge products of a mixture of oxygen and carbon tetrafluoride (88). They have ascribed the observed spectra to the FSO radical although a definite assignment had not been made. No other spectroscopic investigations have been reported yet.

The FSO radical is a member of a series of molecules XSO, and the parent molecule HSO, microwave spectroscopy of which is given in the previous chapter, had only recently been identified through observations of chemiluminescence emitted from reaction systems involving sulfur atom (51,52,85). The chlorine derivative, ClSO, had been detected in low temperature matrices by means of EPR (89), and Wayne et al. also observed its far-infrared LMR spectra (88). The microwave spectroscopy of ClSO also is under way by using the glow discharge cell (86).

Wayne et al. found that the spectrum ascribed to ClSO was much stronger than that of FSO. However, in the case of microwave spectroscopy, spectrum of FSO was much stronger than that of ClSO, so that extensive results for this radical have been obtained at first.

2. Experimental

The Stark spectrometer was used for the study of this radical. FSO was generated by the reaction of carbonyl sulfide and products of a 2450 MHz microwave discharge in an O_2 /CF_4 mixture. According to a suggestion of Wayne et al. (88) CS_2 instead of OCS was used at first, but we found that OCS gave absorption signals several times stronger than CS_2. Therefore, OCS was used throughout the present study. The optimum pressures were 20, 20, and 10 mTorr for OCS, O_2, and CF_4. It was noticed that intensity of FSO lines increased gradually until some amount of sulfur deposit on the cell wall was observed; when the surfaces of the Stark plates and the inside wall of the Pyrex glass tube were cleaned, intensities of the lines became considerably weaker. All subsequent measurements were made with sulfur deposits on the inside wall of the cell.

In our reaction mixture, we have identified SO, SO_2, SF, SF_2, and F_2SO by observing their microwave spectral lines. It is well known that OCS reacts with O to produce SO (4) and SO_2, and with F to generate SF (81) and SF_2 (83). An interesting aspect of these reactions have been noticed; when a small amount of CF_4 was added to O_2 before microwave discharge, intensity of $X^3\Sigma^-$ SO lines increased by a factor of ten, whereas those of $a^1\Delta$ SO lines became weaker (90). On the other hand, an addition of a small amount of O_2 to CF_4 made

spectrum of SF several times stronger.

The absorption spectrum of FSO was strong enough to be seen on CRO. By using a small permanent magnet, it was demonstrated that the radical existed for 1/2 to 1/3 of the cell length down stream from the inlet. Because the linear velocity of the gas flow in the cell was about 5 to 10 m/sec., the lifetime of the radical was estimated to be 20 to 40 msec. in the cell.

At first, the frequency region from 40 to 70 GHz was scanned on a CRO. Many paramagnetic quartet and doublet lines were observed throughout the region. Several transitions of the b-type Q-branch $N_{1,N-1} \leftarrow N_{0,N}$ (here, Q-branch means $\Delta N = 0$ in this case) were easily identified among the strong quartets. Fig. 1 Shows the observed spectrum of the $5_{14} - 5_{05}$ transition, and Fig. 2 shows fine and hyperfine structures observed for several low-N members of the Q-branch series. The rotational quantum number N was easily determined by an A-C versus κ plot. Other transitions were assigned after approximate constants were obtained from the Q-branch transitions, as is given in the next section. The transition frequencies observed for the normal species in the ground state are listed in Table I.

Spectrum of the ^{34}S species was predicted by using the

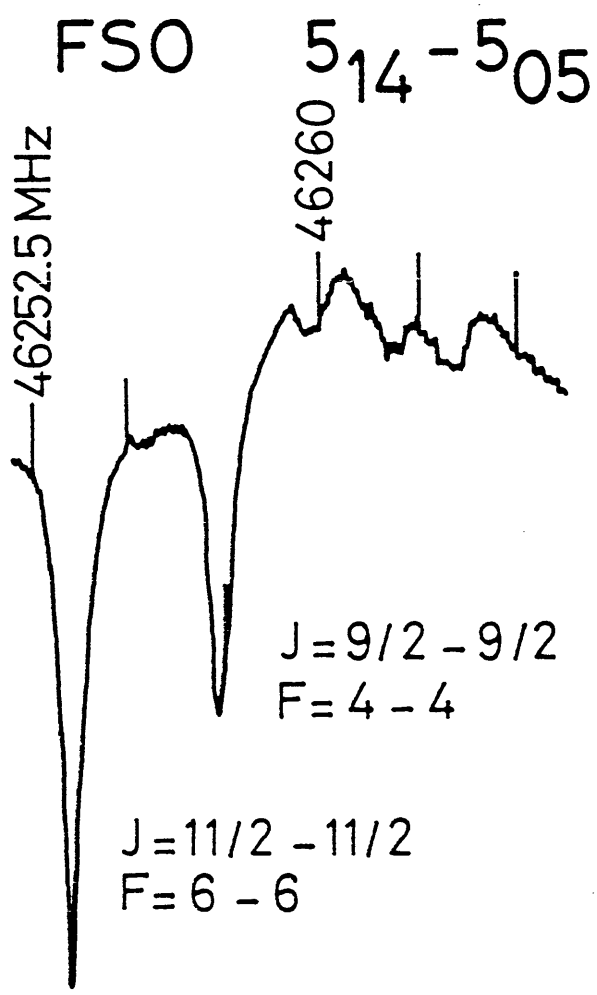

Fig. 1. Two fine and hyperfine components of the $5_{15} - 5_{05}$ transition of $F^{32}SO$ in the ground vibrational state. The spectrum was recorded with a 1 sec time constant and a 813 V/cm p-p square-wave Stark field. FSO was generated by reacting microwave discharge products of 9 mTorr O_2 and 9 mTorr CF_4 with 4 mTorr OCS.

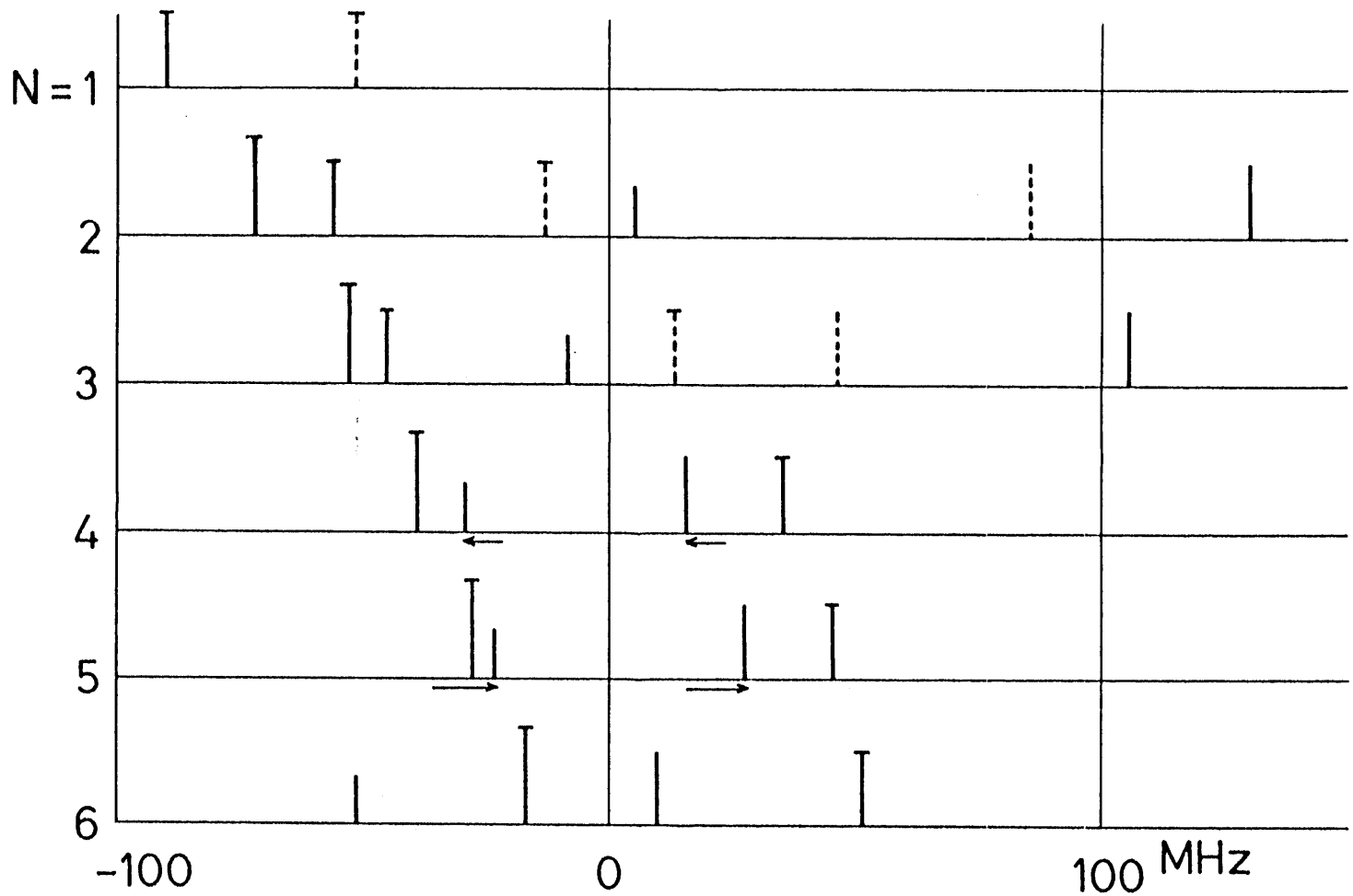

Fig. 2. Observed fine and hyperfine patterns of the Q-branch $N_{1,N-1} - N_{0,N}$ transitions. Solid lines denote the $\Delta J = 0$ transitions, whereas broken lines denote the $\Delta J = \pm 1$ transitions. Arrows indicate the effects of the perturbations caused by ε_{ab} and ε_{ba}.

fine and hyperfine interaction constnats of the normal species and the rotational constants which were calculated from an approximate molecular structure. Thus lines were observed near the predicted frequencies and easily assigned. The observed lines for the ^{34}S species are listed in Table II.

After most of the transitions of FSO in the ground state were assigned in the region mentioned above, it was not difficult to pick out the $N_{1,N-1} \leftarrow N_{0,N}$ Q-branch lines in the first excited state of the bending vibration (the lowest ν_3 mode) from the remaining spectral lines. The R-branch transitions were found at frequencies calculated using inertia defect about three times larger than that of the ground state. Table III lists the transition frequencies thus measured. Intensities of the $2_{12} - 1_{01}$, J = 2.5 - 1.5, F = 3 - 2 transitions in the excited and the ground states were compared to estimate the bending vibrational frequency; the ratio thus obtained is 11.1. This value was reproducible within several percent. When we assume the gas mixture in the cell to be in thermal equilibrium with the cell wall, the vibrational frequency of the state concerned is calculated to be 490±20 cm^{-1}. Because the transition frequencies of the two lines differ as much as 525 MHz, microwave transmission may change for one frequency to the other, causing a larger error in the observed intensity ratio.

Table I. Observed and Calculated Frequencies of $F^{32}SO$ in the Ground State (MHz)

Transition	J' ← J"	F' ← F"	Obs.	Obs.-Calc.
$1_{10} \leftarrow 1_{01}$	0.5 ← 0.5	1 ← 1	31446.076	-0.070[a]
	1.5 ← 0.5	1 ← 1	31141.038	0.018
	1.5 ← 1.5	1 ← 1	31102.405	-0.031
	1.5 ← 1.5	2 ← 2	31078.227	0.039
$2_{11} \leftarrow 2_{02}$	1.5 ← 1.5	1 ← 1	33117.305	0.019
	1.5 ← 1.5	2 ← 2	33241.550	-0.021
	2.5 ← 1.5	2 ← 2	33098.837	-0.005
	1.5 ← 2.5	2 ← 2	33198.074	0.059
	2.5 ← 2.5	2 ← 2	33055.330	0.044
	2.5 ← 2.5	3 ← 3	33039.466	-0.057
$3_{12} \leftarrow 3_{03}$	2.5 ← 2.5	2 ← 2	36135.602	0.016
	2.5 ← 2.5	3 ← 3	36250.058	-0.016
	2.5 ← 3.5	3 ← 3	36191.099	-0.006
	3.5 ← 2.5	3 ← 3	36158.083	-0.014
	3.5 ← 3.5	3 ← 3	36099.201	0.073
	3.5 ← 3.5	4 ← 4	36091.783	0.059
$4_{13} \leftarrow 4_{04}$	3.5 ← 3.5	3 ← 3	40435.842	0.027
	3.5 ← 3.5	4 ← 4	40481.303	0.049
	4.5 ← 4.5	4 ← 4	40500.886	0.063
	4.5 ← 4.5	5 ← 5	40426.168	0.039
$5_{14} \leftarrow 5_{05}$	4.5 ← 4.5	4 ← 4	46257.410	0.007
	4.5 ← 4.5	5 ← 5	46308.835	0.020
	5.5 ← 5.5	5 ← 5	46326.785	0.018
	5.5 ← 5.5	6 ← 6	46253.546	0.067
$6_{15} \leftarrow 6_{06}$	5.5 ← 5.5	5 ← 5	53744.953	-0.056
	5.5 ← 5.5	6 ← 6	53806.236	-0.026
	6.5 ← 6.5	6 ← 6	53848.251	-0.002
	6.5 ← 6.5	7 ← 7	53779.283	-0.017
$7_{16} \leftarrow 7_{07}$	6.5 ← 6.5	6 ← 6	63096.759	0.015
	6.5 ← 6.5	7 ← 7	63163.014	-0.035
	7.5 ← 7.5	7 ← 7	63225.909	0.023
	7.5 ← 7.5	8 ← 8	63156.215	-0.030
$8_{17} \leftarrow 8_{08}$	7.5 ← 7.5	7 ← 7	74394.001	0.045
	7.5 ← 7.5	8 ← 8	74442.250	0.024
	8.5 ← 8.5	8 ← 8	74506.365	0.000
	8.5 ← 8.5	9 ← 9	74435.399	-0.056
$6_{24} \leftarrow 6_{15}$	5.5 ← 5.5	5 ← 5	77973.092	-0.017
	5.5 ← 5.5	6 ← 6	77988.340	0.001
	6.5 ← 6.5	6 ← 6	77767.542	0.016
	6.5 ← 6.5	7 ← 7	77802.948	0.041

Table I. (continued)

Transition	J' ← J"	F' ← F"	Obs.	Obs.-Calc.
$^{7}_{25} \leftarrow {}^{7}_{16}$	6.5 ← 6.5	6 ← 6	76313.277	-0.025
	6.5 ← 6.5	7 ← 7	76350.491	0.131
	7.5 ← 7.5	7 ← 7	76139.964	-0.010
	7.5 ← 7.5	8 ← 8	76184.008	-0.084
$^{8}_{26} \leftarrow {}^{8}_{17}$	7.5 ← 7.5	7 ← 7	75757.753	-0.079
	7.5 ← 7.5	8 ← 8	75756.700	-0.008
	8.5 ← 8.5	8 ← 8	75712.595	-0.011
	8.5 ← 8.5	9 ← 9	75703.780	-0.092
$^{9}_{27} \leftarrow {}^{9}_{18}$	8.5 ← 8.5	8 ← 8	76767.316	0.065
	8.5 ← 8.5	9 ← 9	76769.634	0.044
	9.5 ← 9.5	9 ← 9	76704.396	0.037
	9.5 ← 9.5	10 ← 10	76684.508	0.010
$^{1}_{11} \leftarrow {}^{0}_{00}$	0.5 ← 0.5	1 ← 0	46398.243	0.070[b]
	0.5 ← 0.5	0 ← 1	46430.286	-0.039[b]
	0.5 ← 0.5	1 ← 1	46330.770	-0.238[b]
	1.5 ← 0.5	1 ← 0	46129.324	-0.014
	1.5 ← 0.5	1 ← 1	46062.185	0.012
	1.5 ← 0.5	2 ← 1	46123.203	0.014
$^{2}_{12} \leftarrow {}^{1}_{01}$	1.5 ← 0.5	1 ← 0	61306.586	0.049
	1.5 ← 0.5	2 ← 1	61298.708	0.088[a]
	2.5 ← 1.5	2 ← 1	61133.181	-0.002[a]
	2.5 ← 1.5	3 ← 2	61164.780	0.028
$^{3}_{13} \leftarrow {}^{2}_{02}$	2.5 ← 1.5	2 ← 1	75416.785	0.083[a]
	2.5 ← 1.5	3 ← 2	75381.815	0.032
	3.5 ← 2.5	3 ← 2	75268.177	0.040
	3.5 ← 2.5	4 ← 3	75303.333	-0.044
$^{4}_{04} \leftarrow {}^{3}_{13}$	3.5 ← 2.5	3 ← 2	41323.300	-0.058
	3.5 ← 2.5	4 ← 3	41359.704	-0.012
	4.5 ← 3.5	4 ← 3	41497.778	0.017
	4.5 ← 3.5	5 ← 4	41476.613	0.017
$^{5}_{05} \leftarrow {}^{4}_{14}$	4.5 ← 3.5	4 ← 3	60400.740	-0.071
	4.5 ← 3.5	5 ← 4	60432.257	0.038
	5.5 ← 4.5	5 ← 4	60542.058	-0.011
	5.5 ← 4.5	6 ← 5	60552.198	-0.026
$^{6}_{06} \leftarrow {}^{5}_{15}$	5.5 ← 4.5	5 ← 4	79443.904	-0.081
	5.5 ← 4.5	6 ← 5	79469.102	-0.018
	6.5 ← 5.5	6 ← 5	79557.882	-0.081
	6.5 ← 5.5	7 ← 6	79540.298	-0.012
$^{7}_{16} \leftarrow {}^{6}_{25}$	6.5 ← 5.5	6 ← 5	50569.919	-0.010
	6.5 ← 5.5	7 ← 6	50685.226	0.022
	7.5 ← 6.5	7 ← 6	51300.001	-0.010
	7.5 ← 6.5	8 ← 7	50560.874	-0.001

Table I. (continued)

Transition	J' ← J"	F' ← F"	Obs.	Obs.-Calc.
$8_{17} \leftarrow 7_{26}$	7.5 ← 6.5	7 ← 6	73525.956	-0.017
	7.5 ← 6.5	8 ← 7	73540.309	-0.031
	8.5 ← 7.5	8 ← 7	73762.673	0.036
	8.5 ← 7.5	9 ← 8	73738.367	0.063
$5_{33} \leftarrow 6_{24}$	4.5 ← 5.5	4 ← 5	45991.234	0.040
	4.5 ← 5.5	5 ← 6	45981.171	0.089
	5.5 ← 6.5	5 ← 6	45585.824	-0.018
	5.5 ← 6.5	6 ← 7	45576.155	0.044
$11_{29} \leftarrow 10_{38}$	10.5 ← 9.5	10 ← 9	65752.061	0.061
	10.5 ← 9.5	11 ← 10	65769.611	0.034
	11.5 ← 10.5	11 ← 10	66083.955	-0.092
	11.5 ← 10.5	12 ← 11	66044.228	-0.045
$7_{44} \leftarrow 8_{35}$	6.5 ← 7.5	6 ← 7	75001.983	-0.078
	6.5 ← 7.5	7 ← 8	75009.880	-0.055
	7.5 ← 8.5	7 ← 8	74609.657	-0.021
	7.5 ← 8.5	8 ← 9	74600.723	-0.018
$7_{43} \leftarrow 8_{36}$	6.5 ← 7.5	6 ← 7	76072.484	-0.028
	6.5 ← 7.5	7 ← 8	76084.522	-0.032
	7.5 ← 8.5	7 ← 8	75623.782	-0.001
	7.5 ← 8.5	8 ← 9	75610.955	0.021
$8_{45} \leftarrow 9_{36}$	7.5 ← 8.5	7 ← 8	56795.096	-0.140[a]
	7.5 ← 8.5	8 ← 9	56795.096	0.072[a]
	8.5 ← 9.5	8 ← 9	56435.444	-0.041
	8.5 ← 9.5	9 ← 10	56429.196	-0.043
$8_{44} \leftarrow 9_{37}$	7.5 ← 8.5	7 ← 8	58917.030	-0.053
	7.5 ← 8.5	8 ← 9	58926.366	-0.041
	8.5 ← 9.5	8 ← 9	58612.691	-0.036
	8.5 ← 9.5	9 ← 10	58603.941	-0.022
$11_{56} \leftarrow 12_{49}$	10.5 ← 11.5	10 ← 11	67250.726	0.063
	10.5 ← 11.5	11 ← 12	67255.355	0.102
	11.5 ← 12.5	11 ← 12	66980.658	0.042
	11.5 ← 12.5	12 ← 13	66976.424	0.040
$11_{57} \leftarrow 12_{48}$	10.5 ← 11.5	10 ← 11	66555.164	0.050
	10.5 ← 11.5	11 ← 12	66557.189	0.071
	11.5 ← 12.5	11 ← 12	66232.229	0.058
	11.5 ← 12.5	12 ← 13	66227.604	0.070
$12_{57} \leftarrow 13_{4,10}$	11.5 ← 12.5	11 ← 12	49641.113	-0.036
	11.5 ← 12.5	12 ← 13	49642.999	-0.004
	12.5 ← 13.5	12 ← 13	49358.119	-0.055
	12.5 ← 13.5	13 ← 14	49352.925	-0.040

Table I. (continued)

Transition	J' ← J"	F' ← F"	Obs.	Obs.-Calc.
$^{12}_{58} \leftarrow {}^{13}_{49}$	11.5 ← 12.5	11 ← 12	48341.284	-0.081
	11.5 ← 12.5	12 ← 13	48339.298	-0.008
	12.5 ← 13.5	12 ← 13	48031.921	-0.051
	12.5 ← 13.5	13 ← 14	48027.760	-0.027

Standard deviation is 0.050 MHz.

a. Weight is 0.5.

b. Weight is 0.1.

Table II. Observed and Calculated Frequencies of $F^{34}SO$ (MHz)

Transition	J' ← J"	F' ← F"	Obs.	Obs.-Calc.
$5_{14} \leftarrow 5_{05}$	4.5 ← 4.5	4 ← 4	45622.260	0.342
	4.5 ← 4.5	5 ← 5	45675.843	-0.329
	5.5 ← 5.5	5 ← 5	45699.390	0.041
	5.5 ← 5.5	6 ← 6	45628.168	0.009
$6_{15} \leftarrow 6_{06}$	5.5 ← 5.5	5 ← 5	53393.158	-0.119
	5.5 ← 5.5	6 ← 6	53455.770	0.051
	6.5 ← 6.5	6 ← 6	53501.625	0.098
	6.5 ← 6.5	7 ← 7	53432.570	-0.081
$3_{13} \leftarrow 2_{02}$	2.5 ← 1.5	2 ← 1	73993.440	-0.060
	2.5 ← 1.5	3 ← 2	73958.279	-0.010
	3.5 ← 2.5	3 ← 2	73844.886	0.142
$4_{14} \leftarrow 3_{03}$	3.5 ← 2.5	3 ← 2	87206.393	0.075
	3.5 ← 2.5	4 ← 3	87168.692	-0.090
	4.5 ← 3.5	4 ← 3	87075.006	-0.030
	4.5 ← 3.5	5 ← 4	87107.811	-0.025
$5_{05} \leftarrow 4_{14}$	4.5 ← 3.5	4 ← 3	67250.820	0.019
	4.5 ← 3.5	5 ← 4	61281.303	0.053
	5.5 ← 4.5	5 ← 4	61388.847	-0.017
	5.5 ← 4.5	6 ← 5	61369.824	-0.021
$6_{06} \leftarrow 5_{15}$	5.5 ← 4.5	5 ← 4	80155.828	-0.113
	5.5 ← 4.5	6 ← 5	80179.616	-0.109
	6.5 ← 5.5	6 ← 5	80265.852	0.092
	6.5 ← 5.5	7 ← 6	80249.004	0.113

Standard deviation is 0.164 MHz.

Table III. Observed and Calculated Frequencies of $F^{32}SO$ in the $v_3 = 1$ State (MHz)

Transition	J' ← J"	F' ← F"	Obs.	Obs.-Calc.
$^4_{13} \leftarrow {}^4_{04}$	3.5 ← 3.5	3 ← 3	41092.359	-0.100
	3.5 ← 3.5	4 ← 4	41140.383	-0.060
	4.5 ← 4.5	4 ← 4	41160.787	0.045
	4.5 ← 4.5	5 ← 5	41088.937	-0.009
$^5_{14} \leftarrow {}^5_{05}$	4.5 ← 4.5	4 ← 4	46941.065	0.029
	4.5 ← 4.5	5 ← 5	46991.997	0.076
	5.5 ← 5.5	5 ← 5	47005.532	0.007
	5.5 ← 5.5	6 ← 6	46931.782	0.096
$^6_{15} \leftarrow {}^6_{06}$	5.5 ← 5.5	5 ← 5	54436.096	-0.031
	5.5 ← 5.5	6 ← 6	54497.976	-0.081
	6.5 ← 6.5	6 ← 6	54542.484	0.003
$^7_{16} \leftarrow {}^7_{07}$	6.5 ← 6.5	6 ← 6	63809.754	0.048
	6.5 ← 6.5	7 ← 7	63876.402	0.010
	7.5 ← 7.5	7 ← 7	63942.381	-0.004
	7.5 ← 7.5	8 ← 8	63873.648	0.057
$^8_{17} \leftarrow {}^8_{08}$	7.5 ← 7.5	7 ← 7	75105.621	0.044
	7.5 ← 7.5	8 ← 8	75172.660	-0.020
	8.5 ← 8.5	8 ← 8	75255.622	-0.025
	8.5 ← 8.5	9 ← 9	75185.582	-0.048
$^6_{24} \leftarrow {}^6_{15}$	5.5 ← 5.5	5 ← 5	79661.940	0.097
	5.5 ← 5.5	6 ← 6	79678.100	0.021
	6.5 ← 6.5	6 ← 6	79465.108	0.009
	6.5 ← 6.5	7 ← 7	79502.212	0.013
$^7_{25} \leftarrow {}^7_{16}$	6.5 ← 6.5	6 ← 6	77934.210	-0.036
	6.5 ← 6.5	7 ← 7	77907.514	0.017
	7.5 ← 7.5	7 ← 7	77831.918	-0.018
	7.5 ← 7.5	8 ← 8	77812.968	0.030
$^8_{26} \leftarrow {}^8_{17}$	7.5 ← 7.5	7 ← 7	77314.638	-0.053
	7.5 ← 7.5	8 ← 8	77312.172	-0.006
	8.5 ← 8.5	8 ← 8	77258.468	0.140
	8.5 ← 8.5	9 ← 9	77249.532	0.173
$^9_{27} \leftarrow {}^9_{18}$	8.5 ← 8.5	8 ← 8	78219.208	-0.015
	8.5 ← 8.5	9 ← 9	78222.180	-0.073
	9.5 ← 9.5	9 ← 9	78154.510	-0.111
	9.5 ← 9.5	10 ← 10	78136.316	-0.083
$^2_{12} \leftarrow {}^1_{01}$	1.5 ← 0.5	1 ← 0	61820.999	0.008
	1.5 ← 0.5	2 ← 1	61812.831	0.022
	2.5 ← 1.5	2 ← 1	61659.059	0.080
	2.5 ← 1.5	3 ← 2	61690.233	0.057

Table III. (continued)

Transition	J' ← J"	F' ← F"	Obs.	Obs.-Calc.
$3_{13} \leftarrow 2_{02}$	2.5 ← 1.5	3 ← 2	75838.024	-0.039
	3.5 ← 2.5	3 ← 2	75735.142	-0.150
	3.5 ← 2.5	4 ← 3	75771.126	-0.005
$5_{05} \leftarrow 4_{14}$	4.5 ← 3.5	4 ← 3	59653.103	-0.010
	4.5 ← 3.5	5 ← 4	59684.714	-0.016
	5.5 ← 4.5	5 ← 4	59790.096	0.004
	5.5 ← 4.5	6 ← 5	59770.088	-0.017
$6_{06} \leftarrow 5_{15}$	5.5 ← 4.5	5 ← 4	78697.348	-0.019
	5.5 ← 4.5	6 ← 5	78721.840	-0.012
	6.5 ← 5.5	6 ← 5	78809.608	0.028
	6.5 ← 5.5	7 ← 6	78790.852	-0.007
$8_{17} \leftarrow 7_{26}$	7.5 ← 6.5	7 ← 6	71568.341	-0.005
	7.5 ← 6.5	8 ← 7	71589.407	-0.028
	8.5 ← 7.5	8 ← 7	71833.112	-0.001
	8.5 ← 7.5	9 ← 8	71797.447	0.020
$11_{29} \leftarrow 10_{38}$	10.5 ← 9.5	10 ← 9	62159.911	0.053
	10.5 ← 9.5	11 ← 10	62177.121	0.042
	11.5 ← 10.5	11 ← 10	62484.212	-0.053
	11.5 ← 10.5	12 ← 11	62444.235	-0.008
$7_{44} \leftarrow 8_{35}$	6.5 ← 7.5	6 ← 7	79658.452	-0.020
	6.5 ← 7.5	7 ← 8	79666.298	0.041
	7.5 ← 8.5	7 ← 8	79299.900	-0.074
	7.5 ← 8.5	8 ← 9	79290.790	-0.020
$8_{45} \leftarrow 9_{36}$	7.5 ← 8.5	7 ← 8	61514.479	-0.062
	7.5 ← 8.5	8 ← 9	61513.691	0.003
	8.5 ← 9.5	8 ← 9	61181.801	0.048
	8.5 ← 9.5	9 ← 10	61174.580	0.027
$8_{44} \leftarrow 9_{37}$	7.5 ← 8.5	7 ← 8	63588.214	-0.035
	7.5 ← 8.5	8 ← 8	63597.834	-0.019
	8.5 ← 9.5	8 ← 9	63339.878	-0.029
	8.5 ← 9.5	9 ← 10	63333.014	0.040
$11_{57} \leftarrow 12_{48}$	10.5 ← 11.5	10 ← 11	72617.664	-0.001
	10.5 ← 11.5	11 ← 12	72619.526	0.027
	11.5 ← 12.5	11 ← 12	72326.264	-0.103
$11_{56} \leftarrow 12_{49}$	10.5 ← 11.5	10 ← 11	73287.563	0.050
	10.5 ← 11.5	11 ← 12	73292.837	0.066[a]
	11.5 ← 12.5	11 ← 12	73128.516	0.080[a]
	11.5 ← 12.5	12 ← 13	73128.516	-0.062[a]

Standard deviation is 0.061 MHz.

a. Weight is 0.5.

3. Analysis

A Hamiltonian applicable to the rotational spectra of FSO has been given in Part I, Chapter II. Numerical procedure and a method for the least squares fitting have also given. The method described there requires a fairly large computer program, and the Hamiltonian is treated rigorously by a numerical diagonalization procedure. However, in the work of FSO, another method, which is approximate and easy to handle, was used in an earlier stage of the analysis. In the method, the matrix elements are evaluated in an asymmetric rotor basis set, whithout including the centrifugal correction in the spin-rotation interaction, and the $\varepsilon_{ab}+\varepsilon_{ba}$ terms are treated by a second order perturbation (32).

Low N transitions of the $N_{1,N-1} \leftarrow N_{0,N}$ Q-branch series, the fine and hyperfine patterns of which are shown in Fig. 2, were subjected to the analysis at first. As seen in the figure, it was not easy to discriminate contributions due to the spin-rotation interaction from those due to the magnetic hyperfine interaction. We used the following procedure to obtain parameters for the two interactions, which is based on the approximate method mentioned above.

If $\Delta N = \pm 1$ matrix elements are ignored and the asymmetric rotor basis set is used, the levels of $F = N+1$, $J = N+1/2$ and $F = N-1$, $J = N-1/2$ have only diagonal matrix elements, and the levels of $F = N$, $J = N+1/2$ and $F = N$, $J = N-1/2$ are

derived from 2×2 energy matrices. Instead of diagonalizing the matrix, sums and/or differences of transition frequencies were used which, for Q-branch transitions, reduces to the following simple expressions:

$$[\nu(F=N+1,J=N+1/2) + \nu(F=N-1,J=N-1/2)] - [\nu(F=N,J=N+1/2) + \nu(F=N,J=N-1/2)] = N(N+1)\Delta S_I/[(N-1/2)(N+3/2)], \quad (2\text{-}3\text{-}1)$$

$$\nu(F=N+1,J=N+1/2) - \nu(F=N-1,J=N-1/2) = (2N+1)\{\Delta S_S - 3\Delta S_I/[4(N-1/2)(N+3/2)]\}/2, \quad (2\text{-}3\text{-}2)$$

where $\nu(F,J)$ is the frequency of the $\Delta F = \Delta J = \Delta N = 0$ transition, and,

$$\Delta S_I = \sum_{i=abc} T_{ii}\Delta\langle N_i^2\rangle/[N(N+1)], \quad (2\text{-}3\text{-}3)$$

$$\Delta S_S = \sum_{i=abc} \varepsilon_{ii}\Delta\langle N_i^2\rangle/[N(N+1)], \quad (2\text{-}3\text{-}4)$$

$$\Delta\langle N_i^2\rangle = \langle N_i^2\rangle_{upper} - \langle N_i^2\rangle_{lower}. \quad (2\text{-}3\text{-}5)$$

By making tentative assignments of J and F for the Q-branch transitions and by using approximate rotational constants, preliminary values of the fine and hyperfine interaction constants were obtained from eqs. (2-3-1) and (2-3-2). The analysis, however, was not straightfoward, becasuse some components of the Q-branch transitions were found to suffer from local perturbations. As indicated by the lengths of the arrows in Fig. 2, frequency shifts due to perturbations are large in the N = 4 and 5 transitions, and the J = N-1/2

components of the two transitions were found to be shifted in opposite direction. These shifts were explained by considering the $\varepsilon_{ab} + \varepsilon_{ba}$ term, which has matrix elements of $\Delta K = \pm 1$. The rotational levels, 3_{21} and 4_{22}, are the main perturbers for the levels, 4_{13} and 5_{14}, respectively. The frequency difference between 3_{21} and 4_{13} and between 4_{22} and 5_{14} are 14800 MHz and -5400 MHz, which well explained the relative magnitude of the shifts. The overall fitting of all the Q-branch transitions given in Fig. 2 was, in fact, greatly improved by taking into account those interaction by a second order perturbation method.

Several "extra" transitions were observed for the transitions with N less than 3. These extra lines are as intense as the "normal" transitions. After making some trial assignments for J and F, these extra transitions were concluded to be due to $\Delta N = \Delta F = 0$ but $\Delta J = \pm 1$ transitions. Ordinarily, these transitions have very small line strengths, i.e. at most 1/10 of those of normal ($\Delta N = \Delta J = \Delta F$) transitions. However, because the magnitudes of the spin-rotation and the hyperfine interactions are of the same order, $\Delta J = \pm 1$ transitions gain intensity from $\Delta J = 0$ transitions through the considerable mixing between levels with N = F. This situation is explained in Fig. 3 for the levels with N = 3 and 4, where the coefficients of eigenfunctions expressed in terms of the case (b) symmetric-

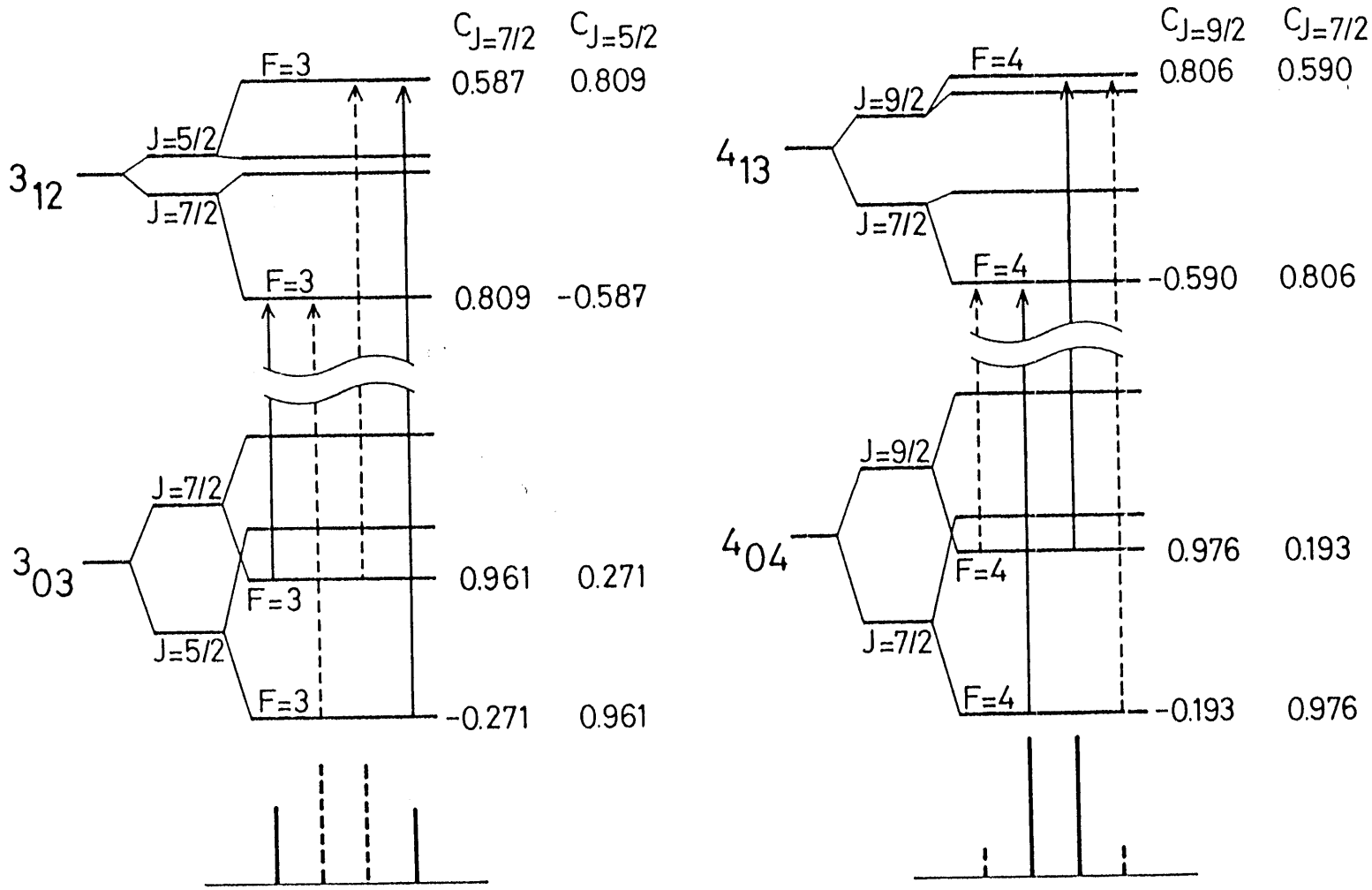

Fig. 3. Level diagrams of $3_{12} - 3_{03}$ and $4_{13} - 4_{04}$ transitions and coefficients (C_J) of the eigenfunctions, which were used to calculate the transition intensities. Solid lines denote the 'normal' transitions and broken lines denote the 'extra' transitions. Lower traces show the calculated intensities.

top basis functions are given. As shown in this figure, the fine structure of 3_{12} is inverted, which explains the abrupt change of the positions of the N = F transitions from N = 3 to 4. Line intensities calculated using these coefficients are consistent with the observed intensities. In addition, $\Delta J = \pm 1$ (or extra) transitions were found to be more sensitive to the magnetic field than $\Delta J = 0$ (or normal) lines, as expected from the fact that the signs of the Zeeman coefficients are opposite for the upper and lower levels.

This preliminary treatment was then followed by the rigorous method which used the computer program explicitly taking into account the $\varepsilon_{ab} + \varepsilon_{ba}$ term. All the measured frequensies in Tables I, II, and III were subjected to the least-squares fitting. The weight was 1 for most of the lines, but was reduced for slightly overlapped or unresolved lines. Severely overlapped lines were not included in the fitting. Table IV lists molecular constants thus determined. The numbers in parentheses in this Table represent 2.5 times standard deviations from the least-squares fitting and apply to the last digits of the constants, as are the case throughout this paper. The number of transitions for the ^{34}S species or for the excited state of the bending mode is not large enough to determine all molecular constants. For the ^{34}S species all centrifugal distortion parameters of both

the overall rotation and the spin-rotation interaction were fixed to the values of the normal species in the ground state, and for the excited state the centrifugal distortion constants of the spin-rotation interaction were fixed to the corresponding ground-state values. Although the individual signs are not determinable for the off-diagonal parameters, $\varepsilon_{ab} + \varepsilon_{ba}$ and T_{ab}, the relative signs were found to be the same for the two parameters.

Table IV. Molecular Constants of FSO (MHz)[a]

	$F^{32}SO(G.S.)$	$F^{34}SO(G.S.)$	$F^{32}SO(v_3=1)$
A	38 698.179(19)	37 536.604(63)	39 295.969(28)
B	9 340.810(4)	9 334.694(7)	9 325.356(6)
C	7 505.064(5)	7 456.138(6)	7 479.494(8)
Δ_N	0.009 970(45)	b	0.009 987(70)
Δ_{NK}	-0.082 86(42)	b	-0.085 26(69)
Δ_K	0.881 77(48)	b	0.961 69(67)
δ_N	0.002 899(18)	b	0.002 915(24)
δ_K	0.027 11(88)	b	0.029 1(14)
ε_{aa}	-339.543(83)	-333.48(66)	-313.288(40)
ε_{bb}	34.896(30)	35.89(16)	35.695(26)
ε_{cc}	1.861(26)	1.82(15)	1.915(32)
$1/2\lvert\varepsilon_{ab}+\varepsilon_{ba}\rvert$[c]	207.952(45)	214.2(22)	210.82(11)
Δ_N^s	0.000 47(49)	b	b
$\Delta_{NK}^s+\Delta_{KN}^s$	-0.013 1(31)	b	b
Δ_K^s	0.042 6(63)	b	b
a_F	67.228(57)	66.82(53)	66.86(11)
T_{aa}	-118.16(19)	-115.7(20)	-118.24(33)
T_{bb}	-117.06(13)	-117.7(9)	-116.85(19)
$\lvert T_{ab}\rvert$[c]	10.29(74)	—	10.5(15)

a. Values in parentheses denote 2.5 times standard deviations and apply to the last digits.

b. Fixed to the values of $F^{32}SO$ in the ground state.

c. The relative signs were found to be the same.

4. Stark effect

To determine the dipole moment, the Stark effect was measured for several low N transitions of the normal species in the ground state. The Stark field was chosen parallel to the microwave electric field, so that $\Delta M_F = 0$ was satisfied. The total pressure of the sample was kept as low as possible throughout the measurements. This was necessary for the observations of the Stark effect at an electric field as high as 1200 V/cm, to prevent discharges from taking place between Stark electrodes. Sine or square wave modulation of small amplitude was used; 40 V peak-to-peak was a typical amplitude. The electric field was calibrated by using Stark shift of the J = 2 - 1 transition of OCS (91).

The transitions measured are listed in Table V. As an example, the observed Stark shifts of the $2_{12} - 1_{01}$, J = 1.5 - 0.5, F = 1 - 0, $M_F = 0$ transition are shown in Fig. 4. As is the case for this example, many transitions show deviations from second order Stark effects at higher electric fields. As discussed before, the energy levels of FSO are complicated by the spin-rotation and hyperfine interactions, and their separations are not necessarily larger than the Stark energy. The ordinary second-order perturbation method is, thus, not adequate for analyzing the Stark effect in FSO.

As explained in Part I, Chapter II, the matrix elements

Table V. Stark Effects and Dipole Moment of FSO

Transition				range of voltage
$N' \leftarrow N''$	$J' \leftarrow J''$	$F' \leftarrow F''$	M_F [a]	applied (V/cm)
$1_{10} \leftarrow 1_{01}$	1.5 ← 1.5	1 ← 1	1	100 - 600
$1_{11} \leftarrow 0_{00}$	1.5 ← 0.5	1 ← 0	0	210 - 1210
$2_{12} \leftarrow 1_{01}$	1.5 ← 0.5	1 ← 0	0	220 - 1220
$3_{13} \leftarrow 2_{02}$	2.5 ← 1.5	2 ← 1	0	110 - 810
			1	810 - 1210
$3_{12} \leftarrow 3_{03}$	2.5 ← 2.5	2 ← 2	2	210 - 660
			1	850 - 1050

$\mu_a = 0.374\ (12)$ D, $\mu_b = 1.624\ (9)$ D, $\mu_{total} = 1.666\ (13)$ D [b]

a. All transitions observed obey $\Delta M_F = 0$ selection rules.

b. Values in parentheses denote 2.5 times standard errors.

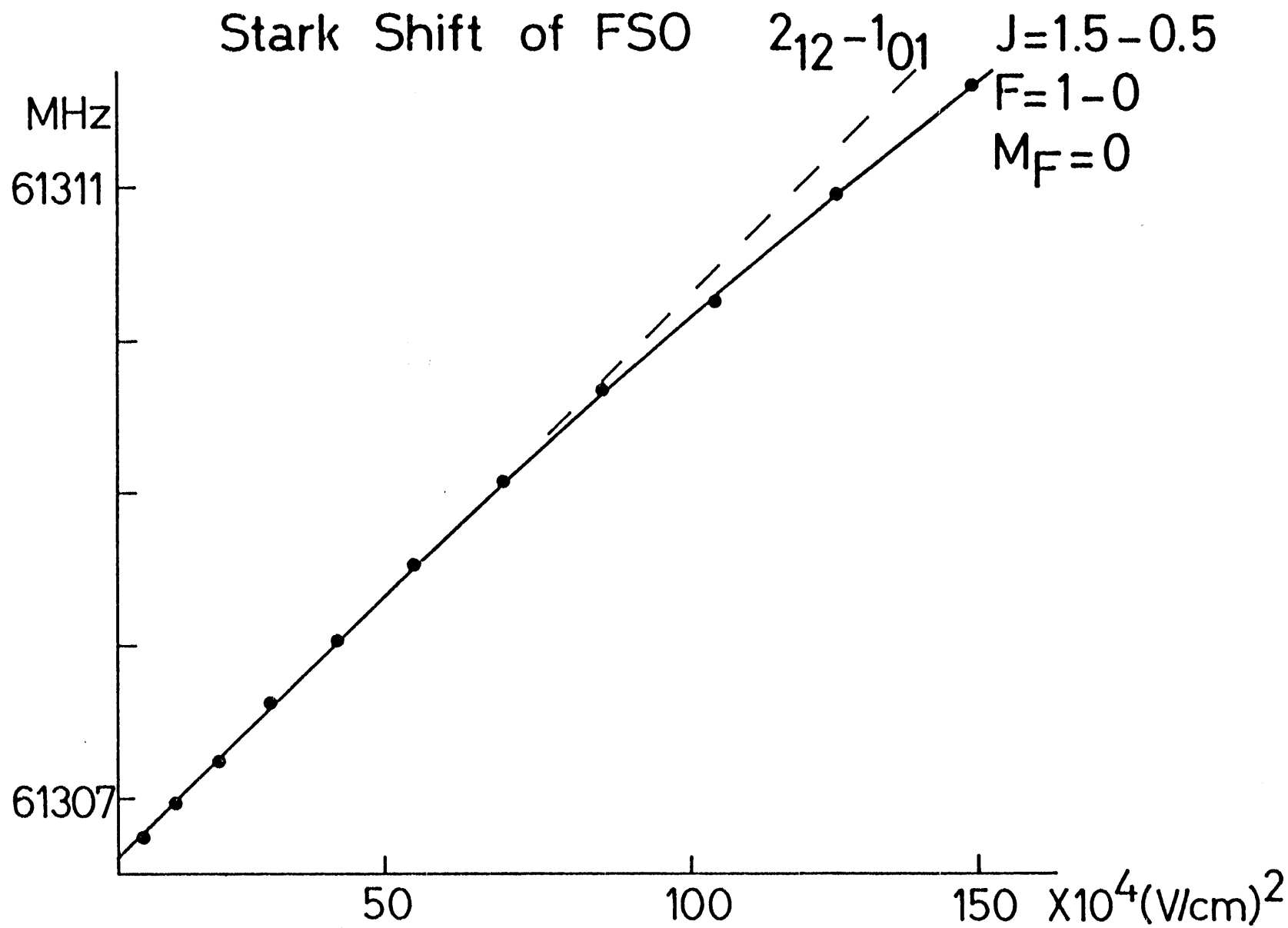

Fig. 4. The observed Stark shift of FSO. Dots denotes the observed Stark shifts, the solid line the calculated Stark effect, and the broken line the second order Stark effect.

of the Stark Hamiltonian are nonzero for $\Delta F = 0,\pm1$, $\Delta J = 0,\pm1$, and $\Delta N = 0,\pm1$, and they are diagonal in M_F. Therefore, the resulting energy matrix is of infinite dimension. Because the maximun F value involved in the observed transitions is 2 in the present study, the energy matrix was truncated at F = 3. The matrix contains all symmetry species of the rotational four group because the $\varepsilon_{ab} + \varepsilon_{ba}$ term and T_{ab} obay c-type selection rules and both μ_a and μ_b are nonzero, so that the energy matrix to be diagonalized becomes fairly large, e.g. 64×64 for $M_F = 0$, although the matrix is truncated at F = 3.

All the frequency shifts due to the Stark effect at different D. C. voltages were fitted by a least-squares method to determine two components of the dipole moment, while other molecular constants were fixed to those given in Table IV. The standard deviation of the fit was 0.042 MHz, and the dipole moment determined is $\mu_a = 0.374(12)$ D, $\mu_b = 1.624(9)$ D, and $\mu_{total} = 1.666(13)$ D, with 2.5 times standard errors in parentheses. The solid line in Fig. 4 represents the calculated Stark effect.

5. Molecular structure

The FSO molecule has three structure parameters: r(S-F), r(S-O), and ∠FSO. Since the spectrum of the ^{18}O species in natural abundance was too weak to be detected, the r_0 structure of FSO was calculated from the rotational constants of the normal and ^{34}S species. The moments of inertia, $I_{aa}^{(0)}$, $I_{bb}^{(0)}$, and $I_{cc}^{(0)}$, for both species were fitted by a least-squares method to determine three structure parameters. The determined molecular structure is :

$$r(S\text{-}F) = 1.602(3)\ \text{Å},$$

$$r(S\text{-}O) = 1.452(3)\ \text{Å},$$

$$\angle FSO = 108.32(6)^\circ.$$

6. Harmonic force field

Because no vibrational frequencies of FSO had been reported, we have tried to estimate the harmonic force field from the centrifugal distortion constants we determined. The centrifugal distortion constants in τ form are expressed in terms of the elements of inverse force constant matrix, F^{-1}, as follows (92):

$$\tau_{\alpha\beta\gamma\delta} = -\frac{(h/8\pi^2 I_{\alpha\alpha})(h/8\pi^2/I_{\gamma\gamma})}{RI_{\beta\beta}I_{\delta\delta}} \Sigma (J_{\alpha\beta}^{(i)})_0 (F^{-1})_{ij} (J_{\gamma\delta}^{(j)})_0 \qquad (2\text{-}3\text{-}5)$$

with $R = 10^{-22}/2h$. Here, the elements of $J_{\alpha\beta}^{(i)} = \delta I_{\alpha\beta}/\delta S_i$ relevant to FSO are listed in Table VI. There are only four τ's for planar molecules to be used for force field calculation, viz. τ_{aaaa}, τ_{bbbb}, τ_{aabb}, and τ_{abab}. From the Watson's Δ parameters given in Table IV, five τ constants were recalculated (93), which are shown in Table VII. As in other triatomic molecules the planarity conditions are not satisfied among the five τ's derived; three pairs of τ_{aabb} and τ_{abab} constants having slightly different values were obtained by using two of the three constants τ_{cccc}, τ_1, and τ_2 (94). Because the errors arising from those of Δ's of each pair were large, the averages of the three sets, as given in Table VII, were used for the calculation of the force field.

Six force constants are necessary to specify the force field of this type of molecules, while only four planar centrifugal distortion constants are available. We thus

Table VI. Relations between the molecular structure and $J_{\alpha\beta}^{(i)}$

	$J_{aa}^{(i)}$	$J_{bb}^{(i)}$	$J_{ab}^{(i)}$
S_1	$-2m_1b_1\cos\alpha_1$	$-2m_1a_1\sin\alpha_1$	$(2m_1/I_{cc})(I_b a_1\cos\alpha_1+I_a b_1\sin\alpha_1)$
S_2	$-2m_2b_2\cos\alpha_2$	$2m_2a_2\sin\alpha_2$	$(-2m_2/I_{cc})(-I_b a_2\cos\alpha_2+I_a b_2\sin\alpha_2)$
S_3	$2m_1b_1r_1\sin\alpha_1$	$-2m_1a_1r_1\cos\alpha_2$	$(-2m_1r_1/I_{cc})(I_b a_1\sin\alpha_1-I_a b_1\cos\alpha_1)$

$S_1 = \delta r_1$, $S_2 = \delta r_2$, and $S_3 = \delta\alpha$.
a_i, b_i: center of mass coordinates.
$I_x = m_i x_i^2$, e. t. c., $x_i = a_i, b_i$.
$I_{cc} = m_i(a_i^2+b_i^2)$

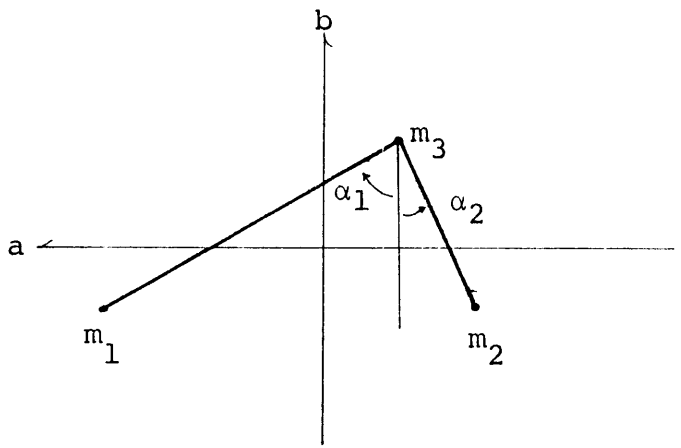

Table VII. Centrifugal Distortion Constants (MHz)[a]

τ_{aaaa}	-3.2355(28)	τ_1	0.2118(28)
τ_{bbbb}	-0.06307(20)	τ_2	0.01436(48)
τ_{cccc}	-0.01668(25)		
Derived from the planarity conditions[b]			
τ_{aabb}	0.293(13)	τ_{abab}	-0.059(12)

a. Recalculated from the constants in Table IV. Values in parentheses denote 2.5 times standard deviations and apply to the last digits of constants.

b. Weighted averages of the three sets of constants derived by taking values of τ_{cccc}, τ_1, and τ_2 in pairs.

estimated F_{11}, the diagonal element associated with the S-O stretching coordinate, by using Badger's rule (95), where the constants of SO, SO_2, and F_2SO were employed as references. Furthurmore, the difference between the inertia defects of the first excited bending state and the ground state, $\Delta_3 - \Delta_0$, contains only the information on the harmonic force field, while the inertia defect of the ground state itself involves contributions of other sources; we included the difference as a data for the estimation of the force field. Although, five data are thus available for determination of five F-matrix elements, we also fixed F_{13}, the off-diagonal element between the S-O stretching and the bending coordinate, to be zero because the frequencies of the ν_1 and ν_3 modes differ greatly and the contribution of the element to τ's and $\Delta_3 - \Delta_0$ are negligible.

Four centrifugal distortion constants and the difference of the inertia defects were used to determine the remaining four F-matrix elements by a least-squares fit. The five data were weighted according to the inverse of the square of their uncertainties because they have different accuracies and dimensions. The force field thus determined is shown in Table VIII, where the vibrational frequencies and the inertia defect of the ground state are also given. The calculated inertia defect of the ground state is corrected for the contribution

Table VIII. Harmonic Force Field, Vibrational Frequencies, and Inertia Defects of FSO

Force constants (in md/Å)[a]		error 1[b]	error 2[c]
F_{11}	9.2[d]	———	0.5
F_{22}	4.08	0.13	0.07
F_{33}	0.5382	0.0036	0.0002
F_{12}	0.140	0.083	0.018
F_{23}	0.050	0.011	0.006
Vibrational frequency (in cm^{-1})		**error 1[b]**	**error 2[c]**
ω_1	1215	2	33
ω_2	763	12	6
ω_3	396.2	1.3	0.1

Inertia defect (in amuÅ^2)	Δ_0	$\Delta_3 - \Delta_0$
obs.	0.17449 (5)	0.33978 (8)
calc.	0.1763 (7)[f]	0.33978[e]

a. Internal coordinates chosen are $S_1 = \delta r(S\text{-}O)$, $S_2 = \delta r(S\text{-}F)$, and $S_3 = \sqrt{r_1 r_2}\,\delta(\angle F\text{-}S\text{-}O)$. $F_{13} = 0$ was assumed.

b. 2.5 times standard errors of the least-squares fitting.

c. Due to an uncertainty in F_{11} of ±0.5 md/Å.

d. Fixed. This value was estimated using Badger's rule.

e. Fitted.

f. Includes contributions from centrifugal distortion terms.

of τ_{abab}, while the electronic contribution is not corrected. Two sources of errors are listed; error 1 corresponds to 2.5 times the standard errors from the least-squares fit, and error 2 is due to an estimated uncertainty in F_{11} of ±0.5 md/Å

7. Discussion

The present results have firmly established the existence of a new free radical FSO in the reaction system of OCS with discharge products of an O_2/CF_4 mixture. The following discussion on the observed spin-rotation and magnetic hyperfine interaction constants listed in Table IV clearly indicates that the ground electronic state of this radical is $^2A"$, as it was the case for HO_2 and HSO (see the discussion in the previous chapter).

Because the FSO radical belongs to C_s symmetry and is rather heavy, its energy levels are complicated and often suffer from local perturbations. However, these characteristics have made it possible for us to precisely determine the off-diagonal components of the spin-rotation interaction tensor and also of the magnetic dipole-dipole interaction tensor of the fluorine nucleus.

Curl's relation (35) was used to calculate the rotational g-factor from the spin-rotation constants and the rotational constants given in Table IV. The deviation of the diagonal components of the g-tensor from the free electron value, $g_S = 2.0023$, are as follows: $-\varepsilon_{aa}/2A = 0.0044$, $-\varepsilon_{bb}/2B = -0.0019$, and $-\varepsilon_{cc}/2C = -0.0001$. These values may be of some use for future studies of the Zeeman effect of FSO.

The absolute magnitude of the isotropic term of the magnetic hyperfine interaction is only 0.1 % of the value of atomic fluorine (84). This indicates that FSO is a π-type radical. Furthurmore, the result that $T_{cc} = -2T_{aa} = -2T_{bb}$, as shown in Table IV, suggests that the p-orbital occupied by the unpaired electron is perpendicular to the molecular plane when viewed from the fluorine atom. From the T_{cc} value of 235.22 MHz the unpaired spin density on the fluorine p_c orbital is calculated to be about 8 % (84).

Since the off-diagonal component of the dipolar hyperfine tensor, T_{ab}, is known, the in-plane principal axis of the tensor can be determined. The angle between the a-axis and one principal axis of the tensor is calculated to be 43.5°, whereas the angle between the a-axis and the S-F bond is about 30°.

The bond moments of FSO are calculated from the μ_a and μ_b components of the dipole moment determined. The direction of the total dipole moment is chosen as shown in Fig. 5, by considering the electronegativities of the three atoms concerned. It makes an angle of 13.0° with the b-axis and an angle of 34.8° with the S-O bond. This choise is consistent with bond moments of the S-F and S-O bonds known so far. The calculated bond moments are $\mu_{S-O} = 1.68$ D and $\mu_{S-F} = 1.00$ D. The S-O bond moment is close to that of F_2SO, 1.69 D, whereas the S-F bond moment is considerably larger than

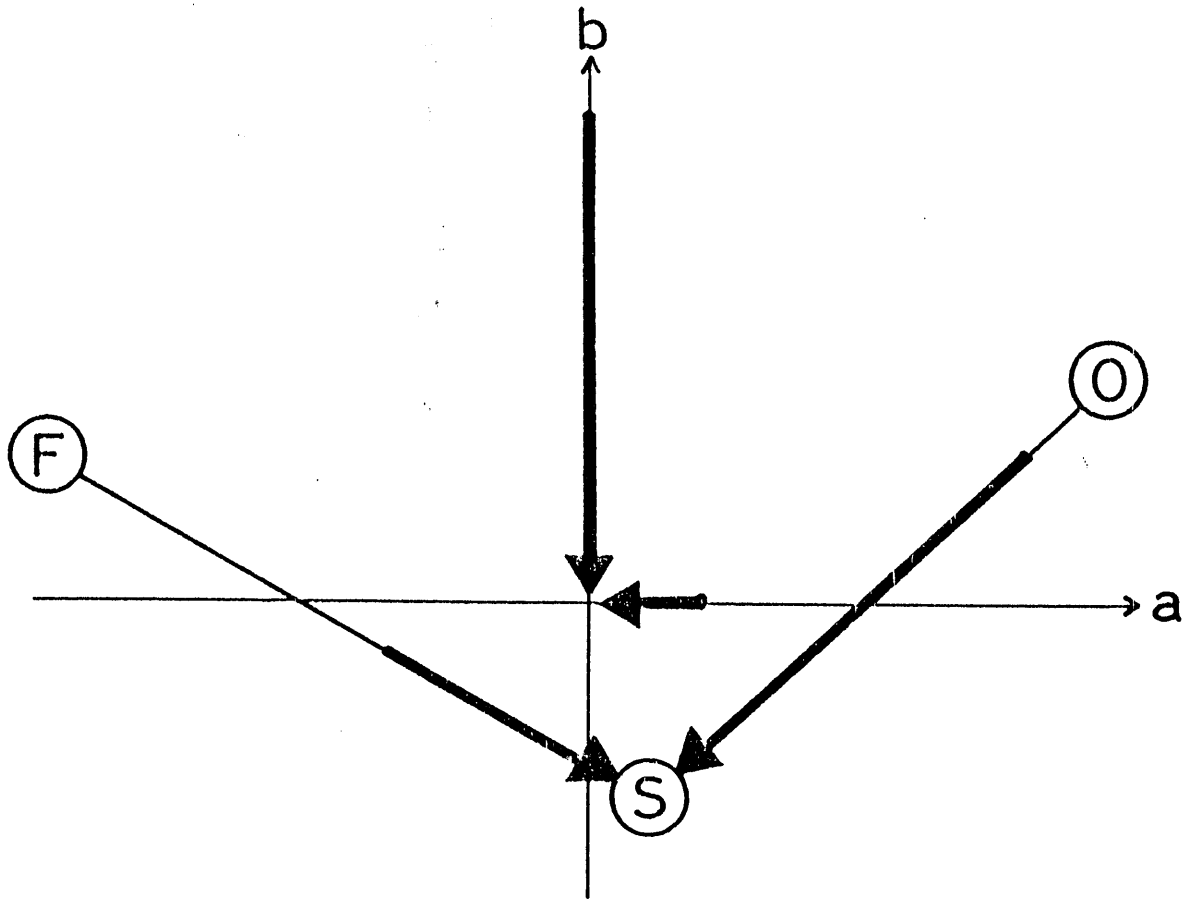

Fig. 5. Orientation of the dipole moment and the inertial axis.

that of F_2SO, 0.78 D.

Attempts to determine the force field without introducing the Badger's rule were not satisfactory because of correlation between the force constants associated with the two stretching modes. To improve the force constants estimated here, at least one of the stretching frequencies must be determined. In fact, the vibration-rotation transitions of the two stretching modes were observed quite recently by diode laser spectroscopy, where we are expecting that the force field will be much improved. On the other hand, as seen in Table VIII, the vibrational frequency of the bending mode, 396.2 cm^{-1}, is well determined in the present work, because this mode makes dominant contributions to the centrifugal distortion constants and the inertia defects obtained.

Chapter IV. General Discussion

1. Spin-rotation interaction

Among many additional interactions existing for molecules with unpaired electron(s), the spin-rotation interaction of asymmetric rotor molecules is the most prominent effect, and has been studied for various molecular species. In Table I are listed the spin-rotation interaction constants of HSO and FSO along with those of several other triatomic free radicals so far studied by high resolution spectroscopic methods. Dominant terms for the origin of the spin-rotation interaction constant, $\varepsilon_{\alpha\beta}$, can be written as follows (35,96)

$$\varepsilon_{\alpha\beta} = -\hbar/hc \sum_{\delta} \mu_{\alpha\delta} \sum_{n'}{}' \frac{[\langle n|L_\delta|n'\rangle\langle n'|C_\beta|n\rangle + \langle n|C_\beta|n'\rangle\langle n'|L_\delta|n\rangle]}{E_n - E_{n'}} \qquad (2\text{-}4\text{-}1)$$

where $\mu_{\alpha\delta}$ denotes the component of the inverse inertia tensor, and C_β is related to the spin-orbit interaction constants of the atoms composing the molecule (35). Thus, for example, ε_{aa} is proportional to the rotational constant A, and that of light molecules tend to be large. Another factor is the energy difference between the ground state and excited electronic states contributing to the interaction. Large part of the molecules listed here have their first excited electronic state in near IR or visible region. For example,

Table I. Spin-Rotation Interaction Constants for Bent Triatomic Radicals so far Studied by Microwave Spectroscopy

	ε_{aa}	ε_{bb}	ε_{cc}	$1/2\lvert\varepsilon_{ab}+\varepsilon_{ba}\rvert$
FSO[a]	-339.543	34.896	1.861	207.952
HSO[a]	-10365.99	-426.656	0.226	378.0
HO_2[b]	-49571.15	-442.573	8.623	387.9
HCO[c]	11617.6	18.9	-206.0	-
ClO_2[d]	-1388.7	-216.6	4.6	
NF_2[e]	-951.79	-92.86	4.49	
NO_2[f]	5401.76	7.65	-95.24	

a. Present studies.

b. Ref. 70.

c. B. J. Boland, J. M. Brown, A. Carrington, and A. C. Nelson, Mol. Phys., 34, 453 (1977); Proc. Roy. Soc. London, A360, 507 (1978).

d. Ref. 34.

e. Ref. 54.

f. Ref. 39.

HSO has its first excited $^2A'$ state 14367 cm^{-1} above the ground state (51). If we substitute C_a in eq. (4-2-1) with the spin-orbit interaction constant of neutral sulfur atom, A_{SO} = -397 cm^{-1} (35,97) and assume $|\langle n|L_a|n'\rangle|$ to be unity, ε_{aa} si calculated to be -33 GHz. This value is about twice as large as the observed value. The discrepancy may be accounted for by considering that $|\langle n|L_a|n'\rangle|$ is not unity, as the matrix element is proportional to the Franck Condon factor. On the other hand, ε_{aa} of FSO is much smaller even if scaled by the rotational constant A; this fact suggests that the first excited electronic state is much higher. However, nothing has been known so far for the electronic spectra of this radical.

The molecules in Table I should be divided into two groupes: molecules in one group have their unpaired electron in p_c-orbital, and have negative ε_{aa}, and others have in-plane unpaired electron orbital (HCO and NO_2). Latter molecules have positive ε_{aa}. Both HSO and FSO belong to the first group, as have been expected because they have similar electronic structures with HO_2. All the molecules belonging to the forst group (symmetriy species of the ground electronic state are of $^2A''$ or $^2B_1$) have almost zero ε_{cc} values; this fact is explained that there is no one electron orbital symmetrically allowed to couple with the ground state to produce c-axis

component of the spin-rotation interaction constant (35). On the other hand, for molecules in the second group the orbital of the unpaired electron is nearly parallel to the b-axis, so that the component parallel to this axis becomes almost zero.

Because the constant $(\varepsilon_{ab} + \varepsilon_{ba})/2$ has no first order contribution to the rotational energy levels, accuracies attained by microwave spectroscopy are required to determine this constant. In fact, we were able to determine the constants precisely both for FSO and HSO. However, it is not easy to discuss quantitatively the constants, since they were determined only as a linear combination and, moreover, each component is expressed as a sum of complicated second order interaction terms. One point should be noted, however, that the constant for FSO is considerably large compared with its ε_{aa}; this could be ascribed to large angles between the FS and/or SO bonds with the a-axis. On the other hand, those of HSO and HO_2 are quite small compared with their ε_{aa}; this suggests that the principal axis of the spin-rotation interaction tensor is nearly parallel to the a-axis.

For diatomic molecules in a $^2\Pi$ electronic state, the spin-rotation interaction which corresponds to that of asymmetric top molecules is expressed differently. The interaction expressed in eq. (2-4-1) corresponds

to one of the Mulliken and Christy's Λ-doubling constant p_v^* (26), viz. $\varepsilon_{bb} = \varepsilon_{cc} = -p_v^*/2$. As has been discussed in Part I, Chapter II, p_v^* is totally correlated with A_J, and cannot be determined experimentally unless studies of at least two isotopic species are combined (55). For molecules like SF or ClO, p_v^* is expected to be a few hundred MHz. Such a value changes A_J of SF, for example, about 1 MHz. On the other hand observed A_J for SF is 0.7(1.7) MHz.

2. Hyperfine interaction

The hyperfine interaction for free radicals is much clearer to understand than the spin-rotation interaction, because the former is an interaction between the unpaired electron spin and the nuclear spin and is essentially one electron property in the ground state, while the latter is a consequence of second order perturbations involving many often unknown excited electronic states. Nuclei which exhibited the magnetic hyperfine interaction in the present study are hydrogen (and deuterium) for HSO and fluorine for FSO and SF. Since these two nuclei behave differently, we will discuss them separately.

Table II lists the hyperfine interaction constants of fluorine for FSO, SF, and a few other species so far studied by microwave spectroscopy. All the species listed here are π-type radicals; that is the unpaired electron occupies p_π- orbital perpendicular to the molecular plane, or molecular axis for diatomic species. The Fermi interaction constants for such molecules should be zero from a simplest approximation because such p_π-orbital have no s-character. In fact, they are quite small compared with the value of atomic fluorine, 47910 MHz (84). Small positive values for these species may be understood as they are a consequence of spin-polarization on F-X bond, and they are roughly proportional to the spin-density on the fluorine atom.

Table II. Hyperfine Interaction Constants of Fluorine Nuclei for Free Radicals studied by Microwave Spectroscopy

	a_F	T_{aa}	T_{bb}	T_{cc}	T_{ab}	spin density
SF [a,d]	105	-211	-190	401	-	0.13
CF [b]	159.6	-244.3	-274.0	518.2	-	0.17
FSO [a]	67.2	-118.2	-117.1	235.2	10.3	0.08
NF_2 [c]	164.4	-241.8	-226.5	468.2	-	0.15

a. Present.

b. Ref. 53.

c. Ref. 54.

d. The a-axis corresponds to the molecular axis. See text for detailed discussion.

In Table II are also listed the dipole-dipole interaction constants, where dipolar interaction constants for diatomic species, SF and CF, are related to the Frosch and Foley's constants as follows (28);

$$T_{cc} - T_{bb} = d,$$

and $T_{aa} = 3/2c.$

Here, a-axis coincides with the molecular axis. From this table it is easily seen that for all species listed here, including the diatomic radicals, $T_{cc} \sim -2T_{aa} \sim -2T_{bb}$. This is a characteristic feature of the π-type radicals. In fact, for p-orbitals of atoms the expectation values $\langle(3\cos^2 - 1)/r^3\rangle_{x,\ y,\ \text{and}\ z}$ become 4/5, -2/5, and -2/5 times $\langle 1/r^3\rangle$ for the axis parallel to the direction p-orbital is pointing and the axes perpendicular to it, respectively. From the expectation value $2/5\langle 1/r^3\rangle$ for atomic fluorine, 1515 MHz (84), spin-densities of the p_π-orbitals on the fluorine atoms are obtained, which are also listed in the table. As have been mentioned earlier, it is easily seen that the Fermi interaction constants are almost proportional to the spin-densities.

Discussions on the magnetic hyperfine interaction constants for hydrogen nucleus are somewhat difficult because p-orbitals of the hydrogen atom are not occupied in most cases. In Table III are listed the hyperfine interaction constants of HSO and several other species containing hydrogen nuclei. In

Table III. Hyperfine Interaction Constants of Hydrogen Nuclei for a few Free Radicals (in MHz)

	T_{xx}	T_{yy}	T_{zz}	a_F
HSO [a,b]	12.9	-14.4	1.6	-36.4
HS [c,d]	21.63	-24.50	2.87	-52.63
HO_2 [e,f]	19.5	-8.1	-11.4	-27.6
HO [c,g]	88.08	-15.73	-72.35	-74.04
HCO [e,h]	3.8	11.6	-15.5	388.9

a. In principal axis system; the x-axis is nearly parallel to the H-S bond.

b. Present.

c. The x-axis cioncides the molecular axis, and $T_{zz}-T_{yy}=\pm d$.

d. Ref. 100.

e. In principal inertial axis system; x→b, y→a, and z→c.

f. Ref. 70.

g. Ref. 100.

h. See note c in Table I.

this table, constants of HCO are quite different from those of other species. The unpaired electron orbital for HCO has considerable s-character, because the unpaired orbital lies in the molecular plane. Thus, the Fermi coupling constant of HCO is large and positive. The Fermi coupling constants of other species are all negative and much smaller in absolute value than that of HCO. Such negative constants are again explained as a consequence of the spin-polarization (84). Because there is no π spin density on the hydrogen atom, the spin polarization is induced by the neighboring atom and, therefore, produces negative effective spin density.

Dipolar interaction constants in Table III are given in principal axis system for HSO, where x-axis was nearly parallel to the H-S bond and z-axis was perpendicular to the molecular plane. On the other hand, the b-axis was taken to be x-axis for HO_2 and HCO because principal axes are not known for these radicals and the b-axes were considered to be much closer to the H-O and H-C bonds than the a-axes. Among the molecules listed in the table, components of all the molecules except HCO (11) have similar relative values, namely, those along the H-X bonds are the largest and others are negative or very small. Generally speaking, because p-orbital on the hydrogen nucleus is not occupied, the dipolar interaction is of hydrogen nuclear spin with p-orbitals on other atoms; the situation is quite similar for the Fermi coupling constants. In fact,

Adrian et al. (98) performed a simple SCF calculation to explain the dipolar interaction constants for HO_2 observed by matrix EPR, where they used a following unpaired electron wave function,

$$\psi_e = (1-\alpha^2)^{1/2}\psi(O_{1\pi}) - \alpha\psi(O_{2\pi}). \qquad (2\text{-}4\text{-}2)$$

$\psi(O_{1\pi})$ and $\psi(O_{2\pi})$ are oxygen $2p_\pi$ orbitals located on the end and center O atoms, respectively. Based on the calculation, Barnes et al. (99) obtained the spin-density on the center O atom, α^2, to be 0.27 in their analysis of the microwave results (87). If we use the calculated values by Adrian et al. for $\alpha^2 = 1$ and correct the differences in bond lengths for HO_2 and OH, following constants are obtained for OH,

$$T_{xx} = 88.3 \text{ MHz},$$

$$T_{yy} = -21.7 \text{ MHz},$$

and

$$T_{zz} = -66.8 \text{ MHz}, \qquad (2\text{-}4\text{-}3)$$

which agrees quite well with the observed.

For HSO, instead of performing an SCF calculation, we have simply compared the dipolar interaction constants with those of the diatomic HS radical (100), based on the above argument. The ratios between the x, y, and z components are 0.60, 0.59, and 0.56, respectively. Thus, we can estimate that the spin-density on center S atom is about 0.60 for HSO. If we simply take the ratios for HO_2 and OH, they are 0.22, 0.51, and 0.16, for x, y, and z components, respectively. The discrepancy is

explained that the contribution of end O atom cannot be ignored for HO_2, while end O atom is much less contributing to the dipolar coupling constants than the central S atom for HSO.

Spin-densities thus estimated for HO_2 and HSO are supported by the ratios of the Fermi coupling constants between HO_2 and OH, and HSO and HS. The ratio for the former pair is 0.37 (99) and the latter is 0.69. They are roughly consistent with the values derived from the dipolar interaction constants.

In this section, we discussed the magnetic hyperfine interaction constants of SF, FSO, and HSO together with other radicals. We concluded that the unpaired electron orbitals of these species are all p_π type orbitals, or, in other word, they are all π-type radicals. We also estimated the spin-densities on fluorine or neighboring sulfur atoms from a simple discussions on these constants. However, comparisons of the hyperfine coupling constants determined here with those derived based on extensive MO calculations would be more informative to fully understand the electronic structures of these free radicals. Furthermore, such comparisons may be of great help to check and improve ab initio MO calculations of molecules with unpaired electrons.

3. Production of the free radicals

In the investigations of the three free radicals SF, FSO, and HSO in this thesis, we used three different absorption cells. FSO was observed with a rather conventional parallel plate Stark cell. We reacted OCS with 2450 MHz microwave discharge products of a mixture of O_2 and CF_4. Recently we observed its rotation-vibration spectrum with a diode laser spectrometer (101), where we also used the same reaction system. We found that A. C. glow discharge of a mixture of OCS, O_2 and CF_4 in the cell gave 1/10 or less signal than the reaction system given above. Thus, for the observation of the FSO radical, the Stark spectrometer and the parallel plate cell with the microwave discharge have been an appropriate combination among the methods we can utilize in our laboratory.

On the other hand, HSO was observed only by the glow discharge cell. Several trials to observe its spectrum with the Stark cell were all unsuccessful, so that the dipole moment of HSO, which is essential to quantitatively discuss its concentrations in reaction systems, could not be obtained so far.

Contrary to the above two species, SF was observable both with the Stark cell and with the glow discharge cell. Problems which had made observations by the Stark cell difficult are its small Stark effect at high frequency region and small Zeeman effect to distinguish its absorption lines from those of other undesirable species. We constructed smaller size discharge

cell (1 m in length) to obtain sufficient magnetic field. This smaller cell, when connected to a large mechanical booster pump with a very short vacuum line, has higher pumping speed than the 3.5 m cell. Therefore, for some species, this high pumping speed is expected to be advantageous although the absorption length becomes 3 to 4 times shorter. In fact, we succeeded to detect the microwave spectrum of CCl quite recently (102) which had not been observed with the 3.5 m cell in spite of several trials in the correct frequency regions. On the other hand, there exist some species for which longer path length is in fact essential. For example, Saito (103) found that the 3.5 m cell is much better than the 1 m cell for the observation of the DO_2 radical.

Thus, these variations of spectrometers and absorption cells we can choose in our laboratory are considered to be of great help to further develop our investigations on unknown free radicals. We can select almost the best reaction system and detection system for a particular species to be studied.

4. Concluding remarks

As have been described in this thesis we have newly constructed two types of microwave spectrometers: one utilizes conventional Stark modulation with a parallel plate cell, and the other utilizes source modulation with internal glow discharge free space cells (either 1 m or 3.5 m in length). We studied three free radicals SF, FSO, and HSO with these spectrometers, and obtained detailed molecular constants for these species. Among the constants thus obtained, the spin-rotation interaction constants and the magnetic hyperfine interaction constants are unique constants for free radicals with unpaired electrons in the ground electronic states, and they have provided us of important information on the electronic structures of these species, as have been discussed in this chapter.

Although both the spectrometers have had high enough sensitivity to study short-lived free radicals, the spectrometer with either of the free space cells was found to have reamarkable performances for free radical spectroscopy. The spectrometer works very well above 100 GHz, even up to 200 GHz, without any loss of sensitivity owing to the good microwave transmission of the free space cells, the difficulties arising from source modulation have been overcome by the use of a mini-computer, and consequently the spectrometer has very high sensitivity. This high sensitivity,

when combined with the internal glow discharge for the production of short-lived species, enabled us to further develop free radical spectroscopy in the microwave frequency region. In fact, after completion of the studies described in this thesis, we succeeded in detecting ClSO (86), CF (53), CCl (102), ClBO (104), and CF_3 (105) with the glow discharge cells. These studies, together with the studies written in this thesis, are hoped to greatly widen our knowledge on unstable species in various reaction systems, which is still restricted to a small number of molecules so far.

References

1. G. Herzberg, 'Molecular Spectra and Molecular Structure I, Spectra of Diatomic Molecules', Van Nostrand, New York, 1950, and G. Herzberg, 'Molecular Spectra and Molecular Structure III, Electronic Spectra of Polyatomic Molecules', ibid., 1966.
2. G. R. Bird and R. C. Mockler, Phys. Rev., 91, 222 (1953), and R. C. Mockler and G. R. Bird, ibid., 98, 1837 (1955).
3. T. M. Sanders, A. L. Schawlow, G. C. Dousmanis, and C. H. Towns, Phys. Rev., 89, 1158 (1953), and G. C. Dousmanis, T. M. Sanders, and C. H. Towns, ibid., 100, 1735 (1955).
4. F. X. Powell and D. R. Lide, J. Chem. Phys., 41, 1413 (1964) (SO).
5. T. Amano, E. Hirota, and Y. Morino, J. Mol. Spectrosc., 27, 257 (1968) (ClO).
6. F. X. Powell and D. R. Johnson, J. Chem. Phys., 50, 4596 (1969) (BrO).
7. T. Amano, S. Saito, E. Hirota, and Y. Morino, J. Mol. Spectrosc., 32, 97 (1969) (NS).
8. S. Saito, J. Chem. Phys., 53, 2544 (1970) ($SO\ ^1\Delta$).
9. S. Saito and T. Amano, J. Mol. Spectrosc., 34, 383 (1970) (NCO).
10. L. W. Hrubesh, E. A. Rinehart, and R. E. Anderson, J. Mol. Spectrosc., 36, 354 (1970) (NF_2).
11. S. Saito, Astrophys. J., 178, L95 (1972) (HCO).
12. S. Saito, J. Mol. Spectrosc., 48, 530 (1973) (IO).
13. T. Amano and E. Hirota, J. Mol. Spectrosc., 45, 417 (1973) (SF).
14. Y. Beers and C. J. Howard, J. Chem. Phys., 64, 1541 (1976) (HO_2).
15. A. Carrington, D. H. Levy, and T. A. Miller, Adv. Chem. Phys., 18, 149 (1970).
16. K. M. Evenson, R. J. Saykally, D. A. Jennings, R. F. Curl, and J. M. Brown, 'Chemical and Biochemical Application of Lasers', ed. C. B. Moore, Academic Press, 5, 95 (1980).

17. A. R. W. McKellar, Chem. Soc., Faraday Discussion, to be published.
18. J. M. Cook, G. W. Hills, and R. F. Curl, Astrophys. J., 207, L139 (1976), and G. W. Hills, J. M. Cook, R. F. Curl, and F. K. Tittel, J. Chem. Phys., 65, 823 (1976).
19. J. M. Brown and T. C. Steimle, Astrophys. J. 236, L101 (1980).
20. K. Takagi, S. Saito, M. Kakimoto, and E. Hirota, J. Chem. Phys., 73, 2570 (1980).
21. E. Hirota, 'Chemical and Biochemical Applications of Lasers', ed. C. B. Moore, Academic Press, 5, 39 (1980).
22. G. Winnewisser, E. Churchwell, and C. M. Walmsley, 'Modern Aspects of Microwave Spectroscopy', ed. G. W. Chantry, Academic Press, 313 (1979).
23. E. Hill and J. H. Van Vleck, Phys. Rev., 32, 250 (1928).
24. J. H. Van Vleck, Rev. Mod. Phys., 23, 213 (1951).
25. J. H. Van Vleck, Phys. Rev., 33, 467 (1929).
26. R. S. Mulliken and A. Christy, Phys. Rev., 38, 87 (1931).
27. G. M. Almy and R. B. Horsfall, Phys. Rev., 51, 491 (1937).
28. R. A. Frosch and H. M. Foley, Phys. Rev., 88, 1337 (1952).
29. T. C. James, J. Chem. Phys., 41, 631 (1964).
30. I. Kopp and J. T. Hougen, Can. J. Phys., 45, 2581 (1967).
31. R. N. Zare, A. L. Schmeltekopf, W. J. Harrop, and D. L. Albritton, J. Mol. Spectrosc., 46, 37 (1973).
32. R. F. Curl and J. L. Kinsey, J. Chem. Phys., 35, 1758 (1961).
33. R. F. Curl, J. L. Kinsey, J. G. Baker, J. C. Baird, G. R. Bird, R. F. Heidelberg, T. M. Sugden, D. R. Jenkins, and C. N. Kenney, Phys. Rev., 121, 1119 (1961).
34. R. F. Curl, R. F. Heidelberg, and J. L. Kinsey, Phys. Rev., 125, 1993 (1962).
35. R. F. Curl, J. Chem. Phys., 37, 779 (1962).
36. M. G. K. Pillai and R. F. Curl, J. Chem. Phys., 37, 2921 (1962).

37. W. M. Tolles, J. L. Kinsey, R. F. Curl, and R. F. Heidelberg, J. Chem. Phys., 37, 927 (1962).
38. R. P. Mariella and R. F. Curl, J. Chem. Phys., 52, 757 (1970).
39. R. M. Lees, R. F. Curl, and J. G. Baker, J. Chem. Phys., 45, 2037 (1966).
40. P. D. Foster, J. A. Hodgeson, and R. F. Curl, J. Chem. Phys., 45, 3760 (1966).
41. R. Kewley, K. V. L. N. Sastry, M. Winnewisser, and W. Gordy, J. Chem. Phys., 39, 2856 (1963).
42. G. Ehrenstein, Phys. Rev., 130, 669 (1963).
43. D. R. Johnson and C. C. Lin, J. Mol. Spectrosc., 23, 201 (1967).
44. R. C. Woods, Rev. Sci. Instrum., 44, 282 (1973).
45. T. A. Dixon and R. C. Woods, Phys. Rev. Lett., 34, 61 (1975) (CO^+).
46. R. C. Woods, T. A. Dixon, R. J. Saykally, and P. G. Szanto, Phys. Rev. Lett., 35, 1269 (1975) (HCO^+).
47. R. J. Saykally, P. G. Szanto, T. G. Anderson, and R. C. Woods, Astrophys. J., 204, L143 (1976) (HNC).
48. R. J. Saykally, T. A. Dixon, T. G. Anderson, P. G. Szanto, and R. C. Woods, Astrophys. J., 205, L101 (1976) (N_2H^+).
49. T. A. Dixon and R. C. Woods, J. Chem. Phys., 67, 3956 (1977) (CN).
50. C. S. Gudeman, N. N. Haese, N. D. Piltch, and R. C. Woods, Astrophys. J., ___, L (1981) (HCS^+).
51. M. Kakimoto, S. Saito, and E. Hirota, J. Mol. Spectrosc., 80, 334 (1980).
52. N. Ohashi, M. Kakimoto, S. Saito, and E. Hirota, J. Mol. Spectrosc., 84, 204 (1980).
53. S. Saito, Y. Endo, and E. Hirota, to be published.
54. R. D. Brown, F. R. Burden, P. D. Godfrey, and I. R. Gillard, J. Mol. Spectrosc., 52, 301 (1974).

55. J. M. Brown and J. K. G. Watson, J. Mol. Spectrosc., 65, 65 (1977).
56. D. W. Lepard, Can. J. Phys., 48, 1664 (1970).
57. T. Amano, S. Saito, E. Hirota, Y. Morino, D. R. Johnson, and F. X. Powell, J. Mol. Spectrosc., 30, 275 (1969).
58. J. A. Coxon and R. E. Hamersley, J. Mol. Spectrosc., 58, 29 (1975).
59. K. L. Saenger and R. N. Zare, J. Mol. Spectrosc., 61, 216 (1976).
60. M Mizushima, Phys. Rev., 97, 967 (1955).
61. G. C. Dousmanis, Phys. Rev., 97, 967 (1955).
62. C. C. Lin and M. Mizushima, Phys. Rev., 100, 1726 (1955).
63. A. R. Edmonds, 'Angular Momentum in Quantum Mechanics', Princeton Univ. Press, 1968.
64. W. L. Meerts, Chem. Phys., 14, 421 (1976).
65. C. C. Lin, Phys. Rev., 116, 903 (1959).
66. I. C. Bowater, J. M. Brown, and A. Carrington, Proc. Roy. Soc. London, A333, 265 (1973).
67. R. N. Dixon and G. Duxbury, Chem. Phys. Lett., 1, 330 (1967).
68. J. M. Cook, G. W. Hills, and R. F. Curl, J. Chem. Phys., 67, 1450 (1977).
69. J. M. Brown and T. J. Sears, Mol. Phys., 34, 1595 (1977).
70. J. M. Brown and T. J. Sears, J. Mol. Spectrosc., 75, 111 (1979).
71. J. K. G. Watson, J. Chem. Phys., 45, 1360 (1966).
72. J. K. G. Watson, 'Vibrational Spectra and Structure', ed. J. R. Durig, Elsevier, 6, 1 (1977).
73. L. D. Landau and E. M. Lifshitz, 'Quantum Mechanics, Non Relativistic Theory', Pergamon Press, 1965 (English translation).
74. W. Gordy and R. L. Cook, 'Microwave Molecular Spectra', Wiley, 1970.
75. Y. Endo, S. Saito, and E. Hirota, J. Mol. Spectrosc., 77, 222 (1979).

76. J. F. Verdiek and C. D. Conwell, Rev. Sci. Instrum., 32, 1383 (1961).
77. W. Nagourney, Rev. Sci. Instrum., 49, 1072 (1978).
78. J. H. Carpenter, J. D. Cooper, J.B. Simpson, J. G. Smith, and D. H. Whiffen, J. Phys. E, 7, 678 (1974).
79. E. Hirota and M. Imachi, Can. J. Phys., 53, 2023 (1975).
80. J. P. Porchet and Hs. H. Gunthard, J. Phys. E, 3, 261 (1970).
81. A. Carrington, G. N. Currie, T. A. Miller, and D. H. Levy, J. Chem. Phys., 50, 2726 (1969).
82. G. Di Lonardo and A. Trombetti, Trans. Faraday Soc., 66, 2694 (1970).
83. D. R. Johnson and F. X. Powell, Science, 164, 950 (1969).
84. J. R. Morton, Chem. Rev., 64, 453 (1964).
85. U. Schurath, M. Weber, and K. Becker, J. Chem. Phys., 67, 110 (1977).
86. S. Saito, Y. Endo, and E. Hirota, to be published.
87. S. Saito, J. Mol. Spectrosc., 65, 229 (1977).
88. F. D. Wayne and H. E. Radford, private communication.
89. K. Nishikida and F. Williams, J. Mag. Res., 14, 348 (1974).
90. C. Yamada, K. Kawaguchi, and E. Hirota, J. Chem. Phys., 69, 1942 (1978).
91. J. M. L. J. Reinartz and A. Dymanus, Chem. Phys. Lett., 24, 346 (1974).
92. R. L. Cook, J. Chem. Phys., 42, 2927 (1965).
93. J. K. G. Watson, J. Chem. Phys., 46, 1935 (1967).
94. W. H. Kirchhoff, J. Mol. Spectrosc., 41, 333 (1972).
95. R. M. Badger, J. Chem. Phys., 3, 710 (1935).
96. J. M. Brown, T. J. Sears, and J. K. G. Watson, Mol. Phys., 41, 173 (1980).
97. C. E. Moore, 'Atomic Energy Levels', NBS, Washington, D. C., 1949.
98. F. J. Adrian E. L. Cochran, and V. A. Bowers, J. Chem. Phys., 44, 2979 (1966).

99. C. E. Barnes, J. M Brown, A. Carrington, J. Pinkstone, T. J. Sears, and P. J. Thistlethwaite, J. Mol. Spectrosc., 72, 86 (1978).
100. W. L. Meerts and A. Dymanus, Can. J. Phys., 53, 2123 (1975).
101. Y. Endo, K. Nagai, and E. Hirota, to be published.
102. Y. Endo, S. Saito, and E. Hirota, to be published.
103. S. Saito, private communication.
104. K. Kawaguchi, private communication.
105. Y. Endo, C. Yamada, S. Saito, and E. Hirota, to be published.
106. K. Kawaguchi, C. Yamada, Y. Hamada, and E. Hirota, J. Mol. Spectrosc., 86, 136 (1981).

List of Publications

Spectroscopy of Free Radicals

R. F. Curl, Y. Endo, M. Kakimoto, S. Saito, and E. Hirota, "Hyperfine Structure in the $\tilde{A}$ State of PH_2", Chem. Phys. Lett., 53, 536 (1978).

Y. Endo, S. Saito, E. Hirota, and T. Chikaraishi, "Microwave Spectrum of Sulfur Difluoride in the First Excited Vibrational States. Vibrational Potential Function and Equilibrium Structure", J. Mol. Spectrosc., 77, 222 (1979).

Y. Endo, S. Saito, and E. Hirota, "Microwave Spectrum, Spin-Rotation, and Hyperfine Interaction Constants, Dipole Moments, Molecular Structure, and Harmonic Force Constants of the FSO radical", J. Chem. Phys., 74, 1568 (1981).

Y. Endo, S. Saito, and E. Hirota, "Microwave Spectra of the HSO and DSO Radicals", to be published in J. Chem. Phys.

Y. Endo, S. Saito, and E. Hirota, "Microwave Spectrum of the SF Radical", to be published.

Others

E. Hirota, S. Saito, and Y. Endo, "Second Order Coriolis Resonance between ν_2 and ν_5 of $^{13}CH_3F$ by Microwave Spectroscopy", J. Mol. Spectrosc., 70, 469 (1978).

E. Hirota, S. Saito, and Y. Endo, "Microwave Spectra of Deuterated Ethanes. Internal Rotation Potential Function and r_z Structure", J. Chem. Phys., 71, 1183 (1979).

Y. Endo, K. Yoshida, S. Saito, and E. Hirota, "The Microwave Spectrum of Carbon Dioxide-^{18}O", J. Chem. Phys., 73, 3511 (1980).

K. Matsumura, T. Tanaka, Y. Endo, S. Saito, and E. Hirota, "Microwave Spectrum of Acetylene-d in Excited Vibrational States", J. Phys. Chem., 84, 1793 (1980).